



HAL
open science

Modeling heterogeneous vehicular traffic for intelligent transport system applications

Sosina Mengistu Gashaw

► **To cite this version:**

Sosina Mengistu Gashaw. Modeling heterogeneous vehicular traffic for intelligent transport system applications. Other [cs.OH]. COMUE Université Côte d'Azur (2015 - 2019), 2018. English. NNT : 2018AZUR4202 . tel-02068753

HAL Id: tel-02068753

<https://theses.hal.science/tel-02068753v1>

Submitted on 15 Mar 2019

HAL is a multi-disciplinary open access archive for the deposit and dissemination of scientific research documents, whether they are published or not. The documents may come from teaching and research institutions in France or abroad, or from public or private research centers.

L'archive ouverte pluridisciplinaire **HAL**, est destinée au dépôt et à la diffusion de documents scientifiques de niveau recherche, publiés ou non, émanant des établissements d'enseignement et de recherche français ou étrangers, des laboratoires publics ou privés.

THÈSE DE DOCTORAT

Modélisation de Trafic Routier Hétérogène pour Systèmes de Transport Intelligents

*Présentée en vue de l'obtention du grade de docteur
en Informatique d'UNIVERSITÉ CÔTE D'AZURE*

par

Sosina Mengistu GASHAW

Dirigée par : Prof. Jérôme HÄRRI
Co-encadrée par : Dr. Paola GOATIN

Soutenue le : 30 Novembre, 2018

Devant le jury, composé de:

- | | | |
|-----------------------------|--------------------------------------|--------------------|
| 1. GOATIN Paola | Directeur de Recherche, INRIA | Directeur de thèse |
| 2. HÄRRI Jérôme | Professeur, EURECOM | Directeur de thèse |
| 3. LECLERCQ Ludovic | Professeur, Université du Lyon | Rapporteur |
| 4. PICCOLI Benedetto | Professeur, Rutgers University | Rapporteur |
| 5. SACONE Simona | Professeur, Université du Genova | Examineur |
| 6. SPYROPOULOS Thrasyvoulos | Professeur Assistant, EURECOM | Examineur |
| 7. VITI Francesco | Professeur, Université du Luxembourg | Rapporteur |

Declaration of Authorship

I, Sosina Mengistu GASHAW, declare that this thesis, titled "Modeling Heterogeneous Vehicular Traffic for Intelligent Transport System Applications" and the work presented in it are my own. I confirm that:

Signed:

Date:

Abstract

UNIVERSITÉ CÔTE D'AZUR

Doctor of Philosophy

Modélisation de Trafic Routier Hétérogène pour Systèmes de Transport Intelligents

by Sosina Mengistu GASHAW

Cette dissertation modélise et analyse les flux de trafic hétérogènes, avec une attention particulière portée à la circulation de voitures et de deux-roues. L'augmentation du nombre de congestions de trafic a forcé les personnes désirant se déplacer à se diriger vers les le deux-roues (appelé ici PTWs = powered two wheelers), comme les motos, les mopeds et les scooters, du fait de leur facilité de manoeuvre et leur efficacité dans l'espace. L'augmentation du nombre de PTWs combinée au caractère unique de certaines de leurs fonctionnalités a résulté en un trafic complexe, donc les particularités sont difficiles à recréer avec les approches de modélisation existantes.

Nous développerons ici un modèle analytique permettant de reproduire de manière pertinente les particularités d'un flux de véhicules mêlant à la fois les voitures et les deux-roues. Le trafic se décompose en deux classes de véhicules : les PTWs et les voitures. Les propriétés fondamentales sont déduites en employant une approche "porous flow". On suppose que la vitesse d'un véhicule d'une certaine classe est dictée par les propriétés physiques et motrices du véhicule, ainsi que la distribution d'espace vide sur la route. Nous proposons une méthode d'approximation pour dériver la distribution d'espace vide.

Dans le but d'explorer plus largement les caractéristiques du flux de trafic notamment requis par les applications de système de transport intelligent (ITS), nous formulons le modèle dans les cadres lagrangien et eulérien. Puis, nous ferons appel à une méthode numérique pour la discrétisation du modèle mathématique.

Se basant sur le modèle développé nous analyserons les caractéristiques du flux de trafic pour en identifier les propriétés les plus importantes qui nous permettront de prédire de futures ITS applications et d'organisations du trafic. La possibilité d'appliquer le modèle pour les différentes ITS applications est illustrée par des exemples. Finalement, le modèle développé est validé à l'aide de l'outil de microsimulation .

Abstract

UNIVERSITÉ CÔTE D'AZUR

Doctor of Philosophy

Modeling Heterogeneous Vehicular Traffic for Intelligent Transport System Applications

by Sosina Mengistu GASHAW

This dissertation models and analyzes heterogeneous traffic flow, with a particular focus on mixed traffic flow consisting of cars and two-wheelers. The increase in traffic congestion induces commuters to switch to powered two wheelers (PTWs), i.e. motorcycle, mopeds and scooters, because of their high maneuverability and space efficiency. The growth in number of PTWs, combined with their unique mobility features, results in complex traffic characteristics which are difficult to recreate with the existing modeling approaches.

We develop an analytical model that can accurately reproduce the traffic features in a mixed flow of cars and PTWs. The traffic stream is decomposed into two vehicle classes, PTWs and cars. The fundamental properties are derived by employing a porous flow approach. It is assumed that the speed of a vehicle class is dictated by the physical and motion properties of the vehicle class, and the distribution of free spaces on the road. We propose an approximation method to derive the free-space distribution.

In order to explore broader aspects of the traffic flow characteristics, notably required by intelligent transport system (ITS) applications, we formulate the model in the Lagrangian and the Eulerian frameworks. Further, we provide a numerical method for the discretization of the mathematical model.

We analyze the flow characteristics of mixed PTWs and cars traffic and identify important properties, which give insights for future ITS solutions and traffic policy makers. The applicability of the model for different ITS applications is illustrated. Finally, the developed model is validated using a microsimulation tool.

Acknowledgements

"The LORD is my shepherd, I shall not want. He makes me to lie down in green pastures. He leads me beside still waters;"

All glory to God Almighty, who is the grace of my life, the source of my wisdom and the light of my life.

The completion this Ph.D. journey would have not been possible without the help and support I have received from many people. I would like to extend my sincere appreciation to all of them.

First and foremost, I would like to express my sincere gratitude to my professor Jérôme Härrri. His guidance, continuous support, encouragement and critical feedbacks throughout the years have been great contributions to my Ph.D. research as well as to my professional development. I am grateful for getting the opportunity to work with him. I am also extremely thankful to my co-supervisor Paola Goatin. Her dedication and professionalism have inspired me. I thank both my supervisor for the regular meetings and the patience in reading and commenting the thesis.

I would like to extend my sincere appreciation to all the jury members, specially to the reviewers, Prof. VITI Francesco, Prof. LECLERCQ Ludovic and Prof. PICCOLI Benedetto, for the constructive comments and suggestions.

I would like to thank also all Eurecom staffs. Handling all the issues related to resident permit, missions, doctoral school and others would have been difficult without your kind support. I thank you for making my stay in France less stressful. My sincere thanks also to A-team members for the interesting discussions.

I am indebted to many kindhearted people around me, who have supported me in one way or the other during this journey. First, I extend my deepest gratitude to my amazing and humble friends from AMU, who are more like brothers and sisters to me. Thank you for the support, the encouragement and for being by my side all the time. You are truly my blessings. I also would like to extend my heartfelt thank to my brothers and sisters from MK Europe. Having you around makes my stay in Europe a wonderful and purposeful time. I can not forget the immense support from special individuals such as Selamina and Sure (Mr. B). I thank all my colleagues for the nice time, of course special thanks goes to my friend Raj Patel.

Lastly, I would like to thank my dearest family with all my heart. I couldn't imagine life without your caring and supportive love. You are the reason for me to be thankful and feel blessed every time. Words fail me to express my gratitude to my parents. Menge and Simegn thank you so much for teaching me to work hard and to be an independent person. You take the lion share in shaping me into who I am today. My beloved brothers Emushe and Abiye, I can not thank you enough for being there all the time, for encouraging me to follow my dream and more than anything for being the best brothers I could have wished for. I extend my huge gratitude to all other family members.

Contents

Declaration of Authorship	iii
Acknowledgements	ix
1 Introduction	1
1.1 Background	1
1.2 Research objective	3
1.3 Methodology	3
1.4 Contribution	4
1.5 Thesis Organization	5
2 Heterogeneous Traffic Flow Modeling	7
2.1 Introduction	7
2.2 ITS applications	8
2.3 Heterogeneous traffic flow models	10
2.3.1 Heterogeneous microscopic traffic models	10
2.3.1.1 Car-following models	11
2.3.1.2 Cellular automata model	12
2.3.2 Heterogeneous macroscopic models	12
2.3.2.1 Multi-class LWR model	13
2.3.2.2 Multi-class two-equation models	20
2.3.3 Heterogeneous mesoscopic models	20
2.4 Modeling two-wheelers mobility	20
2.4.1 Maneuvering behavior of PTWs	20
2.4.2 Models for traffic flow including PTWs	22
2.4.3 Microscopic model	22
2.4.3.1 Car-following model	22
2.4.3.2 Cellular automata model	24
2.4.4 Macroscopic model	25
2.4.4.1 Multiclass LWR model	25
2.5 Traffic model calibration and validation	28
2.6 Conclusion	29
3 Model development	31
3.1 Model requirements	31
3.2 Fundamental relation	32
3.2.1 Determination of spacing distribution	33
3.2.2 Speed function	38
3.3 Flow equation	40
3.3.1 Eulerian representation	40
3.3.2 Lagrangian representation	41
3.3.2.1 N-Lagrangian reference frames	42
3.3.2.2 1-Lagrangian reference frame	43
3.4 Discretization scheme	43
3.4.1 Eulerian formulation	43
3.4.2 Lagrangian formulation	44
3.4.2.1 N-Lagrangian reference frames	44
3.4.2.2 1-Lagrangian reference frame	45

3.5	Numerical Test	47
3.5.1	Test setup	47
3.5.2	Results	48
3.6	Summary and conclusion	52
4	Model analysis and comparison	55
4.1	Mathematical properties of the model	55
4.2	Fundamental relation	57
4.3	Model comparison and verification	58
4.3.1	Pore size distribution verification	58
4.3.2	Verifying model properties	60
4.3.2.1	Creeping experiment	62
4.3.2.2	Overtaking experiment	63
4.4	Model calibration and validation	65
4.4.1	Vissim simulation	66
4.4.2	Analyzing the data	66
4.4.3	Model calibration	67
4.4.4	Validation	71
4.5	Summary and conclusion	73
5	Perspectives for future ITS applications	75
5.1	Traffic impact analysis	75
5.1.1	Road capacity	76
5.1.2	Travel time	76
5.2	Assessing traffic control systems	77
5.2.1	Adaptive traffic light control	77
5.2.1.1	Queue dynamics	78
5.2.1.2	Optimization approach	81
5.2.1.3	Evaluation	83
5.2.2	Variable speed limit control	84
5.2.2.1	Methodology	85
5.2.2.2	Lagrangian Prediction Model	86
5.2.2.3	MPC-based VSL Controller	88
5.2.2.4	Evaluation	89
5.3	Summary and conclusion	92
6	Conclusion	95
6.1	Research contributions	95
6.2	Future research direction	97
A	The parameters used For the fundamental diagrams	99
B	Model development	101
B.1	Pore size distribution	101
B.2	Lagrangian discretization method	103
C	VISSIM simulation	105
C.1	Vehicles parameter	105
C.2	Parameter for Wiedemann model and Later distance	105
D	List of publications	107
	Bibliography	109

List of Figures

2.1	The roles of traffic flow models in ITS applications	9
2.2	Schematic diagram of CA space discretization (A) homogeneous traffic (single cell) (B) heterogeneous traffic (multi-cell)	12
2.3	Speed-density relation (A) (G. Wong and S. Wong, 2002) model (B) (J Van Lint, Serge Hoogendoorn, and Schreuder, 2008) model	14
2.4	The variation of (A) speed-density and (B) flow-density relation with traffic composition in (G. Wong and S. Wong, 2002) model	15
2.5	Speed density relation (A) (Chanut and Buisson, 2003; Ngoduy and R. Liu, 2007) model (B) (S Logghe and L. H. Immers, 2008; Qian et al., 2017) model	16
2.6	The variation of (A) speed-density and (B) flow-density relation with traffic composition in (Ngoduy and R. Liu, 2007) model	16
2.7	The variation of (A) speed-density and (B) flow-density relation with traffic composition in (Chanut and Buisson, 2003) model	17
2.8	The variation of (A) speed-density and (B) flow-density relation with traffic composition in (S Logghe and L. H. Immers, 2008; Qian et al., 2017) model	18
2.9	Fundamental relations in (A)(H. Zhang and Jin, 2002) model (B)(Benzoni-Gavage and Colombo, 2003) model	19
2.10	The variation of (A) speed-density and (B) flow-density relation with traffic composition in (H. Zhang and Jin, 2002) model	19
2.11	The variation of (A) speed-density and (B) flow-density relation with traffic composition in (Benzoni-Gavage and Colombo, 2003) model	19
2.12	The representation of PTWs maneuvering behaviors	21
2.13	Illustration of the strip based approach	23
2.14	The schematic representation of safety space	24
2.15	Heterogeneous CA for a mixed cars and PTWs flow	25
2.16	Speed density relation (A) (Fan and Work, 2015) model (B) (Nair, Mahmassani, and Miller-Hooks, 2012) model	27
2.17	The variation of (A) speed-density and (B) flow-density relation with traffic composition in (Nair, Mahmassani, and Miller-Hooks, 2012) model	27
3.1	Example fundamental relation that satisfies the requirements	32
3.2	Example of the road space and vehicles' spatial distribution	33
3.3	The implementation of Delaunay triangulation to define pore size	34
3.4	The obtained probability density function for different traffic compositions.	34
3.5	Delaunay triangle edges length for circles.	34
3.6	Comparison of estimated probability distribution function and fitting theoretical distributions for different vehicles composition	36
3.7	Example mean inter-vehicle spacing ($E(l_c^*)$) and road width relationship, where LTC and HTC represent light traffic condition ($\rho_1 = 0.04veh/m^2$, $\rho_2 = 0.08veh/m^2$) and heavy traffic condition ($\rho_1 = 0.08veh/m^2$, $\rho_2 = 0.12veh/m^2$, respectively)	37
3.8	Spatial distribution of vehicles in 2-lane road (A) disordered flow (B) semi-disorder flow where cars travel within the lane only and PTWs can occupy any position on the road	37
3.9	Probability density function produced from the two setting in 3.8	38

3.10	Speed Vs total occupied area ($\sum \rho_1 A_1 + \sum \rho_2 A_2$), where $\rho_1 A_1$ and $\rho_2 A_2$ are area projected on the road by PTW and car, respectively.	39
3.11	Speed vs total occupied area for constant critical pore size ($r_c^2 = 3m$) and a variable critical pore size (r_c^1) with the following parameters $r_c^{min} = 3m$ and $r = 2m$	40
3.12	A schematic of Lagrangian and Eulerian approaches	41
3.13	Speed-spacing fundamental diagram (a) for Cars (b) for PTWs, $V_{1,max} = V_{2,max} = 20 m/s$	42
3.14	n-t domain discretization, separate coordinate for each vehicle class	46
3.15	The direction of fluxes through the edges of the cluster	46
3.16	Speed-density relation for the case (a) maximum speed of Cars is greater than PTWs (b) maximum speed of PTWs is greater than cars, density of PTWs $\rho_1 = 0.2veh/m$	47
3.17	The Lagrangian representations, when PTWs are the reference class (Lag. 1) and cars are the reference class (Lag. 2), vs. the Eulerian representation	49
3.18	The comparison between the two Lagrangian methods, (Lag. 1, Lag.2) represent the 1-LRF approach and (Lag. 3) represent the n-LRF approach.	50
3.19	The density waves of PTWs (upper subplot) and cars (lower subplot), result produced using the general discretization scheme for 1-LRF approach	51
3.20	The schematic of sub-lane in Lagrangian representation, one-lane road and two sub-lanes for PTWs	51
3.21	Trajectories of vehicles, two sub-lanes for PTWs	52
4.1	Evaluation of the maximum characteristics speed over a point in $S = \{\rho_1, \rho_2\}$, Here $V_1 = 22m/s$ and $V_2 = 27m/s$	56
4.2	Evaluation of minimum characteristics speed over a point in $S = \{\rho_1, \rho_2\}$, Here $V_1 = 22m/s$ and $V_2 = 27m/s$	57
4.3	The four traffic regimes , (A) Speed-density relation (B) Flow-density relation, where $\rho_T = \rho_1 + \rho_2$	57
4.4	The variation of the fundamental relation with road width	58
4.5	Speed versus total occupied area for cars at different traffic composition	58
4.6	The setting used for the extraction of the inter-vehicle spacing distribution	59
4.7	<i>Normal profile</i> , traffic density waves of cars and PTWs at different time steps. (PTW-1, Car-1) and (PTW-2, Car-2) represent result form our model and Nair's model, respectively.	60
4.8	<i>Queue profile</i> , traffic density waves of cars and PTWs at different time steps. (PTW-1, Car-1) and (PTW-2, Car-2) represent result form our model and Nair's model, respectively.	61
4.9	Speed Vs total occupied area ($\sum \rho_1 A_1 + \sum \rho_2 A_2$) Nair's model (Nair, Mahmassani, and Miller-Hooks, 2011), where $\rho_1 A_1$ and $\rho_2 A_2$ are area projected on the road by PTW and car, respectively.	61
4.10	Creeping experiment density-space diagram, upper subplot for PTWs and lower subplot for cars.	62
4.11	Overtaking experiment density-space diagrams, upper subplot for PTWs and lower subplot for cars, free flow speed of $V_1 = 1.8m/s$ greater than $V_2 = 1m/s$. The dashed lines stretching from upper subplot to the lower connect the tail of the density profiles for cars and PTWs' traffic and the spacing between the two lines indicates the distance gap after PTWs overtake.	63
4.12	Overtaking experiment density-space diagrams, upper subplot for PTWs and lower subplot for cars, free flow speed of $V_2 = 1.8m/s$ greater than $V_1 = 1.5m/s$	64
4.13	Speed vs. total number of vehicles plot, when free flow speed of PTWs less than cars and cars account to 80% of the total traffic, upper subplot <i>Porous G</i> , middle subplot <i>Creeping</i> , lower subplot <i>N-pop</i>	65

4.14	Schematic representation of the road network	66
4.15	The Flow-density curve for PTWs and cars, at the traffic composition of [10% PTWs – 90% cars] and [20% PTWs – 80% cars]	67
4.16	Schematic representation of the pore size measurement method	68
4.17	The estimated and measured (A) flow–density relationship (B) speed–density relationship	69
4.18	The estimated and measured speed–density relationship (A) for cars (B) for PTWs, when the fraction of the other vehicle class is zero	70
4.19	Fitting of theoretical distributions with the observed distribution, for different vehicles composition	71
4.20	The observed and estimated average speed over a time	72
4.21	The observed and estimated average speed at higher traffic densities (cars average speed)	73
5.1	Flow-density diagram, for different penetration rates of PTWs.	77
5.2	The change in travel time of cars for different penetration rate of PTWs.	77
5.3	(A) The density profile immediately before traffic light turns red, (B) The evolution of queue length, and (C) The saturation flow rate, traffic proportion [25% PTWs, 75% Cars]	79
5.4	Traffic light with advanced stop line (A) The density profile immediately before the traffic light turns red (B) The evolution of queue length (C) saturation flow rate, traffic proportion [25% PTWs, 75% Cars]	80
5.5	The variation in flow-density and the maximum flow of cars with PTWs density (veh/m^2).	81
5.6	The change in passenger PCU value of PTWs over the green time duration	82
5.7	The saturation flow rate when vehicles discharge from the queue	82
5.8	Simulation experiment scenario	83
5.9	The evolution of the total number of vehicles in the queue over the simulation time, at the 1st intersection approach	83
5.10	The fundamental properties of the traffic flow	85
5.11	An illustrative example of traffic conditions at different PTWs proportion	86
5.12	The representation of the proposed VSL control	86
5.13	Simulation scenario, freeway link	89
5.14	Evolution of the traffic densities and speed for cars under uncontrolled case	90
5.15	Evolution of the traffic densities and speed for cars under 1-VSLs	91
5.16	Time evolution of the speed limit for cars (1-VSL)	91
5.17	Evolution of the traffic densities and speed for cars under 2-VSLs	91
5.18	Speed difference incurred by VSLs for cars and PTWs in (1-VSL) and 2-VSLs controls	92
5.19	Speed limits evolution over the simulation time -2-VSLs	92
B.1	Vehicle distribution in two different settings (A) Disordered flows (B) Semi-ordered flows, $\rho_1 = 0.05veh/m^2$, $\rho_2 = 0.1veh/m^2$	101
B.2	Probability density functions extracted from the settings in FIGURE B.1	101
B.3	Example of the variation in probability density function with road width (number of lanes)(A) Lower traffic densities ($\rho_1 = 0.01veh/m^2$, $\rho_2 = 0.04veh/m^2$) (B) Higher traffic densities ($\rho_1 = 0.05veh/m^2$, $\rho_2 = 0.1veh/m^2$)	102
B.4	Vehicle grouping according vehicle class 2 (cars), for the case $\Delta n = 1$	103

List of Tables

2.1	Summary of the speed-density relation for heterogeneous traffic flow . . .	28
3.1	Goodness of the fit measures obtained from the fitting experiments for different theoretical distributions.	35
3.2	simulation settings	48
4.1	Simulation Parameters	62
4.2	Speed values extracted at time $t = 50sec$ and position $x = 39.15m$	62
4.3	Goodness of the fit measurements for different theoretical distributions.	72
5.1	The change in critical density (<i>veh/km</i> per unit lane width) and the maximum flow rate (<i>veh/hr/lane</i>) at different ratios of PTWs	76
5.2	The change in the clearance time with the ration of PTWs	79
5.3	The change in clearance time with ration of PTW, at traffic light with advanced stop line	80
5.4	The estimated and the actual clearance time, when PTWs are excluded from CT computation	81
5.5	84
5.6	Initial densities (<i>veh/m</i>), ρ_1 for cars and ρ_2 for PTWs	89
A.1	Parameters used to reproduce the fundamental diagrams in Chapter 2	99
C.1	Vehicles parameters	105
C.2	The parameters of the car following model (Wiedemann 99)	105

List of Abbreviations

PTWs	Powered Two Wheelers
ITS	Intelligent Transportation System
C-ITS	Cooperative Intelligent Transport System
CA	Cellular Automata
CCW	Cooperative Collision Warning
ACC	Adaptive Cruise Control
TIS	Traveler Information System
TMS	Traffic Management System
PCU	Passenger Car Unit
FCD	Floating Car Data
RMSE	Root Mean Square Error
SSE	Sum of Squared Error
LRF	Lagrangian Reference Frame
iTT	instantaneous Travel Time
ASC	Adaptive Signal Control
VSL	Variable Speed Limit
MPC	Model PredictiveControl

Chapter 1

Introduction

Facilitating optimal mobility is the core target of several traffic flow related studies. The increase of road traffic coupled with the limited road infrastructures brings about different traffic problems. In the pursuit of understanding and tackling these problems, traffic flow models have played an indispensable role. Traffic flow models represent the traffic dynamics in mathematical equations, Thus giving the capability to analyze different traffic aspects and to forge operation rules. For example, a traffic control plan can be induced based on the current (estimated) and the future (predicted) traffic conditions, wherein traffic flow models are employed to estimate and predict the traffic state. Moreover, having a model that can replicate the real traffic dynamics offers a flexibility to see beyond what is observed in real situations. This opens a door for innovative and intelligent mobility solutions.

This dissertation presents the modeling and the analysis of heterogeneous traffic flow, with a particular focus on mixed traffic flow consisting of cars and Powered Two Wheelers (PTWs). We develop a model that can recreate the traffic features in mixed cars and PTWs flow. The model properties are examined qualitatively and quantitatively. Furthermore, the traffic flow characteristics that are important for intelligent transportation system (ITS) application development are investigated.

The next sections are organized as follows. The first section discusses the problem statement and the motivations (Section 1.1). Section 1.2 and 1.3 present the objectives, and the methodology applied to achieve the objectives, respectively. Section 1.4 summarizes the major contributions of this dissertation. Finally, Section 1.5 outlines the organization of the dissertation.

1.1 Background

While owning a car is considered as a social achievement in most of the eastern countries, drivers in Europe slowly replace them with motorcycles and other types of Powered Two-Wheelers (PTWs) such as scooters and moped. The shift to two-wheelers comes from different reasons, with the primary reason being the maneuverability advantage gained from their compact size. Because of their small size, PTWs can move between lanes of traffic. Thus, PTWs rider can avoid being stuck in congestion by filtering through traffic lanes. This is seen as a potential means to beat congestion by commuters that need to pass through the congested traffic, particularly in big cities.

PTWs represent a growing class of traffic, between the year 2002 and 2011 the fleet of PTWs increased by 17% in Europe (OECD/ITF, 2015). The recent report from European Association of Motorcycle Manufacturers (ACEM) indicates that motorcycle and moped registration in France went up by 4.1 %, in 2017. Although Europe wide it shows a 1.6 % decrease. According to the trend, the number of PTWs on the road is expected to keep growing. However, there are unresolved issues regarding the transport policy toward PTWs. Whether to allow lane splitting or not remains a controversial issue among policy makers. For example, lane splitting is legal only in some regions of France. No matter what the rule says, most of the PTWs riders do lane splitting (Aupetit, Espié, and Bouaziz, 2015). Moreover, despite the advancement in the ITS technologies and

the availability of remarkable amount of ITS solutions to create a safe and efficient traffic flow, PTWs are not integrated into most of the systems. Integration of PTWs into the ITS benefits not only PTWs but also all road users.

To clarify the issues regarding what policy should be applied toward PTWs, a thorough research is required. Moreover, it is also essential to facilitate efficient and safe cohabitation of PTWs with other road users. By this means, the opportunity the shift to PTWs offers in easing congestion can be utilized fully, without compromising their safety and affecting other road users. There are some initiatives looking for the best integration of PTWs to the traffic system. Allowing two-wheelers to use bus lane (York et al., 2010) is one of the measures. Segregation of PTWs from other traffics (Radin Umar, Mackay, and Hills, 1995) is also seen as a solution in countries where there are significantly high number of PTWs. In the European context, where the proportion of PTWs is much less than passenger cars, allocating an exclusive road space for PTWs might be infeasible.

Beside the experimental studies, traffic flow models play a significant role in answering the different questions raised concerning the effective way of integrating PTWs to the traffic system. Answering these questions in turns helps to devise intelligent traffic solutions, e.g, traffic control and management solutions. Traffic flow models also supplement model-based traffic control and management systems with traffic state estimation and prediction functionality.

Since the 1950s traffic flow models have been applied to investigate different traffic phenomena. The dynamics in the real traffic flows is replicated by the models through various representation and approximation methods (S. P. Hoogendoorn and Bovy, 2001). Depending on the level of detail, the mathematical representations attempt to describe the individual driver or the aggregated flow behaviors. The individual driver behaviors are characterized using the 'law of separation' (Louis A Pipes, 1953) also known as follow-the-leader principles and stochastic parameters. For the aggregate level description, the well known Lighthill-Whitham-Richards (LWR) model (Lighthill and Whitham, 1955b; Richards, 1956) approximates the traffic flow with the method of kinematic wave or motion of fluid. This dissertation applies this LWR method.

The original LWR model is developed for a homogeneous traffic, where all the vehicles that make up the traffic stream exhibit identical average behavior. However, in reality traffic streams contain vehicles with different physical (length, size) and operational (speed, acceleration, etc.) characteristics. The heterogeneity of the driver/vehicles characteristics impacts traffic flow properties (Sarvi, 2013; Puppo et al., 2016) at the collective as well as the individual level. Therefore, for accurate representation of traffic flows, it is essential to incorporate the heterogeneity aspect. For this reason, the LWR model is extended by introducing the concept of vehicle classes. The traffic stream is decomposed into homogeneous sub-streams or vehicle classes. Vehicles in the same class are assumed to have identical behavior.

The majority of the heterogeneous, also called multi-class, LWR models is formulated to describe the interaction of cars and trucks or vehicle types which have a resembling characteristic, i.e. the distinguishing factors among the vehicle classes are the maximum speed, the length, the space/time headway, etc. However, the presence of PTWs, which have a unique maneuverability calls for a different approach to describe the interaction between vehicle classes and the fundamental traffic properties. PTWs ride through the space between other vehicles or between vehicles and road borders. This maneuvering capability of PTWs permits them to travel at non-zero speed while other vehicles are stationary. The approximation method used to model traffic flow containing PTWs, therefore, should reflect these behaviors.

Hence, it is necessary to develop models that can accurately reproduce the mobility behavior of PTWs and the resulting interaction. Thereby, the models can be employed for various applications, and also can be utilized as experimentation tool for the evaluation of PTWs related traffic policy and traffic management strategies.

1.2 Research objective

Understanding the mobility characteristics of traffic flows containing PTWs is a major step for the inclusion of PTWs in traffic control and management plans, and for the emergence of other PTW-aware intelligent mobility solutions. Therefore, it is imperative to have analytical models and simulation tools that can replicate the characteristic of such flows. The objectives of the dissertation are the following:

- Develop an analytical model that can accurately replicate the dynamics of mixed cars and two-wheeler flows. The model bases on multi-class LWR model. In order to explore broader aspects of the traffic flow characteristics, we apply the two different LWR representations, namely the Lagrangian and the Eulerian method.
- Develop efficient and accurate discretization schemes that can approximate the solution of the model equations.
- Analyze the traffic flow characteristics and identify important properties, which provide an insight for future mobility solutions and traffic policy maker.
- Study the integration of two-wheelers into traffic management and control systems.

1.3 Methodology

Traffic flow models are usually developed by introducing different assumptions and approximation methods, which base on theoretical and empirical foundation. Therefore, the first step in developing traffic flow model for traffic streams containing PTWs is to establish the required traffic properties. To that end, the maneuvering features of PTWs and the collective mobility characteristics of traffic flows consisting of PTWs and other vehicle types reported in the literature are reviewed, mainly the empirical observation. From this analysis, we identify the required mobility features. Then, the identified properties are used to decide the modeling approach.

Traffic flow models can be formulated at different granularity levels, namely microscopic, macroscopic and mesoscopic. The choice of the level of detail depends on the required application, accuracy level and computational efficiency. In this dissertations, we aim to develop a model that can describe traffic heterogeneity, computationally efficient for a large scale analysis of traffic flow properties, and for real-time ITS applications, and also can allow the tracking of vehicles. For these reasons, the macroscopic approach, particularly the LWR approach, is selected. In the LWR approach, traffic heterogeneity can be modeled by decomposing the heterogeneous flow into homogeneous sub-flows. Further, the flow equations can be described and solved in Eulerian or Lagrangian coordinate systems. The Lagrangian description allows the tracking of vehicles, which makes it useful for cooperative ITS (C-ITS) applications. The Eulerian description also has advantage in terms of simplicity. Therefore, for traffic efficiency applications that do not necessitate the tracking of vehicles, the Eulerian method is preferable. Since each representation has an apparent advantage, we formulate the model equation in the Eulerian as well as the Lagrangian frameworks.

Besides the flow equation, the fundamental relationship, i.e., speed-density or flow-density relationship, is the important component of the LWR models. To derive a law that defines the fundamental relationship, different analogies and approximation methods are used. According to the identified traffic features in traffic flow containing PTWs, we evaluate the fundamental relations applied in the existing heterogeneous LWR models. It is found out that the porous flow analogy is a suitable approach for our interest. However, the porous flow approach is not well explored. In porous flow approach the road space is treated as a porous medium, where the pores are the free space between vehicles, and the vehicles are the solid objects that form the pores. A proper description of pore size (or inter-vehicle spacing) distribution is necessary to formulate the

fundamental relations. We therefore devise an approximation method to characterize the porous medium, and determine the inter-vehicle spacing distribution and its parameters. The distribution parameters are defined based upon a Poisson point process assumption for geometrical distribution of vehicles. Moreover, the correlation of pore size distribution with the size of vehicles and the road geometry is integrated. Afterward, we define the fundamental relationships and analyze the model properties.

Furthermore, the solution of LWR models is approximated by applying a discretization scheme. Thus, we develop a discretization scheme for solving the equation of the model.

The next step is analyzing the model qualitative properties. We check whether the model is able to capture the required traffic characteristics or not. The model is assessed with respect to the requirements which are set out based on the traffic features observed in real-world scenarios. The model is also compared with a model that applies the porous flow approach.

Moreover, to improve the performance of the model, we conduct a model calibration and validation process. Due to the lack of real traffic data, synthetic data obtained from micro-simulation tool Vissim is employed for the model calibration and validation. In the calibration procedures, first the fundamental curves are derived from the traffic data. Then, the model parameters are adjusted to fit the curves. Accordingly, we establish a relation between the traffic composition and the jam densities of the vehicle class. Further, the critical gap is described as a function of the traffic state. In the validation phase, we evaluate the validity of the proposed pore-size (or inter-vehicle spacing) distribution. The applicability of the model is also validated by comparing the prediction and the experimental data.

Afterward, the model is applied to analyze the traffic characteristics that are important for ITS application development. In order to develop PTWs-aware ITS application, it is crucial to understand the underlying traffic features. We study the impact of PTWs on road capacity and travel time. Finally, we study the existing traffic control approaches in the context of adaptive traffic light control and variable speed limit control. The method to integrate PTWs in such systems is introduced.

The developed model is intended to contribute as an enabler for 'PTW aware' ITS solutions and traffic regulations. For example, a variety of traffic control strategies require traffic flow models to predict the traffic state and make an appropriate control decision. Employing our model in such system opens a door to the inclusion of PTWs in traffic control. On the other hand, the model can be used as a framework to assess the optimality of the existing control schemes, including information collection and computation methods. Moreover, the model can help traffic regulator to determine collective and class-specific optima and to induce a vehicle class specific flow adjustment. In this way, new traffic regulations adapted to PTWs can be introduced, which in turn promotes the use of PTWs. Additionally, our model could be applied to design a smart two-wheeler navigation system which is well aware of PTWs' capability to move through congested car traffic and provides a route plan accordingly. The model could also contribute in the proper integration of PTWs into multi-modal transport planning. In general, the model plays a role in enabling 'PTW aware' traffic efficiency related applications/technologies.

1.4 Contribution

The dissertation contributes to the state-of-the-art in many ways, with the main contributions being:

- A methodology to approximate the fundamental relations. The fundamental relation is derived based on the porous flow approach, which requires the distribution of the inter-vehicle spacing and the statistical parameters. A framework to approximate the inter-vehicle spacing distribution and its parameters is provided.

- An analytical model for a mixed cars and two-wheelers traffic flow. The model is formulated in Lagrangian (mesoscopic) as well as in Eulerian (macroscopic) frameworks. The Eulerian description observes the the traffic phenomena at a fixed point, whereas the Lagrangian description observes the traffic phenomena along the trajectory of vehicles. Each representation, therefore, gives different view of the traffic flow.
- Discretization scheme to approximate the model equations. We develop an appropriate discretization method to solve the solution of the model equation.
- Analysis of different traffic characteristics that are important for the development of PTWs-aware ITS application. We investigate the characteristics of the mixed flow of car and PTWs and identify the features that should be considered in the development of ITS applications.
- Model validation and calibration. The validity of the assumptions used to construct the model, and the capability of the model to reflect the observed behaviors in mixed flow of car and PTWs are demonstrated using synthetic data from a micro-simulation tool. Moreover, the model parameters are calibrated.

1.5 Thesis Organization

The remainder of the dissertation is organized in the following manner.

Chapter 2 presents the-state-of-the-art of heterogeneous vehicular traffic flow modeling. This includes the applicability of traffic flow models in intelligent transportation systems (ITS); the need to shift from homogeneous modeling approach to heterogeneous flow modeling; the frameworks of heterogeneous traffic flow modeling at different granularity. This dissertation focuses on a particular case of heterogeneous traffic flow modeling, namely traffic flow containing PTWs. Thus, the specific maneuvering characteristics of PTWs and the modeling approaches are also presented.

Chapter 3 describes the model development. The requirements of the model are set out and the interpretation of the requirements in the model development is explained. The principles employed for the derivation of the fundamental relation, i.e., the interaction between vehicle classes is explained. Furthermore, the formulation of the flow equations in the Lagrangian and the Eulerian coordinate systems as well as the discretization methods used to solve the solution of the flow equations are described. Finally, we present numerical examples to illustrate the validity of the proposed discretization schemes.

Chapter 4 focuses on the analysis, comparison, calibration and validation of the model developed in Chapter 3. The mathematical properties of the model is analyzed. The fundamental relation are examined with respect to the requirements. Moreover, the model properties are tested and compared against the known realistic traffic characteristics and other models. Using synthetic traffic data, the model parameter are calibrated, and the mode is validated.

In Chapter 5, we analyze the important traffic characteristics for ITS application development. Traffic impacts of PTWs are discussed. Furthermore, the existing ITS traffic management and control methods are evaluated by considering particular cases, namely adaptive traffic light and variable speed limit controls. Then, we present a method to improve the control strategies, and the proposed methods are examined.

Chapter 6 concludes this dissertation by outlining the key findings and recommending future research directions.

Chapter 2

Heterogeneous Traffic Flow Modeling

2.1 Introduction

The increase in vehicular traffic becomes the source of traffic congestion. Several researchers have been seeking for congestion relieving solutions. Congestion mitigation strategies ranging from road infrastructure and public transport improvement to influencing and managing traffic behavior have been implemented. To keep pace with new challenges and opportunities (e.g., emergence of new technologies), congestion alleviation is still an ongoing issue. Due to the complexity of the problem and the factors causing it, a comprehensive study is required to understand the causes of different phenomena and how to create a better situation.

Traffic flow models play an indispensable role for understanding the fundamental traffic properties and other wide ranges of characteristics, such as the causes and the dynamics of congestion, and capacity drops. Furthermore, the existence of models that can reproduce the real traffic behaviors in a reasonable accuracy becomes an enabler for various types of traffic monitoring, control and management solutions. Beyond reproducing the observed traffic characteristics, with traffic flow models it is also possible to envision 'what-if' scenarios and think beyond the existing situations. Traffic models also serve as a tool for evaluation of traffic planning, infrastructure design, control measures and traffic policies.

For these reasons, a number of mathematical theories have been developed to describe the complex characteristics of vehicular traffic flow. The theories are usually established based on empirical observations and different analogies or assumptions. The models differ in the scope of their application, the way the flow properties are interpreted and the level of detail in which the traffic dynamics is represented. According to the level of detail at which the traffic dynamics is described, the models can be categorized as microscopic, macroscopic and mesoscopic (S. P. Hoogendoorn and Bovy, 2001; Klar, Kühne, and Wegener, 1995).

Microscopic models describe the manner in which drivers follow each other. The general principle used to represent drivers' behavior is termed follow-the-leader, which characterizes how drivers regulate their motion with respect to the leading vehicle. Broadly speaking, the governing rule for the car-following behaviors can be expressed either in the form of 'safe distance' (Louis A Pipes, 1953; Gipps, 1981) or 'stimulus-response' (Gazis, Herman, and Rothery, 1961) theories. In the former principle, the drivers' motion properties (speed, acceleration) are constrained by the required safe distance with respect to the preceding vehicle. Whereas, in the latter the response (e.g., acceleration/deceleration) of the drivers is triggered by the action of the leading vehicle (e.g., relative speed, relative spacing). The car-following behavior represents the longitudinal movement of vehicles. There are also lane changing models that describe the lateral movement of vehicles (Kesting, Treiber, and Helbing, 2007; Gipps, 1986).

The macroscopic representation attempts to characterize the aggregated flow properties. The traffic flow properties are quantified with macroscopic variables, such as flow, speed and density. The theory developed by Lighthill and Whitham, and Richards

(Lighthill and Whitham, 1955a; Lighthill and Whitham, 1955b; Richards, 1956), usually referred as LWR model, is the foundation for the majority of macroscopic models. In the theory, the dynamics of traffic flow is described in analogy with one dimensional fluid motion. The relationship between the macroscopic quantities speed, flow and density is the other important hypothesis of the LWR model. A lot of other researchers have also established a functional form for the equilibrium speed-density or flow-density relationship, which is called fundamental diagram/relation (Greenshields, Channing, H. Miller, et al., 1935; Greenberg, 1959; Louis Albert Pipes, 1966; Underwood, 1961; Del Castillo and Benitez, 1995; Edie, 1961). Another variant of the macroscopic traffic flow model is the second order model (two equations model) (Aw and Rascole, 2000; Payne, 1971; M. Papageorgiou, 1983). Instead of the equilibrium speed definitions in the LWR model, the two-equations model defines a dynamic speed equation. Macroscopic models are suitable for the dynamic control and traffic condition assessment, e.g., real-time traffic monitoring, prediction and control.

The other level of traffic flow modeling is the mesoscopic approach. Like the macroscopic modeling, vehicles are aggregated according to certain properties, however, the driving behavior of individual drivers and the interaction between vehicles are explicitly expressed with a probability distribution. The models that follow the gas-kinetic approach fall under this category. The kinetic models express the dynamics of distribution functions (Paveri-Fontana, 1975; Wegener and Klar, 1996; Chowdhury, Santen, and Schadschneider, 2000).

Most of the existing models are well fit to describe homogeneous traffic situations. Nevertheless, there is a dissimilarity between vehicles in the traffic flows, and the individual vehicle's behavior is influenced by other interacting vehicles. Apparently, the characteristics in heterogeneous flows diverges from what is observed in homogeneous cases. With the homogeneous assumption, therefore, it is difficult to observe the important traffic phenomena existing in heterogeneous flows. This inability of homogeneous models to correctly reflect the characteristics in non-homogeneous traffics drives the emergence of heterogeneous traffic flow models.

This chapter reviews the relevant work on heterogeneous traffic flow modeling. In Section 2.2, the general overview of intelligent transportation system (ITS), and the roles of traffic flow model is covered. The next section (Section 2.3) presents the traffic flow modeling approaches at different level of details, namely microscopic, macroscopic, and mesoscopic, with more emphasis on macroscopic models. Further, the extension of the modeling approaches to represent heterogeneous traffic flow is also presented. The next section focuses on two-wheelers (Section 2.4). We review the observed traffic characteristics of two-wheelers reported in literature, and based on that we outline the important maneuvering features of PTWs that should be included to model traffic flow containing PTWs. The assumptions and approaches used to translate these features in microscopic and macroscopic models are discussed. Thereafter, we discuss the validation and calibration of traffic flow models (Section 2.5). Finally, we end the chapter with conclusion (Section 2.6).

2.2 ITS applications

ITS aims at realizing a safe, efficient and environment friendly transportation systems, with the help of advanced technologies. The main players in ITS are users, vehicles and road infrastructures. By creating a cooperation between these entities, numerous traffic challenges have been resolved and the operation performance of the transportation systems has been improved.

To address the multifaceted road safety issues, a range of ITS solutions are available. Cooperative collision warning (CCW) systems (Misener, Sengupta, and Krishnan, 2005) alert drivers about the potential collision risks, based on the information collected from surrounding vehicles, road users or road infrastructure. There are various types

of CCW systems, such as forward (rear end) collision warning (Dagan et al., 2004; Jamson, Lai, and Carsten, 2008), intersection collision warning (R. Miller and Huang, 2002; Dogan et al., 2004), lane change assistance (Habenicht et al., 2011; Dang et al., 2014). The forward collision warning systems target to prevent vehicles from colliding with the vehicle in front. This is achieved by monitoring the relative distance and activating a warning message if the threshold is passed. Likewise, the intersection collision warning systems trigger infrastructure or vehicle based warning message when a possible conflict is detected between vehicles crossing intersections from different directions. The lane change warning systems, on the other hand, assist drivers to perform a safe lane change. Since drivers may fail to react to the warning messages, collision avoidance systems which combine the CCW systems functionality with intervening system have been also developed (Doi et al., 1994; Seiler, Song, and Hedrick, 1998). Another important automated driver assistance system, which provides an automatic longitudinal distance control, is adaptive cruise control (ACC) (Marsden, McDonald, and Brackstone, 2001; Ploeg et al., 2011). ACC contributes also to improving traffic efficiency (Van Arem, Van Driel, and Visser, 2006; Schakel, Van Arem, and Netten, 2010).

Furthermore, ITS applications have played remarkable roles in promoting efficient use of transport networks. The main objectives of traffic efficiency ITS applications are: alleviating congestion, minimizing travel time, creating smooth traffic flow, etc. One way of promoting traffic efficiency is to influence drivers' behavior by giving real time traffic information. For this reason, traveler information systems (TIS), which disseminate information about real time traffic and road conditions, are developed (Adler and Blue, 1998; Levinson, 2003). Thus, drivers make a pre-route (e.g., departure time and transport mode) or en-route decisions (e.g., route choice) according to the traffic state update received from TIS. Moreover, ITS also has introduced smart traffic management systems (TMS) that control traffic demands. Nowadays, there are numerous advanced TMS, for example traffic responsive and coordinated traffic signal control for urban traffic control (Priemer and Friedrich, 2009; Lämmer and Helbing, 2008), ramp metering (M. Papageorgiou and Kotsialos, 2002) and variable speed limit control (Ghods, Kian, and Tabibi, 2009) for freeway traffic can be mentioned.

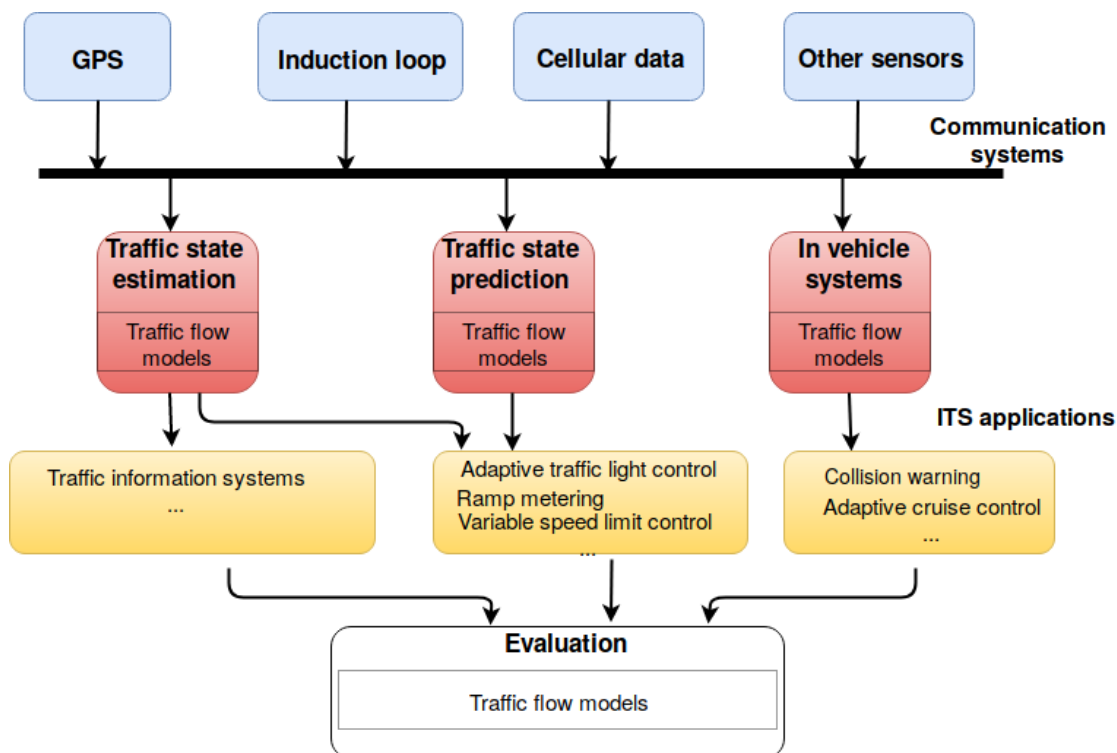


FIGURE 2.1: The roles of traffic flow models in ITS applications

ITS applies a wide range of information and communication technologies in order to solve the transportation problems (Papadimitratos et al., 2009). The emergence of these

technologies is therefore a key enabler for the advancement ITS applications. In different ITS applications, the information exchange between vehicles (V2V) or vehicles and infrastructures (V2I) relies on communication technologies (Dar et al., 2010; Maimaris and G. Papageorgiou, 2016). Sensing and data acquisition technologies (Guerrero-Ibáñez, Zeadally, and Contreras-Castillo, 2018), like sensors, GPS, and loop detectors, used to collect information about traffic and road conditions are also the core parts of ITS. Further, the consolidation and aggregation of traffic information collected from multiple sources require data processing technologies (El Faouzi, Leung, and Kurian, 2011).

Traffic simulation models are also equally important as the aforementioned technologies for ITS (Clark and Daigle, 1997). A thorough understanding of the traffic flow characteristics is essential for devising new ITS applications. Due to the issues related to cost, safety and security, sometimes it is difficult to evaluate ITS applications in real scenarios. In such cases, simulation based study is a more convenient and efficient alternative than field experiment. Moreover, traffic flow models are used for traffic state prediction and estimation in real-time traffic management systems.

2.3 Heterogeneous traffic flow models

In reality, traffic streams are composed of various types of vehicles and drivers. The term heterogeneous (also called mixed and multi-class) traffic flow is used to indicate this difference in the operating characteristics of vehicles (e.g., physical dimension, maximum speed, acceleration and deceleration capability) as well as drivers' behavior. In heterogeneous traffic flows, because of the difference among vehicles/drivers, under identical traffic conditions vehicles/drivers behave differently.

Earlier traffic flow models were designed for homogeneous traffic flows, implying a given characteristic is exhibited by all of the vehicles. However, the homogeneous assumption neglects the very in-homogeneity of traffic flows, and therefore fails to correctly describe the real characteristics. It is hardly possible to find a single characteristic that can represent the diverse behavior of vehicles/drivers in heterogeneous traffic flows. When vehicles with different moving features share a road, vehicles/drives show a different behavior than in homogeneous flows due to the interaction between vehicles. Accordingly, there is a disparity in the individual vehicle (microscopic) as well as the collective (macroscopic) behaviors between homogeneous and heterogeneous flows. For example, the study in (Ossen and S. P. Hoogendoorn, 2011) shows that the car following behaviors of trucks and cars are different. Further, the behavior of the vehicles appears to be influenced by the lead vehicle type. Similarly, the effect of the presence of different vehicle types is also revealed in the macroscopic traffic characteristics. The fundamental relation in heterogeneous traffic flow depends on traffic composition (type and ratio of vehicles) (Wang et al., 2007; Kockelman, 1998). The presence of heavy vehicles like trucks also causes a reduction in road capacity.

To correctly describe the traffic flow characteristics, it is therefore important to distinguish between vehicle types and drivers' behaviors. Treiber and Helbing (Treiber and Helbing, 1999) show that the scattering phenomenon in fundamental relationship can be reproduced by integrating traffic heterogeneity in the model. Moreover, including the behavior of each vehicle type and the resulting collective traffic characteristics in traffic models improves the effectiveness of traffic efficiency and safety ITS solutions.

2.3.1 Heterogeneous microscopic traffic models

Microscopic traffic flow models deal with a detailed description of individual vehicle behavior and the interaction between vehicles. The existing microscopic models try to develop a governing rule of leader-to-follower interaction (car-following models) and lane changing rule for multi-lane scenarios (lane changing models). The rules can be

formulated as a continuous mathematical equation (car-following models) or in discrete time-space format (cellular automata).

2.3.1.1 Car-following models

Driver to driver interaction in a longitudinal movement is often modeled based on car-following theory, which demonstrates how the follower and the leader vehicles interact with each other (Brackstone and McDonald, 1999). The car-following behaviors are characterized by microscopic parameters such as distance and time headway, speed, acceleration, reaction time and location. Based on the hypothesis used for constructing car-following principles, in broader terms, the existing models can be categorized into two generic groups, 'safe distance' and 'stimulus-response' models.

Safe distance model

The car-following behavior of vehicles in a safe-distance based model is adapted according to a safe distance vehicles should keep with respect to the vehicle in front (Louis A Pipes, 1953; Gipps, 1981). For example, the well known Gipp's (Gipps, 1981) model constructs a car following rule on the assumption that drivers set their speed so that they can stop without colliding when the leader vehicle brakes suddenly. Thus, the speed choice is constrained by the desired speed of drivers (f_1) and the safe-stop condition (f_2).

$$v_n(t + \tau) = \min\{f_1, f_2\} \quad (2.1)$$

where

$$f_1 = v_n(t) + 2.5a_n\tau \left(1 - \frac{v_n(t)}{V_n}\right) \left(0.025 - \frac{v_n(t)}{V_n}\right)^{1/2}$$

$$f_2 = b_n\tau + \sqrt{(b_n^2\tau^2 - b_n[2[x_{n-1}(t) - s_{n-1} - x_n(t)] - v_n(t)\tau - v_{n-1}(t)^2/b^2])}$$

The parameters a_n/b_n , τ , v , V_n and s represent, respectively, the maximum acceleration/deceleration, the reaction time, the speed, the desired speed and the effective length of vehicle. The subscripts $n - 1/n$ denote the leader/follower vehicle.

Stimulus-response model

In stimulus-response based models, the car following behavior of vehicles is governed by a stimulus-response type relationship. In other words, the reaction of a vehicle is a function of the stimulus and its sensitivity. The stimulus is often quantified in terms of relative spacing and/or relative speed, and the decision to accelerate or decelerated is taken as a response. For example, the model developed by the general motors group (referred as GM model) (Gazis, Herman, and Rothery, 1961) formulates the car-following rule as

$$a_n(t + \tau) = \frac{cv_n(t + \tau)[v_{n-1}(t) - v_n(t)]}{[x_{n-1}(t) - x_n(t)]^l} \quad (2.2)$$

where τ , x , v , a and c stand for reaction delay, position, speed, acceleration and a constant coefficient, respectively. $\frac{cv_n(t + \tau)}{[x_{n-1}(t) - x_n(t)]^l}$ represents the sensitivity to the stimulus, which is the relative speed. In general form, it can be rewritten:

$$a_n(t + \tau) = \lambda\Delta v(t) \quad (2.3)$$

Multi-class extension

The car-following models have contributed greatly to a better understanding of traffic flow dynamics. Nevertheless, the models are mainly designed to represent homogeneous traffic flows. For accurate description of traffic flow dynamics, it is imperative to include in the models the heterogeneity observed in real traffic flows. Several empirical studies have reported the variation in the car-following interaction between different vehicle types (Aghabayk et al., 2011; L. Liu, Zhu, and Yang, 2016; Ossen and

S. P. Hoogendoorn, 2011; Tordeux, Lassarre, and Roussignol, 2010). The car-following behaviors such as space headway, time headway and reaction time are observed to be dependent on the vehicle type and the follower-leader combinations. Furthermore, the comparison between different car-following models show that the best performing model differs between vehicle classes (Ossen and S. P. Hoogendoorn, 2011).

However, since the microscopic description represents the individual vehicle behavior, the incorporation of heterogeneity is relatively straightforward, which can be done either by varying the parameters between vehicle classes (Helbing and Tilch, 1998) or using different models for each vehicle class (Kesting and Treiber, 2013).

In addition, in multi-lane traffic flow the difference between drivers or vehicle type causes overtaking, i.e. a faster moving vehicle passes a slower one. For this purpose, lane-changing models, which are used in conjunction with car-following models, are introduced (Gipps, 1986; Kesting, Treiber, and Helbing, 2007).

2.3.1.2 Cellular automata model

A cellular automata (CA) approach for modeling traffic flow is first introduced in (Nagel and Schreckenberg, 1992). In CA models, unlike car-following models, the movement of vehicles is represented in a discrete way. The space is divided into fixed and identical sized cells (2.2(a)). The speed is also discrete and is expressed as the number of cells a vehicle advances per unit time step. The update rule defines the movement of vehicles. A follower vehicle increases its speed from v to $v + 1$ if $v < v_{max}$ and the distance to the leading vehicle is greater than $v + 1$. Otherwise, if the leader vehicle is located j cells away and $v \geq j$, the follower vehicle reduces its speed to $v = j - 1$. Further, with a random probability p each vehicle decreases its speed by one. Subsequently, the vehicle advances v cells.

Besides its computational efficiency, the CA model proposed by Nagel and Schreckenberg (NASC) reproduces important traffic flow behaviors (Nagel and Schreckenberg, 1992). Several other CA models have been also developed to incorporate different traffic characteristics such as slow-to-start behaviors (Maerivoet and De Moor, 2005; Barlovic et al., 1998), lane changing behaviors in multi-lane traffic flows (Wagner, Nagel, and Wolf, 1997; Li et al., 2006). Moreover, the homogeneous CA model is extended to incorporate different vehicles' characteristics. In homogeneous CA, vehicles are assumed to occupy a single cell, and hence the variation in vehicle length is not considered. The heterogeneous CA applies a finer space discretization (see FIGURE 2.2(b)) and a vehicle can occupy multiple cells (multi-cell). The CA model for heterogeneous traffic flow containing cars and trucks is presented in (Yang et al., 2015). The number of cells a vehicle spans depend on its length. Moreover, the maximum speed and acceleration are vehicle type dependent.

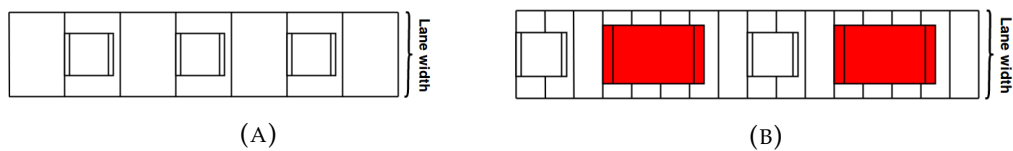


FIGURE 2.2: Schematic diagram of CA space discretization (A) homogeneous traffic (single cell) (B) heterogeneous traffic (multi-cell)

2.3.2 Heterogeneous macroscopic models

Macroscopic models describe traffic flow behaviors at a collective level. The aggregate behavior which emerges from the interaction between vehicles is formulated, rather than the individual vehicle motion. For this purpose, traffic flow is treated in analogy with one-dimensional fluid motion. Hence, the dynamics of the flow is described by continuity equations. Average speed, density and flow are the variables that are often used to represent the traffic flow behavior.

The fluid approximation of traffic flow reproduces a wide range of interesting traffic phenomena. However, to further improve the description capability and accuracy, different modifications are applied. Including the various types of traffic flow heterogeneity is one of the aspects that attracts major attention.

We discuss the extension of the two broadly known macroscopic modeling approaches, namely LWR and two-equation models, to accommodate traffic heterogeneity.

2.3.2.1 Multi-class LWR model

The kinematic wave model developed by (Lighthill and Whitham, 1955a; Lighthill and Whitham, 1955b; Richards, 1956) is a pioneer macroscopic model. This model is known as LWR model. The conservation law and the function relation between the traffic flow variables are the basic elements of the LWR model. The continuity equation which describes the conservation law is formulated as:

$$\frac{\partial \rho(x, t)}{\partial t} + \frac{\partial q(x, t)}{\partial x} = 0, \quad (2.4)$$

where ρ is the density (vehicle per unit length), q is the flow (vehicle per unit time). The flow and the density are hypothesized to have a functional relationship

$$q = Q(\rho) \quad (2.5)$$

Similar relation can also be drawn for speed-density since $v = q/\rho$. The curve that represents the speed-density or the flow-density relationship is referred to as a fundamental diagram.

LWR model is able to reproduce a significant amount of real traffic phenomena. Nevertheless, the model has some limitations. The steady state flow-density assumption leads to infinite acceleration/deceleration when vehicles pass through shocks. The other drawbacks are the inability to describe the desired speed difference in light traffic states and the capacity drop in stop-go traffic (Daganzo, 1995).

The recently introduced multi-class version of LWR model extends the original model to include the heterogeneity among drivers/vehicles. Multi-class LWR model can describe the desired speed variation and other traffic phenomena that appear due to the interaction between heterogeneous vehicles, which counteracts the flaws of the original LWR model.

In multi-class LWR model, road users are distinguished based on drivers' or vehicle characteristics. Accordingly, the traffic stream is decomposed into sub-streams or classes, in which vehicles in a class have identical properties. A multiclass LWR model that takes into account the variation in the desired speed is proposed by (G. Wong and S. Wong, 2002). They demonstrate that the model can explain traffic phenomena which the homogeneous LWR is unable to describe correctly, such as the two capacity, hysteresis and platoon dispersion. Likewise, a theoretical analysis of a multi-lane and a flow of two-type of drivers presented in (Daganzo, 2002) illustrates these phenomena. Another two-class LWR model derived based on the interaction of trucks and cars is presented in (H. Zhang and Jin, 2002). There are also other similar multiclass models proposed by different authors (Benzoni-Gavage and Colombo, 2003; S. Logghe and L. Immers, 2003; Chanut and Buisson, 2003; Ngoduy and R. Liu, 2007; S. Logghe and L. H. Immers, 2008; J. Van Lint, Serge Hoogendoorn, and Schreuder, 2008). These models attempt to characterize various features in heterogeneous traffic flows. The difference among the models mainly lies in vehicle class classification method and the fundamental diagram used to explain the individual vehicle class or the collective flow properties.

Fundamental relation

Multi-class LWR models consist of two or more vehicle classes. All the existing vehicle classes have an impact on the mobility behavior of a particular class. The speed-density

relation is used to express this interaction between the vehicle classes, which can be written in a general form as:

$$v_i = V_i(\rho_1, \rho_2, \dots) \quad (2.6)$$

There are a number of approaches adopted to drive the fundamental relation for multi-class flows. We categorize them based on the principle the vehicle classes are identified and the interaction between them is represented.

Heterogeneous drivers

Daganzo (Daganzo, 1997) presents a representation of the traffic dynamics in multi-lane two-class flow, where drivers in one class are restricted to particular lanes and drivers in the other class can travel freely in any of the lanes. Two regimes are identified, namely 1-regime and 2-regime. In 2-pipe regime there is no interaction between the two classes, thus the speed is a function of the class's density. On the other hand, in 1-regime drivers in both classes travel with the same speed, which is a function of the total density.

$$v_i = \begin{cases} v(\rho_i/\gamma_i) & \text{2-pipe regime} \\ v(\sum_i \rho_i) & \text{1-pipe regime} \end{cases} \quad (2.7)$$

where γ denotes the fraction of accessible lanes.

A multi-class flow model in (G. Wong and S. Wong, 2002) attempts to reproduce the variation in the desired speed of drivers. The vehicle classes are grouped based on their maximum speed. The speed-density relation is formulated in such a way that vehicle classes have different speed for a given traffic condition, and the speed difference diminishes with the increase in the total density (ρ).

$$v_i = v_i^{max} \exp(-(\rho/\rho_0)^2/2) \quad (2.8)$$

The fundamental diagram properties are shown in FIGURE 2.3(a) and 2.4.

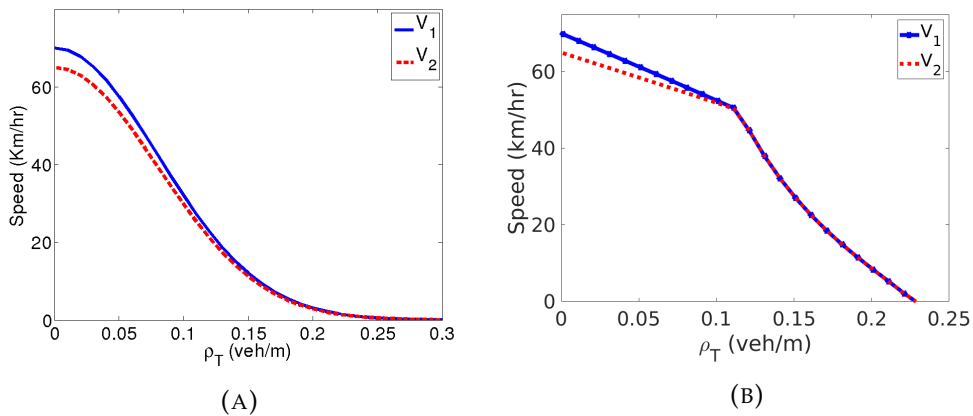


FIGURE 2.3: Speed-density relation (A) (G. Wong and S. Wong, 2002) model (B) (J Van Lint, Serge Hoogendoorn, and Schreuder, 2008) model

Passenger car unit

Passenger car unit (PCU) is defined as the number of passenger cars that would produce a similar effect on the traffic operation to a particular vehicle type. It has been widely applied for capacity analysis of roads under heterogeneous traffic conditions. The PCU value reflects the length and the operation capability of non-passenger car vehicles (Krammes and Crowley, 1986).

For the capacity analysis, the PCU value is used to convert heterogeneous traffic volumes into equivalent passenger-car-only volume (Krammes and Crowley, 1986). In

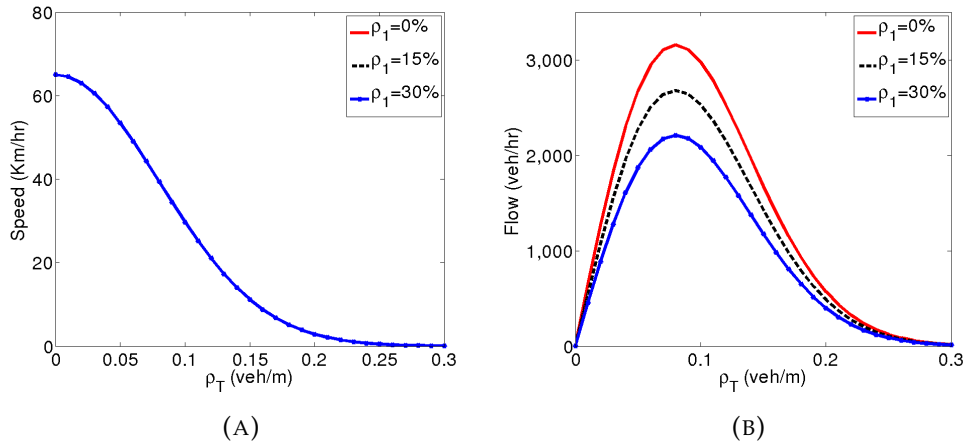


FIGURE 2.4: The variation of (A) speed-density and (B) flow-density relation with traffic composition in (G. Wong and S. Wong, 2002) model

the same fashion, the concept of PCU has been implemented in multi-class LWR models developed for mixed flow of cars and trucks. The models use a constant or a traffic state dependent PCU value.

Constant PCU

Chanut and Buisson (Chanut and Buisson, 2003) propose a multi-class fundamental relation that satisfies the following properties. In free flow condition, vehicles drive at their desired speed, and all vehicles have identical speed in the congested state. Vehicle classes are differentiated by their maximum speed and length. The PCU value for vehicle classes is defined as $\alpha_i = \frac{L_i}{L_r}$, wherein L_i is the length of vehicle class i and L_r is the length of the reference class (i.e. passenger car). The fundamental relation is given by:

$$v_i = \begin{cases} \frac{\rho}{\rho_{cr}} v_{cr} + (1 - \frac{\rho}{\rho_{cr}}) v_i^{max} & \rho \leq \rho_{cr} \\ \frac{\rho_{jam} - \rho}{(\rho_{jam} - \rho_{cr}) \rho^*} q_{cap} & \rho > \rho_{cr} \end{cases} \quad (2.9)$$

$$\rho = \sum_i \rho_i, \quad \rho^* = \sum_i \rho_i \alpha_i$$

where ρ_{cr} , ρ_{jam} and α_i are, respectively, the critical density, the jam density and the PCU value. q_{cap} denotes the road capacity in PCU. The jam and the critical densities are optimized with the traffic condition.

$$\rho_{jam} = \rho_{jam}^r \frac{\rho}{\sum_i \rho_i \alpha_i}, \quad \rho_{cr} = \zeta \rho_{jam}, \quad \text{where } \zeta \in [0.2, 0.5], \quad q_{cap} = \rho_{cr}^r v_{cr} \quad (2.10)$$

The PCU value is used to incorporate the variation of the jam density and the critical density (road capacity) with the ratio of trucks. Thus, the fundamental diagram parameters are adapted to the traffic composition.

A similar approach is used in (Ngoduy and R. Liu, 2007). The speed-density relation takes the the form as in equation (2.9), except that $\rho = \rho^* = \sum_i \rho_i$.

$$\rho_{jam} = \rho_{jam}^r \frac{\sum_i \rho_i \beta_i}{\rho}, \quad \rho_{cr} = \rho_{cr}^r \frac{\sum_i \rho_i \beta_i}{\rho}, \quad q_{cap} = \rho_{cr} v_{cr} \quad (2.11)$$

where $\beta_i = \frac{1}{\alpha_i}$.

The fundamental diagrams are shown in figures 2.5(a), 2.5(a) and 2.6.

Traffic state dependent PCU

PCU value for vehicles with the traffic conditions (Praveen and Venkatachalam

Thamizh Arasan, 2013) and the value should be selected depending on the vehicles' speed, vehicles' size, headway and other traffic variables (Adnan, 2014). The PCU value of truck is also reported to increase with traffic volume (Huber, 1982). To integrate this dependence of the PCU value on traffic state, different from (Ngoduy and R. Liu, 2007; Chanut and Buisson, 2003), (J Van Lint, Serge Hoogendoorn, and Schreuder, 2008) defines traffic state dependent PCU value.

$$\alpha_i = \frac{L_i + T_i v_i}{L_r + T_r v_r} \quad (2.12)$$

L and T stand for the minimum space gap (i.e. bumper to bumper distance) and time headway. The speed-density relation has the same formulation as in equation (2.9) except that ρ in this case equals $\rho = \rho^* = \sum_i \alpha_i \rho_i$.

The fundamental diagram for the model in Chanut and Buisson; Ngoduy and R. Liu; J Van Lint, Serge Hoogendoorn, and Schreuder is depicted in FIGURE 2.5(a) and the variation of the fundamental relation with the traffic composition is shown in FIGURE 2.6 and 2.7.

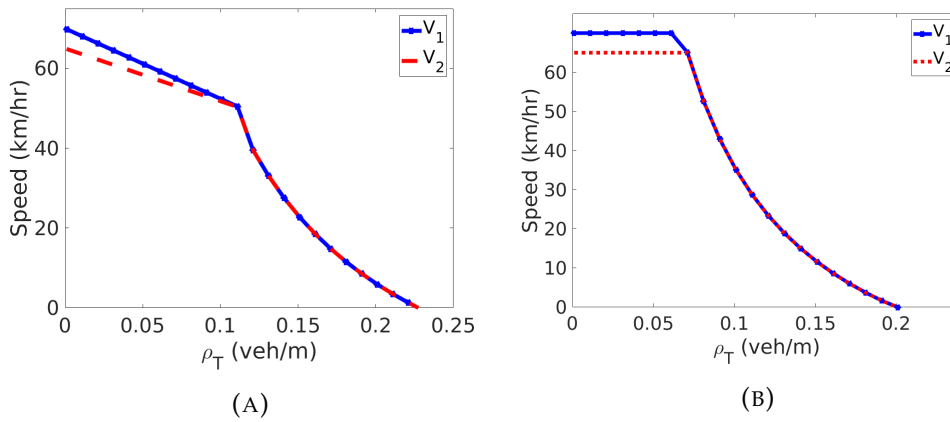


FIGURE 2.5: Speed density relation (A) (Chanut and Buisson, 2003; Ngoduy and R. Liu, 2007) model (B) (S Logghe and L. H. Immers, 2008; Qian et al., 2017) model

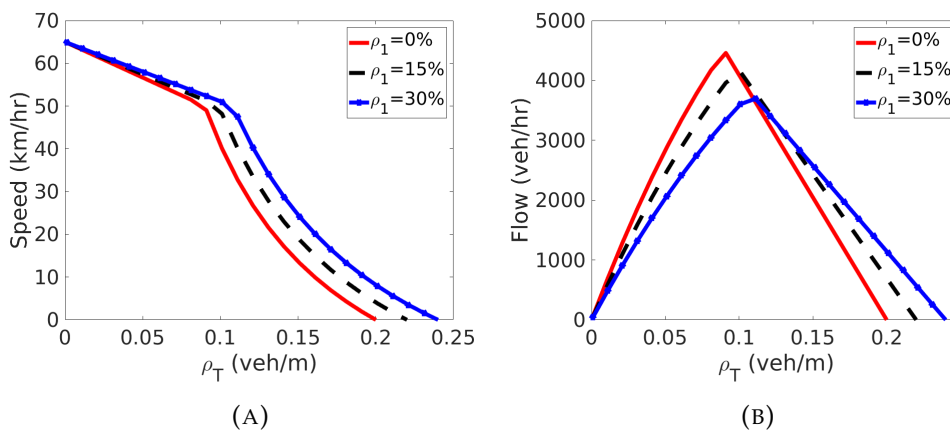


FIGURE 2.6: The variation of (A) speed-density and (B) flow-density relation with traffic composition in (Ngoduy and R. Liu, 2007) model

Scaling factor

The concept of scaling factor can be interpreted as a way of deriving PCU to relate the homogeneous and the heterogeneous fundamental diagrams of a vehicle class or the

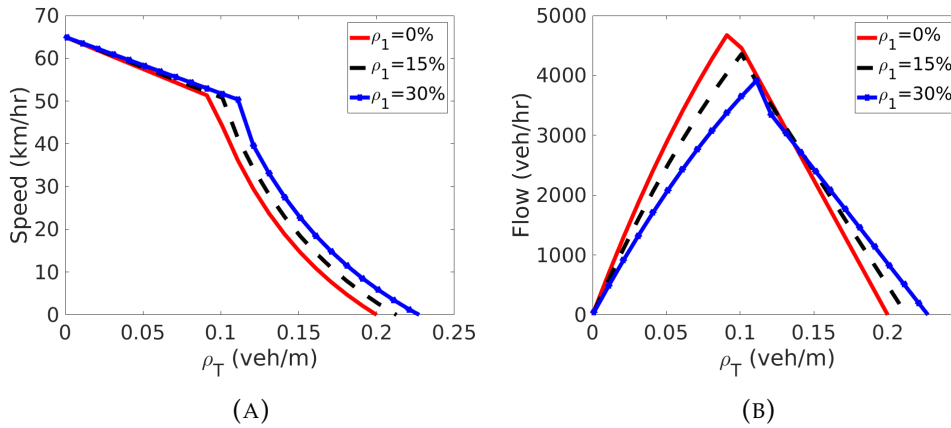


FIGURE 2.7: The variation of (A) speed-density and (B) flow-density relation with traffic composition in (Chanut and Buisson, 2003) model

homogeneous fundamental diagrams of vehicle classes. The scale factor is first introduced in (S. Logghe and L. Immers, 2003). The fundamental diagrams of the vehicle classes are assumed to be a scaled version of each others. For two vehicle classes the following relation holds

$$q_2(\rho_2) = \alpha q_1\left(\frac{\rho_2}{\alpha}\right), \quad \rho_{2,jam} = \alpha \rho_{1,jam}, \quad \rho_{2,cr} = \alpha \rho_{1,cr} \quad (2.13)$$

The relation in equation (2.13) requires $v_1^{max} = v_2^{max}$.

The scaling factor α correlates the two classes. As such, the heterogeneous traffic flow properties is expressed in terms of the properties of an equivalent homogeneous flow of one of the vehicle classes. That is, the heterogeneous traffic flow (ρ_1, ρ_2) takes the same properties as class 1 flow $(\rho_1 + \rho_2/\alpha)$.

The same authors (S Logghe and L. H. Immers) later used the scaling factor to drive the fundamental diagram of a vehicle class in heterogeneous traffic flow condition from its homogeneous fundamental diagram (S Logghe and L. H. Immers, 2008). Here, the scaling factor represents the fraction of road space assigned for a vehicle class. The scaling factor for each class is different and satisfies

$$\sum_i \alpha_i \leq 1.$$

For a given mixed traffic condition (ρ_1, ρ_2, \dots) , the fundamental diagram for each class is equivalent to

$$q_i(\rho_1, \rho_2) = \alpha_i q_i^h(\rho_1/\alpha_i) \quad (2.14)$$

where q_i^h is the homogeneous flow. The homogeneous fundamental diagram for each class is represented by a triangular fundamental diagram.

$$q_i^h(\rho_i^h) = \begin{cases} \rho_i^h v_i^{max} & \rho_i^h \leq \rho_{i,cr}^h \\ \omega(\rho_{i,jam}^h - \rho_i^h) & \rho_i^h > \rho_{i,cr}^h \end{cases} \quad (2.15)$$

where the wave speed $\omega = \frac{\rho_{i,cr}^h v_i^{max}}{\rho_{i,jam}^h - \rho_{i,cr}^h}$. Each class has a distinct jam density (ρ_{jam}^h), critical density (ρ_{cr}^h) and wave speed.

For two classes, the heterogeneous speed-density relation is derived using the scaling factor α and the homogeneous fundamental diagram.

$$v_i(\rho_1, \rho_2) = v_i(\rho_i / \alpha_i) = \begin{cases} v_i^{max} & \frac{\rho_i}{\alpha_i} \leq \rho_{i,cr}^h \\ \frac{1}{\rho_i} \alpha_i q_i^h(\frac{\rho_i}{\alpha_i}) & \frac{\rho_i}{\alpha_i} > \rho_{i,cr}^h \end{cases} \quad (2.16)$$

The scaling factor reflects the interaction between vehicle classes at different traffic conditions, therefore the value changes with the traffic state. Three traffic regimes are identified: free flow, semi-congested and congested. The value of the scaling factors vary with the traffic regime.

Similarly, Qian et al. (Qian et al., 2017) interpret the scaling factor with perceived equivalent density. Each vehicle class perceives as the traffic flow consists of only that type of vehicle class. Thus, the heterogeneous flow is converted to a homogeneous flow that would result in an equivalent traffic state. The perceived density (ρ^p) is computed using a conversion factor (δ), which has an analogy to the theory of PCU.

$$\rho_1^p = \rho_1 + \delta_1 \rho_2 = \rho_1 / \alpha_1$$

$$\rho_2^p = \delta_2 \rho_1 + \rho_2 = \rho_2 / \alpha_2$$

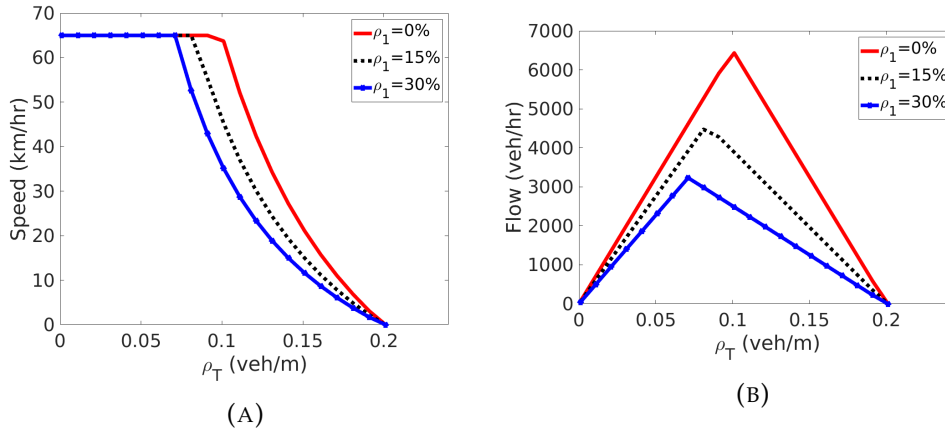


FIGURE 2.8: The variation of (A) speed-density and (B) flow-density relation with traffic composition in (S Logghe and L. H. Immers, 2008; Qian et al., 2017) model

Figures 2.5(b) and 2.8 show the properties of the fundamental relation in (S Logghe and L. H. Immers, 2008; Qian et al., 2017).

Area occupancy

The models in this category describe the mixed traffic properties on the basis of the space gap between vehicles in free-flow or jam conditions. The sum of space gaps between vehicles (bumper to bumper) in free-flow or jam condition should be less than the length of the road. That is, the length (area) occupancy should be less than 1.

H. Zhang and Jin (H. Zhang and Jin, 2002) give a formulation for a group speed that accounts the variation among vehicle classes. It is written as

$$v = \begin{cases} \frac{\sum_i v_i^{max} \rho_i}{\sum_i \rho_i} & \sum_i (l_i + v_i^{max} \tau_i) \rho_i < 1 \\ \frac{1 - \sum_i \rho_i l_i}{\sum_i \rho_i \tau_i} & \sum_i (l_i + v_i^{max} \tau_i) \rho_i \geq 1 \end{cases} \quad (2.17)$$

The vehicle classes have a unique maximum speed (v^{max}), length (l) and time headway τ . Hence, the jam and critical densities change with the traffic composition.

Based on the area occupancy in jam state, speed-density relation for each class of a multi-class flow is derived in (Benzoni-Gavage and Colombo, 2003) as follows.

$$v_i = v_i^{max}(1 - \sum \rho_i l_i) \tag{2.18}$$

Figures 2.9, 2.10, 2.11 illustrate the properties of the speed-density relation in the models (H. Zhang and Jin, 2002; Benzoni-Gavage and Colombo, 2003).

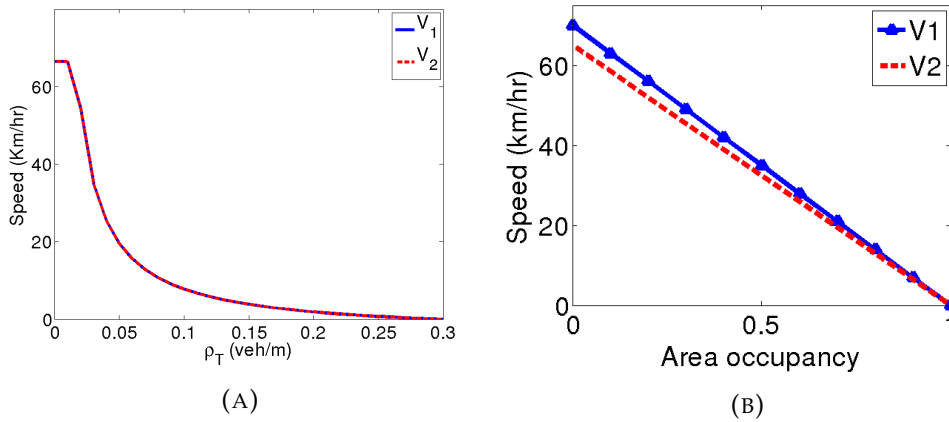


FIGURE 2.9: Fundamental relations in (A)(H. Zhang and Jin, 2002) model (B)(Benzoni-Gavage and Colombo, 2003) model

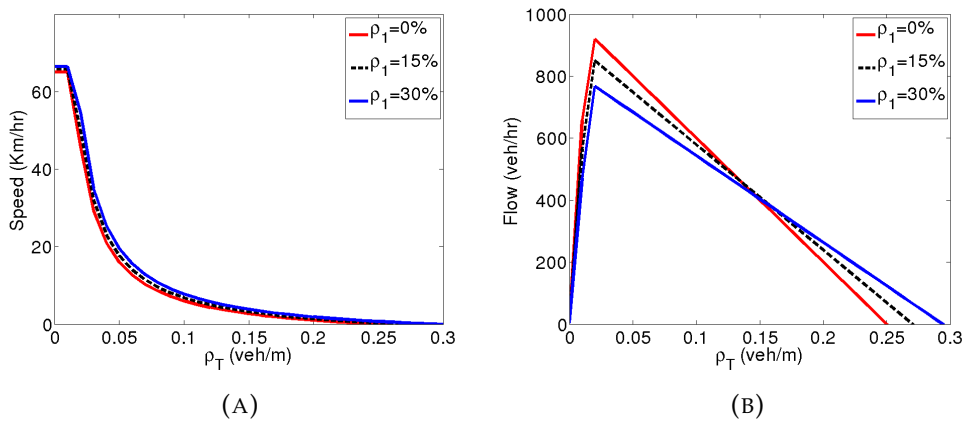


FIGURE 2.10: The variation of (A) speed-density and (B) flow-density relation with traffic composition in (H. Zhang and Jin, 2002) model

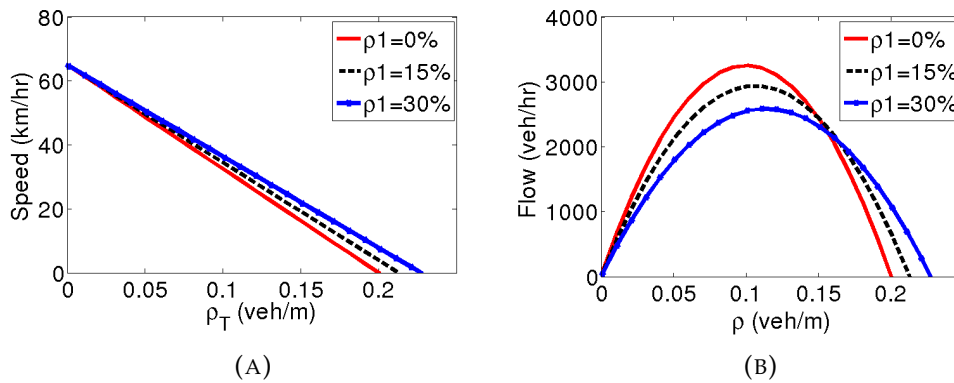


FIGURE 2.11: The variation of (A) speed-density and (B) flow-density relation with traffic composition in (Benzoni-Gavage and Colombo, 2003) model

2.3.2.2 Multi-class two-equation models

Two-equation, also called second order models, aim to address the limitations of LWR model that are related to equilibrium speed-density relation. Instead, the two-equation models replace it with an equation that describes the average speed dynamics. Based on car-following theory, different speed dynamics equation are derived (Payne, 1971; H. M. Zhang, 1998). However, the proposed equations are found not to respect the anisotropic property of traffic flow, i.e., drivers are only influenced by the front stimuli Daganzo, 1995. Later, (Aw and Rascle, 2000; H. M. Zhang, 2002) provide an improved speed dynamic equation

$$\frac{\partial v}{\partial t} + v \frac{\partial v}{\partial x} = -\rho V_e'(\rho) \frac{\partial v}{\partial x} \quad (2.19)$$

where $V_e(\rho)$ is the equilibrium speed.

Furthermore, to take into account heterogeneous drivers that have a different speed dynamics, multi-class second order models are developed (Gupta and Katiyar, 2007; Tang et al., 2009). The models define the speed equation and conservation equation for each class. In this way, for the individual vehicle class different parameters can be specified, for instance class-dependent equilibrium speed-density relation.

2.3.3 Heterogeneous mesoscopic models

Traffic flow models derived from gas kinetic theory are the most popular mesoscopic representation of traffic flow. Numerous types of kinetic traffic flow models have been developed (Paveri-Fontana, 1975; Wegener and Klar, 1996; Chowdhury, Santen, and Schadschneider, 2000). The traffic flow equation describes the dynamics of the phase-space density $f(v, x, t)$, where $f(v, x, t)dvdx$ represent the number of vehicles at time t in $[x, \Delta x]$ and with speed $[v, \Delta v]$.

$$\frac{\partial f}{\partial t} + v \frac{\partial f}{\partial x} = \left(\frac{\partial f}{\partial t} \right)_{int} + \left(\frac{\partial f}{\partial t} \right)_{rel} \quad (2.20)$$

Different assumptions have been made to determine the interaction (*int*) and relaxation (*rel*) terms (Paveri-Fontana, 1975).

A heterogeneous version of gas kinetic model presented by (S. P. Hoogendoorn and Bovy, 2000) integrates class specific desired speed and acceleration term that considers intra-class and inter-class interactions. Another multi-class extension of of gas kinetic model is also proposed by Helbing, Hennecke, et al. (Helbing, Hennecke, et al., 2001).

2.4 Modeling two-wheelers mobility

2.4.1 Maneuvering behavior of PTWs

PTWs have peculiar mobility features, which are attributed to their compact size. The standard lane demarcation of roads is designed for vehicles like passenger cars and other heavy vehicles. These vehicles require a wider lane to operate than PTWs. Consequently, when PTWs share road with other road users, they exhibit a different behavior. PTWs traffic behavior has commonality with bicycles traffic. However, unlike bicycles, PTWs often share road with other vehicles, and their speed is comparable to cars' speed. The unique behaviors of PTWs in mixed traffic flow can be summarized as lane sharing, smaller longitudinal and lateral gap, and travel at non-zero speed while cars are completely stopped. These behaviors are not mutually exclusive; one has a consequence on the other.

Lane sharing

PTWs ride through the space between cars or between cars and road borders. This practice of PTWs is expressed by different terms such as lane sharing, lane filtering,

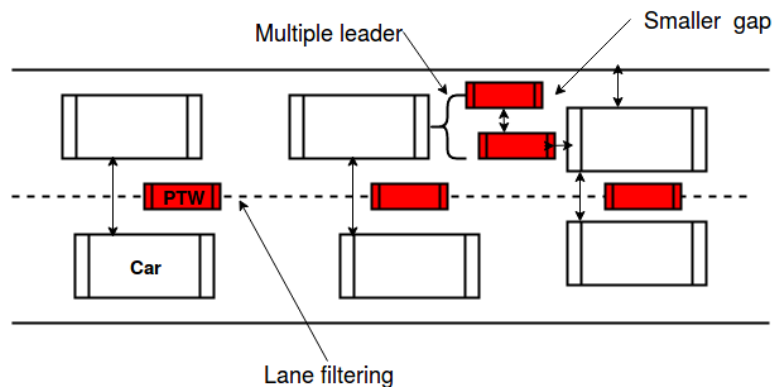


FIGURE 2.12: The representation of PTWs maneuvering behaviors

lane splitting, and creeping. Generally, lane splitting and creeping refer to the specific case where PTWs pass between the rows of stationary traffic (Fan and Work, 2015; FEMA, 2009; Robertson, 2002). Whereas, lane splitting denotes the condition where PTWs pass between a moving traffic (FEMA, 2009). Lane sharing is the encompassing term for lane splitting and filtering (Sperley, Pietz, et al., 2010).

Although lane sharing is not allowed everywhere, it is a commonly observed behavior. There are also different rules about when and how PTWs are allowed to do lane-sharing. An experimental study done in Paris (Aupetit, Espié, and Bouaziz, 2015) reports that PTWs ride between traffic on average for 72% of their riding time or 77 % of the traveled distance. PTWs use the spaces between traffic, which are not accessible by other vehicles, to overtake. Lane sharing often occurs under medium and heavy traffic conditions. That is, the rate of lane-sharing increases with traffic volume (Ouellet, 2012). The width of the free spaces between vehicles and the traffic volume (or the speed of traffic) are the determinant factors for PTWs riders to engage in lane sharing or not (Aupetit, Espié, and Bouaziz, 2015). On the other hand, the width of the gaps between vehicles or between vehicles and road border has a direct relation with the total lane width. The wider the total lane width is, the higher the chance for PTWs to find enough space to do lane filtering/splitting (Sperley, Pietz, et al., 2010). The critical space for lane sharing (filtering) depends on the speed of PTWs (Minh, Sano, and Matsumoto, 2012), the relative speed to the rest of traffic, and the presence of heavy vehicles and platoon of PTWs (Vlahogianni, 2014).

Longitudinal and lateral gaps

PTWs, compared to other vehicles, maintain shorter longitudinal and lateral gaps (K. Wong, LEE, and CHEN, 2016; T.-C. Lee, J. W. Polak, et al., 2012). In car-following state, drivers follow the leader vehicle at a safe distance in order to avoid collision. The safe distance depends on the traffic state. Yet, due to their compact sizes PTWs are able to make lateral movements (e.g., swerving (T.-C. Lee, J. W. Polak, et al., 2012)) to avoid collision (Walton and Buchanan, 2012). Besides, PTWs have a higher deceleration capability than passenger cars (T.-C. Lee, J. W. Polak, et al., 2012). Thus, PTWs keep smaller longitudinal distance to the leader and still manage to avoid collision by braking or swerving. In the same manner, PTWs do not respect lane demarcations, rather create a dynamic virtual lane using the space between vehicles. Obviously, the lateral gap maintained by PTWs is smaller than other vehicles, which respect lane-based discipline. The lateral gap also has a correlation with the speed of PTWs (K. Wong, LEE, and CHEN, 2016; Minh, Sano, and Matsumoto, 2012), but the sensitivity to the speed is less than the longitudinal distance (K. Wong, LEE, and CHEN, 2016). Furthermore, the differential speed and the type of vehicle alongside influence the lateral distance (C Mallikarjuna, Tharun, and Pal, 2013).

Travel speed

At low traffic densities, the interaction among vehicles classes is negligible. Thus, vehicles travel at a speed close to their desired speed. In lane-based heterogeneous traffic flows, slow moving vehicles (e.g., trucks) may impact the speed of fast vehicles (e.g., cars), particularly at medium to high traffic densities. However, PTWs utilize different lateral maneuvers to avoid such constraints. For this reason, PTWs have a better opportunity to travel at a higher speed than cars (T.-C. Lee, J. W. Polak, et al., 2012; K. Wong, LEE, and CHEN, 2016). The speed of PTWs is dependent on the factors that influence the lateral/longitudinal gap and the lane sharing behaviors, such as traffic composition and lane width. The trend of the differential speed between PTWs and other traffic stream is analyzed in (Rice, Troszak, and Erhardt, 2015; Aupetit, Espié, and Bouaziz, 2015). Accordingly, the highest differential speed occurs when the other traffic stream is completely stopped. Thanks to their filtering capability, PTWs can have non-zero speeds while the other vehicles are stopped due to congestion. In general, the relative speed of PTWs is related to lane changing probability in the other traffic stream. In other words, the speed difference increases with the decrease of the lane-changing probability (Aupetit, Espié, and Bouaziz, 2015).

2.4.2 Models for traffic flow including PTWs

There are only a few available models for traffic flow that consists of PTWs and other vehicle types. The aforementioned driving behaviors of PTWs are different from any other vehicles types. In addition, the presence of PTWs influences the moving behaviors of other vehicles. For instance, since PTWs share a lane with other vehicles, a vehicle may have more than two leaders. Thus, the conventional car following models cannot be applied directly. Same lane overtaking is also another phenomenon that is observed in mixed traffic flows that contain PTWs. To account such properties, special traffic flow models for PTWs traffic, and heterogeneous traffic flow that include PTWs are developed.

2.4.3 Microscopic model

Modeling traffic flow containing PTWs is challenging as there are several unique properties. These properties include, but not limited to, multiple leader, no-lane based movement and same lane overtaking. In a microscopic approach, the heterogeneity of driver and vehicle characteristics is modeled by defining different behavioral rules and parameters, such as longitudinal and lateral movement rule (Pandey, Rao, and Mohan, 2017), speed choice, lateral and longitudinal headway (Lenorzer et al., 2015), and reaction time. The parameters and driver behaviors are described differently depending on the interacting vehicle classes (SHIOMI et al., 2012). Space discretization methods are also introduced to accommodate the lateral movement within a lane and the variation in vehicle size (Chen et al., 2013; Mathew, Munigety, and Bajpai, 2013).

2.4.3.1 Car-following model

The basic car-following theories base on the assumption of ordered flow of vehicles. The existence of PTWs, which have a deviant characteristic from car-like behavior, necessitate modified car-following theories. Traffic features like multiple leader, same-lane overtaking, and zero-headway are unique to the traffic flows containing PTWs. A mixed flow of cars and PTWs can be seen as a complete disorder flow like what is commonly observed in developing countries (V Thamizh Arasan and Koshy, 2005) or a mixture of ordered (for cars) and disorder (PTWs) flows. Different car-following models are proposed to characterize the individual vehicle behavior in pure PTWs traffic and traffic flows including PTWs.

In strip-based car-following model (Mathew, Munigety, and Bajpai, 2013), the lane is divided into strips, and a lane analogy is applied to the strips. Depending on the

size, a vehicle may occupy more than one strip. The closest vehicle inside the strip/s occupied by the follower vehicle becomes the leader. The speed of the follower vehicles is formulated according to the safe gap theory.

$$v_n = -\tau b + \sqrt{(\tau b)^2 + v_{n-1}(t-1)^2 + 2bg_{n-1}(t-1)} \quad (2.21)$$

where τ , b , g are the reaction time, the maximum deceleration and the distance head-

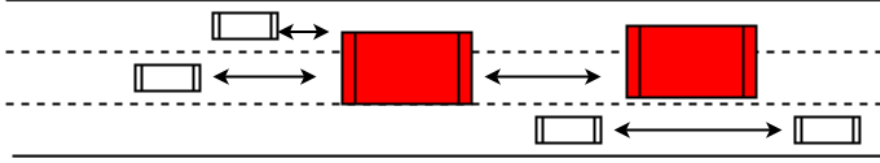


FIGURE 2.13: Illustration of the strip based approach

way, respectively. The distance headway (g) is adapted to the vehicle types in the follower-leader combination. Besides, the model defines the strip/lane changing rules. The multi-anticipative approach would be more convenient for strip models, in order to include the impact of the front vehicles in the same lane but not in the same strips.

T.-C. Lee, J. Polak, and Bell (T.-C. Lee, J. Polak, and Bell, 2009) also develop a longitudinal movement model based on the principle that PTWs either stop at a safe distance behind the leader vehicle or swerve to the left of the leading vehicle to avoid collision. The model given in (T.-C. Lee, J. Polak, and Bell, 2009) can be reformulated similar to equation (2.21). Nonetheless, the value of g_{n-1} is determined by the choice of PTWs to swerve or not, i.e., g_{n-1} for swerving maneuver is less than non-swerving. Instead of the fixed virtual lanes (strips), the model introduces dynamic virtual lanes, which are specified by a path choice rule.

Another stimulus-response type microscopic model for pure motorcycle traffic is proposed in (L. Nguyen, Hanaoka, and Kawasaki, 2012; L. X. Nguyen, Hanaoka, and Kawasaki, 2014). The model applies a safety level concept to quantify the influence of the leader vehicle on the follower (Figure 2.14). The safety area is denoted by a half ellipse and a rectangle, where the perceived safety level to the leader vehicle in the front and moving at the side is measured with respect to the ellipse and the rectangular area, respectively. For selecting a leader PTW or the most influential PTW out of the surrounding PTWs, following angle and route width are used as filtering criterion. Then, the follower vehicle adjusts its acceleration according to the perceived safety level (SL) and the relative speed.

$$a(t + \tau) = \begin{cases} SL \frac{1}{\Delta v} \left(\frac{\Delta x \Delta v_x}{(\tau v)^2} + \frac{\Delta y \Delta v_y}{(w + dy)^2} \right) & \Delta x \geq 0 \\ SL \frac{1}{\Delta v} \left(\frac{\Delta y \Delta v_y}{(w + dy)^2} \right) & -2dx \leq x < 0 \end{cases} \quad (2.22)$$

where

$$SL = \begin{cases} A \exp\left(-\left(\frac{\Delta x^2}{(\tau v)^2} + \frac{\Delta y^2}{(w + dy)^2}\right)/B\right) & \Delta x \geq 0 \\ A \exp\left(-\left(\frac{\Delta y^2}{(w + dy)^2}\right)/B\right) & -2dx \leq x < 0 \end{cases} \quad (2.23)$$

τ , v , dx , dy stand for the reaction time, the speed, the length and the width of the follower vehicles, and ΔV is the relative velocity. The semi-major and semi-minor axis of the ellipse area equal τv and $w + dy$, respectively. The rectangular safety space has a length of $2dx$ and a width of $w + dy$.

However, $\left(\frac{\Delta x^2}{(\tau v)^2} + \frac{\Delta y^2}{(w + dy)^2}\right) > 1$ if the the leader vehicle is outside the half ellipse area and $\left(\frac{\Delta x^2}{(\tau v)^2} + \frac{\Delta y^2}{(w + dy)^2}\right) \leq 1$ otherwise, implying the safety level decreases with the increase of the distance between the leader and the follower, while the reverse is true in the real condition.

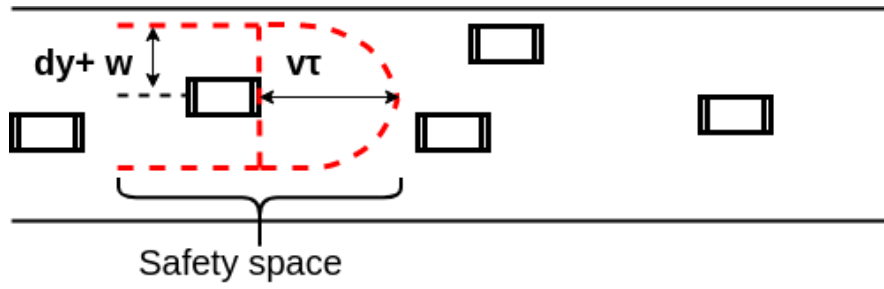


FIGURE 2.14: The schematic representation of safety space

The model in (Cho and Wu, 2004) attempts to represent PTWs longitudinal movement as a function of the desired speed and the repulsion force from the leading PTWs. The model assumes that PTWs interact with the two nearest leading PTWs. Thus, the repulsion force is a weighting sum of the repulsion from each leading PTW. The weight is proportional to the lateral distance.

$$v_n(t + \tau) = v_{n,d} \left(1 - \sum_i^2 w(y_{n-i} - y_n) \exp^{-\lambda \frac{v_n^\alpha - v_i(t)}{v_n(t)^\beta} \left(\frac{x_{n-i} - x_n - s_n}{L} \right)^\gamma} \right) \quad (2.24)$$

where v , x , y , w denote, respectively, the speed, the longitudinal position, the lateral position and a weighting factor. The remaining variables L , γ , λ , β , α are the mode parameters. The model also includes a description for the lateral movement of PTWs. However, the model is limited to pure PTWs flow and cannot replicate a collision free flow.

In a similar manner, the social force model proposed in (L. X. Nguyen and Hanaoka, 2011) relates the repulsion force and the desired speed (or acceleration force). These acceleration and repulsion forces determine the maneuvering behavior of PTWs.

$$a_\alpha(t) = F_\alpha^A + \sum_\beta F_{\alpha\beta}^R + \sum_B F^B + \text{fluctuation} \quad (2.25)$$

The acceleration force F_α^A describes the attempt of PTWs to accelerate to the desired speed. $F_{\alpha\beta}^R$ represents the repulsion force from the leading PTWs, that leads in reduction of the following PTWs speed. Different weight is applied to the repulsion from leading PTWs within and outside the angle of sight. The repulsion from road border is denoted by F^B .

In addition to the above model, a model that describes the acceleration/deceleration behavior of PTWs at signalized intersection is proposed in (MINH, SANO, et al., 2007). An operating zone, which is equivalent to dynamic virtual lane, proportional to the speed of a subject PTW is applied to characterize the non-lane based moving behavior of PTWs. Furthermore, a discrete choice method, which is borrowed from pedestrian modeling (Robin et al., 2009), is also used to represent the maneuvering behavior of PTWs and car in mixed flows (SHIOMI et al., 2012). A set of discrete choices, that characterizes the decision of vehicles, are defined. The preference of vehicles to each alternatives is determined by a utility function.

2.4.3.2 Cellular automata model

The cellular automata model presented in Section 2.3.1.2 considers lane-based heterogeneous traffic flow. However, to model traffic flows which include PTWs or any disordered flows, the update rules and space discretization have to be adapted. In lane-based CA model, the width of a cell is assumed to be equal to the lane width since there is no lateral movement within a lane. Nonetheless, to model the side-by-side movement of vehicles and the same lane overtaking, the lane is subdivided into sub-lanes

(FIGURE 2.15. That is, the space is discretized laterally and longitudinally (Lan and C.-W. Chang, 2005; Meng et al., 2007; Ch Mallikarjuna and Rao, 2009; Lan, Chiou, et al., 2010). The number of consecutive lateral and longitudinal cells occupied by vehicles is determined by the safe lateral and longitudinal space maintained by vehicles and the cell dimension. In addition to the rule to update the longitudinal movement, a lateral movement model is added (Lan and C.-W. Chang, 2005; Meng et al., 2007; Ch Mallikarjuna and Rao, 2009; Lan, Chiou, et al., 2010).

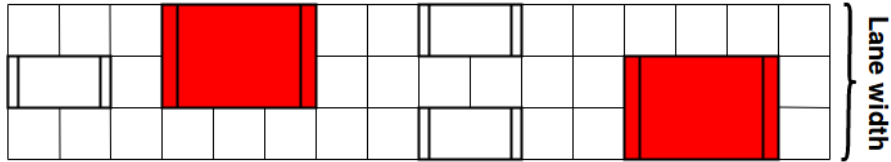


FIGURE 2.15: Heterogeneous CA for a mixed cars and PTWs flow

2.4.4 Macroscopic model

The macroscopic traffic characteristics observed in traffic flow containing PTWs differ from other heterogeneous traffic flows in many ways. Due to the lane sharing properties of PTWs, the average speed depends not only on the longitudinal spacing but also on the lateral spacing. Therefore, the speed-density relation should reflect this property. Moreover, when other vehicle classes (e.g., cars) are completely stopped, PTWs can travel with non-zero speed through the gaps between vehicles. The critical and the jam densities should be identified for each traffic stream. Most of the existing heterogeneous macroscopic models are unable to describe these unique properties or need to be modified to accommodate the required properties. In this section, we discuss the approaches applied in macroscopic models for capturing such behaviors.

2.4.4.1 Multiclass LWR model

The principle followed is similar to the heterogeneous LWR model in section 2.3.2.1. The governing principle is represented using the system equations in equation (2.4-2.6). However, the speed-density relation are derived in a way that captures the traffic characteristics resulted from the unique maneuvering behavior of PTWs.

Fundamental relation

Numerous multi-class models are stemmed from the desire to characterize mixed flows of cars and trucks, which is an ordered flow. For instance, the model in (H. Zhang and Jin, 2002) formulates a mixed flow of passenger cars and trucks based on their free flow speed difference. A two-class flow model proposed in (Chanut and Buisson, 2003) differentiates vehicles according to their length and speed. Furthermore, the heterogeneity among vehicles is modeled in relation to the maximum speed, length and minimum headway of vehicles in (J Van Lint, Serge Hoogendoorn, and Schreuder, 2008). Despite providing a separate representation for each vehicle classes, in all these models (Chanut and Buisson, 2003; J Van Lint, Serge Hoogendoorn, and Schreuder, 2008; P. Zhang et al., 2006) vehicle classes have identical critical and jam density parameters, but the parameters are scaled according to the actual traffic state. The multi-class model in (G. Wong and S. Wong, 2002) extends the LWR model for heterogeneous drivers, by distinguishing the vehicle classes by the choice of the speed. The assumption is that drivers respond in a different way to the same traffic density. Correspondingly, the work in (Benzoni-Gavage and Colombo, 2003) presents a mixed flow for several populations of vehicles, where the vehicle classes are differentiated by the maximal speed, and the equilibrium speed is expressed as a function of total occupied space. The models in (S Logghe and L. H. Immers, 2008; Qian et al., 2017) derive a multi-class model, based on the interaction between vehicles classes (trucks and cars) at different traffic conditions.

However, mixed flows consisting of PTWs yet exhibit distinctive features from the assumption taken in the aforementioned multi-class models. Their narrow width indeed grants PTWs flexibility to share lanes with other vehicles or filter through slow moving or stationary traffic, requiring traffic stream attributes to be defined differently from traffic following lane rules (Ch Mallikarjuna and Rao, 2006). Only a few models exist that attempt to reproduce these unique traffic behaviors. We can categorize the LWR models for mixed flow of cars and PTWs, based on the principles applied to formulate the speed-density relation, as area occupancy and porous flow approach.

Area occupancy

The model proposed in (Fan and Work, 2015) formulates the speed-density relation following the method in (Benzoni-Gavage and Colombo, 2003). To reproduce the lane filtering or creeping behavior of PTWs, the model distinguishes the area occupancy, in which the vehicles come to a complete stop, for each vehicle class. The area occupancy for PTWs is greater than other vehicles classes, as such the creeping behavior can be reproduced. The speed-density relation is given as

$$v_i = v_i^{max} \left(1 - \frac{r}{r_i^{max}}\right) \quad (2.26)$$

where the area occupancy $r = \sum_i \rho_i l_i$, and r^{max} is the maximum area occupancy. The model captures the basic traffic characteristics. Nevertheless, the area occupancy cannot reflect all the properties and the interaction between the vehicle classes. For instance, for a given area occupancy when all the vehicles are PTWs or cars, the traffic condition differs depending on the vehicle class, which can not be identified by the model. The fundamental diagram is shown in FIGURE 2.16(a). The speed-density and flow-density variation with traffic composition in the model proposed by (Fan and Work, 2015) have similar characteristics with (Benzoni-Gavage and Colombo, 2003) (see FIGURE 2.11).

Porous flow approach

The model proposed by Nair, Mahmassani, and Miller-Hooks (Nair, Mahmassani, and Miller-Hooks, 2011; Nair, Mahmassani, and Miller-Hooks, 2012) treats the mixed flow of cars and PTWs in analogy to the flow of fluid through a porous medium. In disordered traffic flows, vehicles do not follow lane demarcation, rather fast-moving vehicles drive through the free space between vehicles to overtake slow vehicles. To represent such traffic characteristics, Nair *et al.* define the average vehicle speed as a function inter-vehicle gap (pore size) distribution.

$$v_i = v_i^f \left(1 - \int_0^{r_i^{cr}} f(l_p(\rho_1, \rho_2, \dots)) dl_p\right) + v_i^r \int_0^{r_i^{cr}} f(l_p(\rho_1, \rho_2, \dots)) dl_p \quad (2.27)$$

where $f(l_p)$ and r_i^{cr} denote, respectively, the probability density function of the pore size distribution and the critical pore size, which is a minimum pore size that allows the passage of a vehicle class. The average speed is the weighted sum of two speed terms, free speed (v_i^f) and restrained speed (v_i^r), with the weight factor being the fraction of accessible and inaccessible pores. Furthermore, the two speeds are defined as

$$v_i^f = v_i^{max} \left(1 - \int_0^{r_i^{cr}} f(l_p(\rho_1, \rho_2, \dots)) dl_p\right)^{\alpha_f}, \quad v_i^r = v_i^{max} \left(1 - \int_0^{r_i^{cr}} f(l_p(\rho_1, \rho_2, \dots)) dl_p\right)^{\alpha_r} \quad (2.28)$$

The following relation is also specified: $\alpha_r \geq \alpha_f$. Nair *et al.* (Nair, Mahmassani, and Miller-Hooks, 2012) employ exponential distribution to characterize the pore size distribution.

$$\int_0^{r_i^{cr}} f(l_p(\rho_1, \rho_2, \dots)) dl_p = 1 - \exp^{-\lambda(\rho_1, \rho_2, \dots)r_i^{cr}} \quad (2.29)$$

The average pore size $1/\lambda$ is given by ¹

$$1/\lambda = (l_{max} - l_{min}) \left(1 - \sum_i a_i \rho_i \right) + l_{min}$$

where a and ρ are the projected area of a vehicle and the areal density (veh/m^2), respectively. l_{min} , l_{max} are the distribution parameters.

The fundamental diagram for the model in (Nair, Mahmassani, and Miller-Hooks, 2012; Fan and Work, 2015) is shown in FIGURE 2.16 and 2.17.

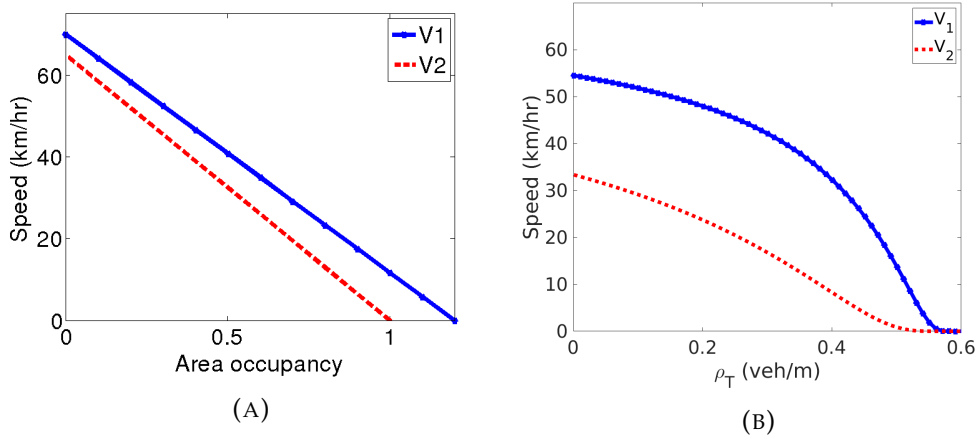


FIGURE 2.16: Speed density relation (A) (Fan and Work, 2015) model (B) (Nair, Mahmassani, and Miller-Hooks, 2012) model

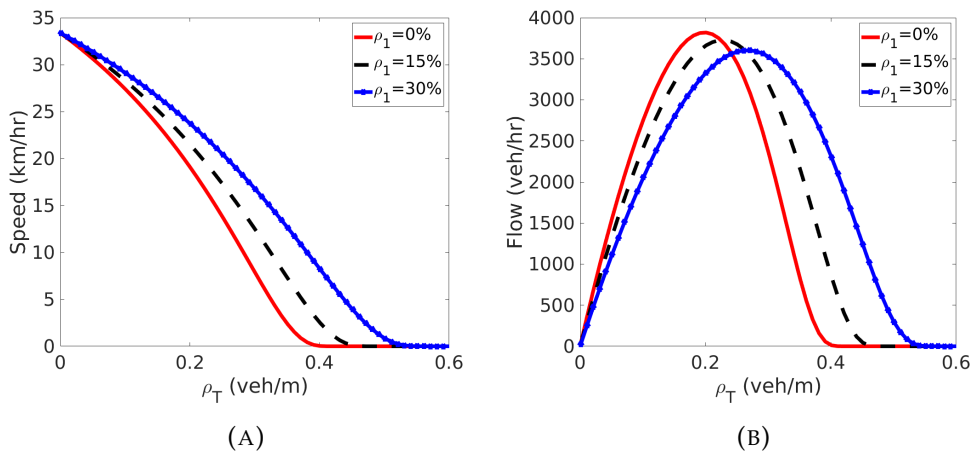


FIGURE 2.17: The variation of (A) speed-density and (B) flow-density relation with traffic composition in (Nair, Mahmassani, and Miller-Hooks, 2012) model

¹The equation in (Nair, Mahmassani, and Miller-Hooks, 2012) is modified here

Model	Speed function	
Heterogeneous drivers		
Daganzo, 1997	$v_i = \begin{cases} v(\rho_i/\gamma_i) & \text{2-pipe regime} \\ v(\sum_i \rho_i) & \text{1-pipe regime} \end{cases}$	
G. Wong and S. Wong, 2002	$v_i = v_i^{max} \exp(-(\rho/\rho_0)^2/2)$	$\rho = \sum_i \rho_i$
PCU		
Chanut and Buisson, 2003	$v_i = \begin{cases} \frac{\rho}{\rho_{cr}} v_{cr} + (1 - \frac{\rho}{\rho_{cr}}) v_i^{max} & \rho \leq \rho_{cr} \\ \frac{\rho_{jam} - \rho}{(\rho_{jam} - \rho_{cr}) \rho^*} q_{cap} & \rho > \rho_{cr} \end{cases}$	$\rho = \sum_i \rho_i$ $\rho_{jam} = \rho_{jam}^r \frac{\rho}{\sum_i \rho_i \alpha_i}$ $\rho_{cr} = \zeta \rho_{jam}$
Ngoduy and R. Liu, 2007		$\rho = \sum_i \rho_i$ $\rho_{jam} = \rho_{jam}^r \frac{\sum_i \rho_i \beta_i}{\rho}$ $\rho_{cr} = \rho_{cr}^r \frac{\sum_i \rho_i \beta_i}{\rho}$
J Van Lint, Serge Hoogendoorn, and Schreuder, 2008		$\rho = \sum_i \rho_i \alpha_i$ $\alpha_i = \frac{L_i + T_i v_i}{L_r + T_r v_r}$
Scaling factor		
S Logghe and L. H. Immers, 2008 Qian et al., 2017	$v_i = \begin{cases} v_i^{max} & \frac{\rho_i}{\alpha_i} \leq \rho_{i,cr}^h \\ \frac{1}{\rho_i} \alpha_i q_i^h(\frac{\rho_i}{\alpha_i}) & \frac{\rho_i}{\alpha_i} > \rho_{i,cr}^h \end{cases}$	$\sum_i \alpha_i \leq 1.$
Area occupancy		
H. Zhang and Jin, 2002	$v = \begin{cases} \frac{\sum_i v_i^{max} \rho_i}{\sum_i \rho_i} & \sum_i (l_i + v_i^{max} \tau_i) \rho_i < 1 \\ \frac{1 - \sum_i \rho_i l_i}{\sum_i \rho_i \tau_i} & \sum_i (l_i + v_i^{max} \tau_i) \rho_i \geq 1 \end{cases}$	
Benzoni-Gavage and Colombo, 2003	$v_i = v_i^{max} (1 - \sum \rho_i l_i)$	
Fan and Work, 2015	$v_i = v_i^{max} (1 - \frac{\sum_i \rho_i l_i}{v_i^{max}})$	
Porous flow		
Nair, Mahmassani, and Miller-Hooks, 2011	$v_i = v_i^f \int_{r_{cr}^f}^{\infty} f(l_p) dl_p + v_i^r \int_0^{r_{cr}^r} f(l_p) dl_p$	
Nair, Mahmassani, and Miller-Hooks, 2012	$v_i^f = v_i^{max} \left(\int_{r_{cr}^f}^{\infty} f(l_p) dl_p \right)^{\alpha_f}, v_i^r = v_i^{max} \left(\int_{r_{cr}^r}^{\infty} f(l_p) dl_p \right)^{\alpha_r}$	$f(l_p) = \lambda \exp^{-\lambda r_{cr}^f}$

TABLE 2.1: Summary of the speed-density relation for heterogeneous traffic flow

2.5 Traffic model calibration and validation

Theoretical traffic flow models are developed by hypothesizing the individual and/or aggregated driver behavior, which usually base on an empirical observation. To apply the model for practical application, it is important to compare and analyze their properties against real data. The calibration and validation procedures are intended to improve the descriptive accuracy of the models by adapting the assumption and the

model parameters to the real situations, and testing the models capability to reproduce the required properties (Rakha et al., 1996). As such, the deviation between the models and the real traffic situation is reduced.

The complexity and the method of validation and calibration process depend on the type of the traffic flow model. Microscopic models have large set of parameters, and some of the parameters are difficult to determine from experimental data (e.g., reaction time, sensitivity (Serge Hoogendoorn and R. Hoogendoorn, 2010)). Either aggregated or individual vehicle data is applied to validate and calibrate microscopic models (Benekohal, 1991; Kesting and Treiber, 2013). For macroscopic models, different techniques are employed for the validation and the calibration. The validation experiments focus on assessing the accuracy level of the models to predict the targeted traffic phenomena (e.g., congestion (Spiliopoulou et al., 2014), capacity drop (Monamy, Haj-Salem, and Lebacque, 2012), etc.). Accordingly, the empirical and the computed data are compared to quantify the deviation of the model from the real behavior. On the other hand, the model parameters are optimized to fit the real traffic data in the calibration process. For LWR models usually the fundamental diagram parameters, such as jam density, critical density and wave speed (Dervisoglu et al., 2009) are calibrated. Whereas for the two-equation models the unknown parameters are determined from empirical data (Cremer and M. Papageorgiou, 1981; Ngoduy and SP Hoogendoorn, 2003).

The traffic data required for the calibration and the validation can be obtained from different sources. Probe vehicles (floating car data), loop detectors, cameras, and sensors are the widely employed methods. Depending on the required type of data, for instance, microscopic or aggregated data, any of the data acquisition methods can be used. Despite the existence of numerous traffic data collection methods, only a few of them are applicable for the validation of traffic flow containing PTWs. The challenge is mainly on getting the required traffic parameters and an accurate geo-location of vehicles, specifically PTWs. For example, data collected from sensors like inductive loops are not sufficient as extrapolation of vehicles spatial location is very difficult, if not impossible. Floating Car Data (FCD) could be an efficient method for collecting vehicles' trajectory data, where smartphones or GPS devices in vehicles continuously send location, speed, etc. information. However, the inefficiency of smartphone GPS to produce the true location of PTWs (Koyama and Tanaka, 2011), and the low penetration rate of vehicles equipped with an accurate GPS receiver make FCD method less applicable. Another potential alternative is to use video cameras and to extract the required traffic data (e.g., vehicle number, vehicle type, location) utilizing image processing techniques (Ch Mallikarjuna, Phanindra, and Rao, 2009). Given the complexity of data collection, synthetic data from calibrated commercial simulators like VISSIM can serve as a means of model calibration and validation tool (Chu et al., 2011). Yet, as the simulator might be calibrated to a particular scenario, the model validation would be valid only to that specific scenario.

Furthermore, before using data it is also necessary to undergo a preprocessing in order to extract the important information, which may entail aggregating or re-sampling, filtering the data and constructing the necessary parameters (Kesting and Treiber, 2013; Leclercq, 2005).

2.6 Conclusion

Traffic flow models are the major enablers of intelligent transportation systems (ITS). The models are employed for evaluation, analysis, planning, design, control and a lot of other applications. Several hypotheses and mathematical formulations are developed to interpret the observed traffic characteristics.

The models interpret the traffic flow features at different granularity, i.e. microscopic, mesoscopic and macroscopic. Since there is no model that outperforms and fits for all applications, the choice of a model depends on the requirements, such as level

of accuracy, computational efficiency, descriptive capability. To boost the models effectiveness to describe realistic traffic features, different extensions and adaptations have been done. Traffic heterogeneity is one these properties that needs to be included in the models.

The existing models are extended to describe the heterogeneity among drivers and vehicle types. Besides, when the existing modeling approach fall short of correctly describe the traffic features, new approaches are introduced. For instance, heterogeneous traffic flow are often studied and modeled from the perspective of trucks and cars. However, the traffic pattern in traffic flows containing PTWs differs from what is observed in car and truck mixed flow. New modeling approaches are therefore required to characterize traffic flows containing PTWs.

Of the macroscopic models, the LWR model is widely used due to its potential to express different traffic phenomena. Furthermore, the model can be easily extended to better reproduce various traffic characteristics. The multi-class extension intended to characterize heterogeneous traffic flow is recently getting attention. This dissertation also focuses on the multi-class LWR model.

In the next chapters, we develop and analyze a macroscopic model for traffic flow consisting of cars and PTWs. The approach used to depict different vehicle characteristics and the interaction among the vehicle types are presented in detail. The model properties are analyzed. The model is aimed to be employed to incorporate PTWs into different ITS applications.

Chapter 3

Model development

In this chapter, a macroscopic model for a mixed flow of cars and PWTs is presented. The required properties and the modeling principle are outlined first. The modeling approach employs the multi-class LWR framework. Each vehicle class has an independent fundamental diagram. The fundamental relations are derived by extending the principles applied in a porous flow approach (Nair, Mahmassani, and Miller-Hooks, 2011; Nair, Mahmassani, and Miller-Hooks, 2012). The methodology for extracting the inter-vehicle spacing distribution is introduced. In order to use the model for a variety of ITS applications, the flow equation is formulated in Eulerian and Lagrangian reference frames. More specifically, the Lagrangian representation tracks the motion property of vehicles along the trajectory, making it suitable for ITS applications that control and predict the flow properties of vehicles. On the other hand, the Eulerian description, which analyzes the flow properties at a fixed point in space, is convenient for ITS applications that control and predict traffic flow properties at a fixed location. The applied discretization schemes to solve the flow equations in the Eulerian and the Lagrangian representations are also discussed. For the Eulerian representation, the Lax-Friedrichs scheme is used, whereas a new discretization scheme is introduced for the Lagrangian representation.

The chapter is organized as follows: first the required model properties, related to the fundamental relation, are presented (Section 3.1). Then, we describe the method applied to interpret the interaction between vehicle classes (Section 3.2). Afterward, we describe the derivation of the flow equation in the Lagrangian and the Eulerian reference frames, and the corresponding numerical schemes (Section 3.3 and 3.4). Numerical examples are presented in Section 3.5. We finally conclude with summary and conclusion (Section 3.6).

3.1 Model requirements

Without loss of generality, the discussion on the model development focuses on two-populations flow, specifically cars and PTWS. Based on the maneuvering characteristics of PTWs mentioned in Section 2.4.1, the following model properties are established.

1. There are four traffic regimes, free-flow, semi-congested, congested and creeping. In free-flow regime both vehicle classes travel at their desired speed. The semi-congested state represents the situation where PTWs can travel at their desired speed but cars cannot. In congestion state, the speeds of both vehicle classes reduce with increasing density. The creeping regime denotes the traffic condition in which cars are completely stopped but PTWs can travel at non-zero speed.
2. Requirement 1 implies that vehicle classes should have different critical as well as jam (maximum) densities.
3. The difference in the physical dimension (length and projected area) and the maximum speed of vehicles should be included.
4. The equilibrium speed should be defined uniquely for each vehicle class density.

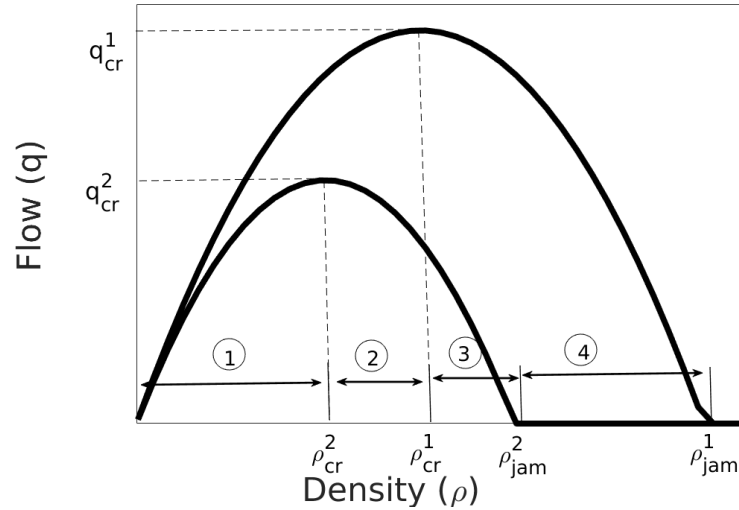


FIGURE 3.1: Example fundamental relation that satisfies the requirements

5. The equilibrium speed should have a correlation with the road geometry (width or number of lanes).

Requirement 1 and 2 are deduced from the fact that PTWs are able to do lane sharing or overtake in the same lane. Thereby, PTWs can get enough space to keep their desired speed while cars slow down due to congestion. Likewise, PTWs can also drive between stopped cars. These behaviors result in the four traffic regimes, and the difference in the critical and the jam densities of the two classes.

The requirement related to the maximum speed (requirement 3) is set to allow vehicle classes to choose their free-flow speed independently. Further, including the difference in the physical dimension of the vehicle classes is important in order to determine the free road space and its accessibility to a given vehicle class.

Requirement 4 describes that a pair of vehicle classes densities defines a unique traffic state and thus a unique equilibrium speed.

The last requirement (requirement 5) is intended to capture the fact that PWTs find more space to practice lane-sharing in multi-lane road space than in one-lane road space. Therefore, the speed of vehicles should be influenced by the number of lanes (or road width).

3.2 Fundamental relation

In this section, we derive the fundamental relation for a mixed cars and PTWs traffic (i.e. two vehicle classes), according to the requirements listed in the previous section.

The fundamental relation describes the interaction between vehicles within the same class and with other vehicle classes. The flow and the average speed of each vehicle class depend on the density of all vehicle classes. Therefore, the class-specific equilibrium flow-density and speed-density relations can be expressed as

$$q_i = Q_i(\rho_1, \rho_2) \quad (3.1)$$

$$v_i = V_i(\rho_1, \rho_2) \quad (3.2)$$

where the variables q , ρ and v represent, respectively, the flow (vehicles per unit time), density (vehicles per unit length) and average speed (distance per unit time).

To express the equilibrium relation as a function of the density of each vehicle class, the speed law is derived under the framework of the porous flow theory (Nair, Mahmassani, and Miller-Hooks, 2011). In porous flow theory, it is assumed that the speed

of vehicles is determined by the vehicle properties and the distribution of the pore size. The pore size defines the gap between the vehicles. The pore size distribution, i.e. the distribution of the gap between vehicles, depends on the traffic volume and the traffic composition. For vehicles to be able to pass through a given pore, the pore size should be greater than the minimum acceptable pore size. Throughout the dissertation, the term 'critical pore size' or 'critical gap' is used to indicate the minimum acceptable pore size, which is denoted by r^{cr} . The speed function is then can be formulated as:

$$v_i = v_i^{max} (1 - F(r_i^{cr})) \quad (3.3)$$

$F(r_i^{cr})$ is the cumulative density function of the pore size distribution, which is equivalent to the fraction of inaccessible free space.

$$F(r_i^{cr}) = \int_0^{r_i^{cr}} f(l_p) dl_p, \quad \int_0^{\infty} f(l_p) dl_p = 1 \quad (3.4)$$

We assume that the critical pore size is similar within a vehicle class but differs across the vehicles classes. Further, the critical pore size is assumed to be constant, later this assumption will be relaxed.

3.2.1 Determination of spacing distribution

A curve fitting technique is employed to characterize the inter-vehicle spacing distribution. Through the curve fitting procedures a standard distribution that fits best to the observation is selected.

In order to determine the inter-vehicle spacing distribution, simplifying assumptions are applied. First, the whole road space is considered as a single unit, i.e. vehicles can occupy any position on the road. The Pores are the free space between vehicles, and vehicles and road boundaries. Then, the vehicles are assumed to be distributed on the road space according to the Poisson point process. Empirical evidence also supports the Poisson point process assumption for spatial distribution of vehicles (Jiang et al., 2016), though limited to light traffic conditions. The vehicles are represented by circular shapes, note that the circular shape assumption does not change the distribution of the inter-vehicle spacing qualitatively.

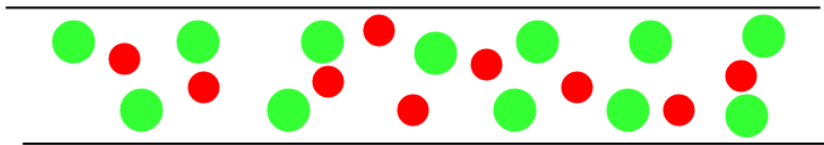


FIGURE 3.2: Example of the road space and vehicles' spatial distribution

Furthermore, Delaunay triangulation is used to define the spacing between vehicles, on the assumption that Delaunay triangle edge length represents the size of the spacing (FIGURE 3.3).

To obtain the probability density function, vehicles are distributed in the domain uniformly and independently according to Poisson point process with intensity λ , where λ is the number of vehicles per unit area. In other words, given the density of each vehicle classes, vehicles are placed uniformly and independently without overlapping in a two-dimensional finite space, with intensity $\lambda = \rho_1 + \rho_2$. Here, ρ_1 and ρ_2 represent PTWs' and cars' areal density, i.e. vehicles per unit area, respectively. The Delaunay triangulation is constructed over the center of vehicles (see FIGURE 3.3), and the triangles edge length data from multiple simulation runs is used to estimate the probability density function (Figure 3.4).

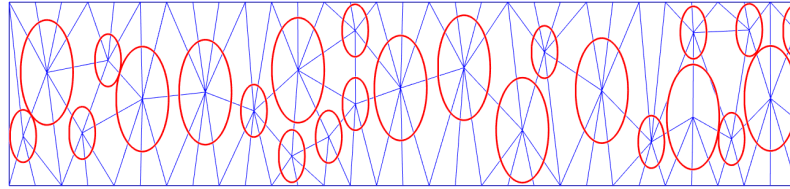


FIGURE 3.3: The implementation of Delaunay triangulation to define pore size

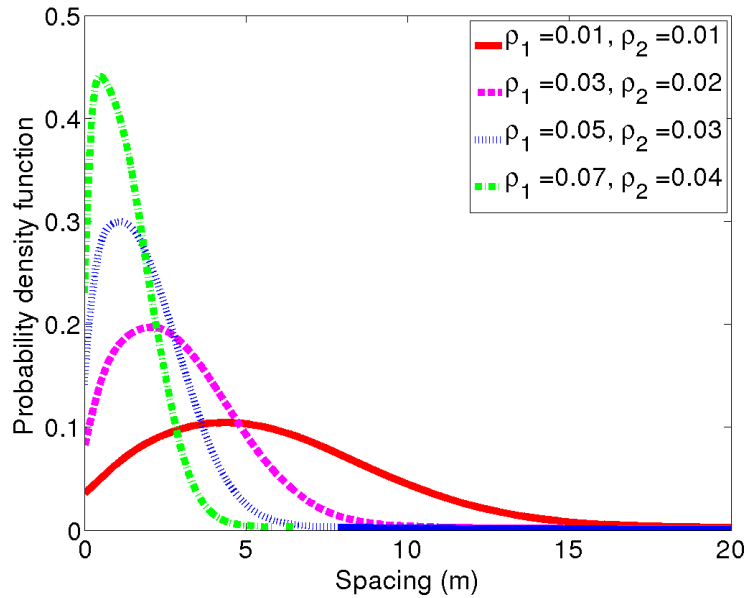


FIGURE 3.4: The obtained probability density function for different traffic compositions.

The parameters of the pore size distribution are estimated based on the statistical properties of Poisson point process. Let l_p be the edge length of a Delaunay triangle, then the mean values are given by (Miles, 1970)

$$E(l_p) = \frac{32}{9\pi\sqrt{\lambda}}, \quad E(l_p^2) = \frac{5}{\pi\lambda} \quad (3.5)$$

where λ is intensity (density) of the Poisson point process distribution.

We convert these formulations to our problem where we have circles, instead of points. When the points are replaced by circles (small circles for PTWs and large circles for cars), edge length measured for points is reduced by the sum of the radius of the circles the two end points of the edge are connected to. For instance, an edge connecting PTWs and cars is reduced by $R_1 + R_2$, where R_1 and R_2 are the radius of the circles representing PTWs and cars respectively.

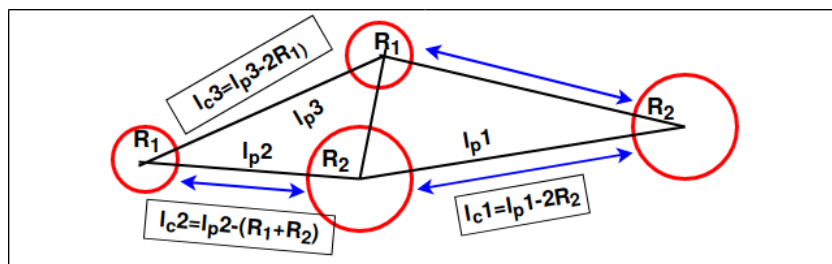


FIGURE 3.5: Delaunay triangle edges length for circles.

In accordance with the mean length of the Delaunay triangle edge over points, we define for circles as (FIGURE 3.5):

$$E[l_c] = E[l_p] - 2(R_1 p_1 + R_2 p_2), \quad (3.6)$$

$$E[l_c^2] = E[l_p^2] - 2E[l_p] (2(R_1 p_1 + R_2 p_2)) + (2(R_1 p_1 + R_2 p_2))^2, \quad (3.7)$$

where p_1 is probability for an edge to touch PTWs, and p_2 for cars. The probabilities are expressed in the form

$$p_i = \frac{\rho_i}{\rho_1 + \rho_2}, \quad i = 1, 2 \quad (3.8)$$

Therefore, equation (3.6) becomes

$$E(l_c) = \frac{32}{9\pi\sqrt{\rho_1 + \rho_2}} - \frac{2(R_1\rho_1 + R_2\rho_2)}{\rho_1 + \rho_2}. \quad (3.9)$$

The standard deviation and variance are the same for the case of points (σ_p^2) and circles (σ_c^2), thus

$$\sigma_c^2 = \sigma_p^2 = E(L_p^2) - E(L_p)^2 \approx \frac{3}{\pi^2(\rho_1 + \rho_2)}. \quad (3.10)$$

The above equations provide the parameters for the distribution function of inter-vehicle spacing. To determine a theoretical probability density function (PDF) that best fits the observed PDF, we use MATLAB's curve fitting tool, and the goodness of the fit is measured by R-square, sum of squared errors (SSE) and root mean square error (RMSE) values.

We consider left-truncated normal, log-normal and exponential as candidate distributions to characterize inter-vehicle spacing. The distributions are chosen based on qualitatively observed similarity on the shape of PDF curve. Besides, the exponential distribution is recommended in (Nair, Mahmassani, and Miller-Hooks, 2012) to characterize the inter-vehicle spacing distribution.

The comparison between the three selected theoretical distribution functions is shown in FIGURE 3.6. Based on the goodness of the fit results (see TABLE 3.1) left-truncated normal (LT-Normal) distribution conforms better to the estimated PDF than the other distributions. Further, it can be noted that the negative exponential assumption taken in (Nair, Mahmassani, and Miller-Hooks, 2012) is not fitting well.

	SSE	R-square	RMSE	SSE	R-square	RMSE
	$\rho_1 = 0.01, \rho_2 = 0.01$			$\rho_1 = 0.05, \rho_2 = 0.02$		
LT-normal	0.24	0.955	0.0069	0.97	0.938	0.0139
Log-normal	0.809	0.851	0.0127	2.67	0.831	0.023
Exponential	2.17	0.602	0.0208	4.05	0.744	0.028
	$\rho_1 = 0.02, \rho_2 = 0.05$			$\rho_1 = 0.1, \rho_2 = 0.01$		
LT-normal	3.21	0.853	0.025	1.46	0.993	0.017
Log-normal	5.51	0.748	0.033	4.07	0.813	0.028
Exponential	3.93	0.82	0.028	5.39	0.753	0.032

TABLE 3.1: Goodness of the fit measures obtained from the fitting experiments for different theoretical distributions.

Therefore, we assume that the spacing distribution follows the left-truncated normal distribution, having the form

$$f_{pTN}(l_p) = \begin{cases} 0 & l_p < 0 \\ \frac{f_p(l_p)}{\int_0^\infty f_p(l_p)} & l_p \geq 0 \end{cases} \quad \text{where } f_p = \frac{1}{\sqrt{2\pi}\sigma_c} \exp \frac{-(l_p - E(l_c))^2}{2\sigma_c^2}. \quad (3.11)$$

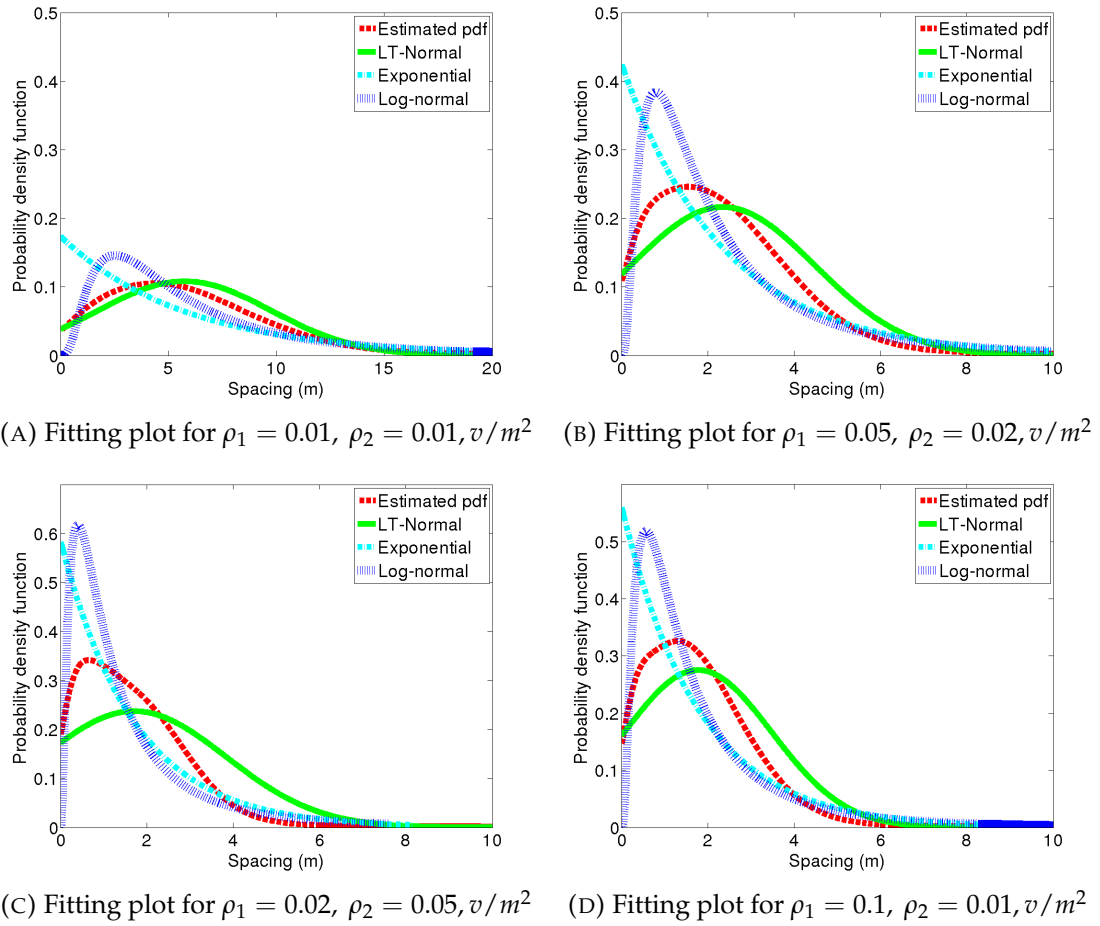


FIGURE 3.6: Comparison of estimated probability distribution function and fitting theoretical distributions for different vehicles composition

The inter-vehicle spacing distribution is dependent on the width (or the number of lanes) of the road space. This becomes more significant at lower traffic densities (see FIGURE B.3 in Appendix B). The shape of the inter-vehicle spacing distribution remains the same, but the parameters change. To include this property, the mean inter-vehicle spacing is redefined based on the $E(l_c)$ formula in equation 3.7 as

$$E(l_c^*) = E(l_c) \left(1 - \frac{1}{w^{\alpha_\rho}} \right) \quad (3.12)$$

where w stands for the width of the road space. The parameter α_ρ is expressed in relation to the traffic intensity so that the effect of road width diminishes with the increase of the traffic density (see FIGURE 3.7).

$$\alpha_\rho = \frac{1}{1 - (\rho_1 a_1 + \rho_2 a_2)} \quad (3.13)$$

where ρ and a denote, respectively, the density in vehicle per unit square and the projected area of a vehicle.

For the determination of the pore size, all the vehicles are distributed randomly. However, unlike PTWs, car drivers tend to respect lane demarcation. In what follows below, we relax the random assumption for cars by restricting the location of cars within the lanes only (FIGURE 3.8(b)). It appears that the probability density function obtained is almost similar to the disordered case (FIGURE 3.9).

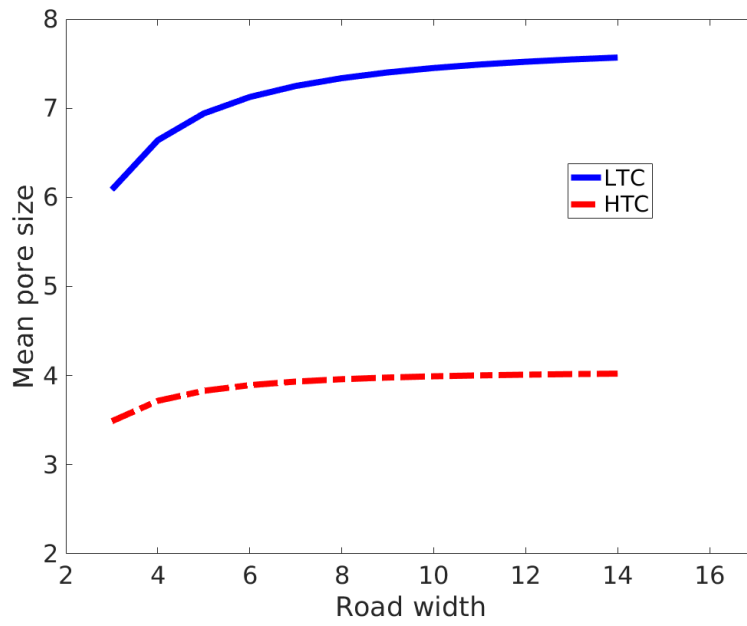
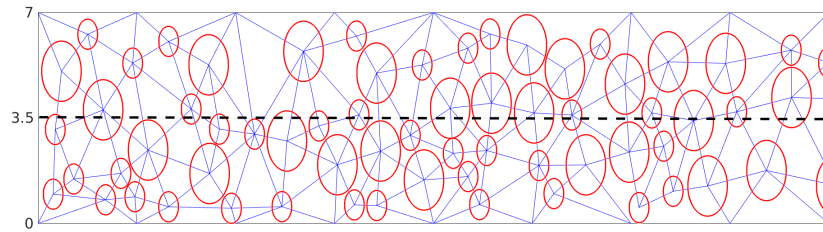
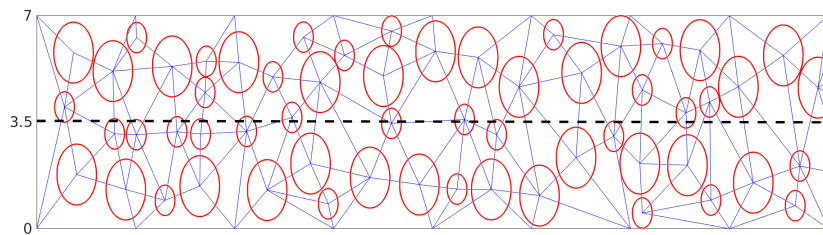


FIGURE 3.7: Example mean inter-vehicle spacing ($E(l_c^*)$) and road width relationship, where LTC and HTC represent light traffic condition ($\rho_1 = 0.04veh/m^2$, $\rho_2 = 0.08veh/m^2$) and heavy traffic condition ($\rho_1 = 0.08veh/m^2$, $\rho_2 = 0.12veh/m^2$, respectively)



(A)



(B)

FIGURE 3.8: Spatial distribution of vehicles in 2-lane road (A) disordered flow (B) semi-disorder flow where cars travel within the lane only and PTWs can occupy any position on the road

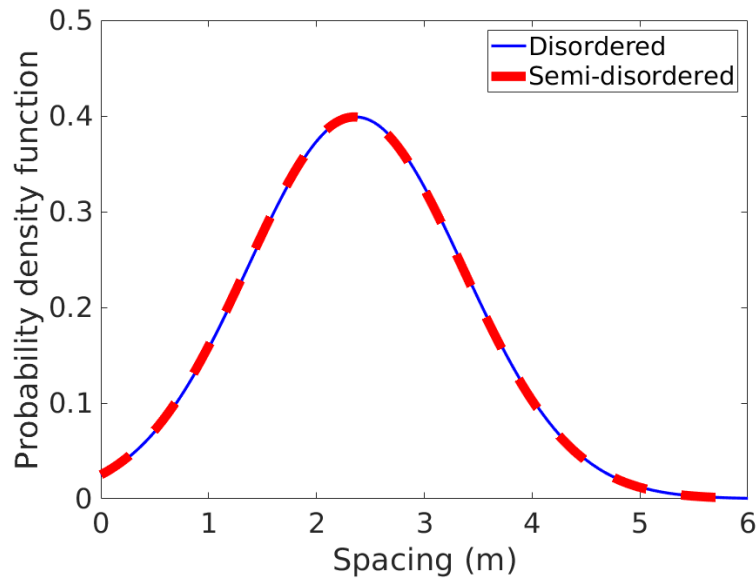


FIGURE 3.9: Probability density function produced from the two setting in 3.8

3.2.2 Speed function

Using the PDF function in equation (3.11), the speed-density relationship in equation (3.3) is re-written as

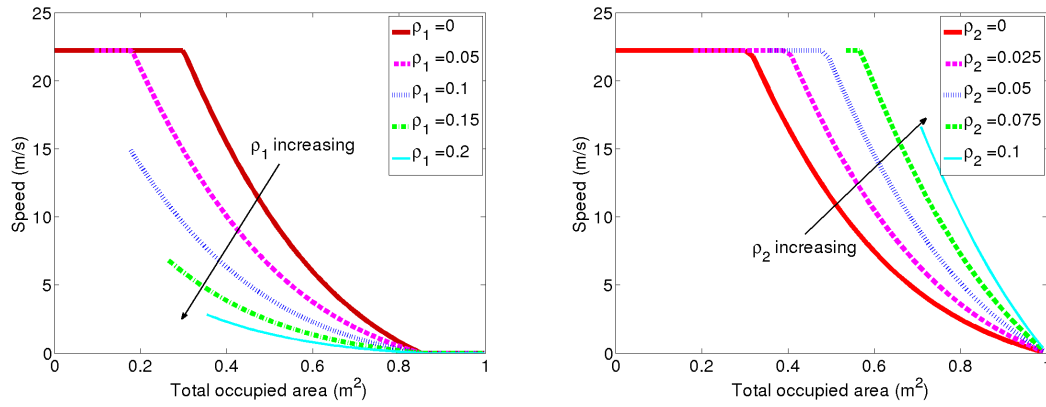
$$v_i = v_i^{max} \left(1 - \int_0^{r_i^{cr}} f_{pTN}(l_p) dl_p \right), \quad (3.14)$$

The limitation of equation (3.14) is that, because of the property of normal distribution function, the speed becomes zero only at infinite density, as for the speed function used in (Nair, Mahmassani, and Miller-Hooks, 2012). In attempt to overcome this infinite jam density, we have distinguished the jam area occupancy for the two classes, and the speed values are normalized to zero at the jam area occupancy. Beside the consideration of vehicles size, we selected the jam area occupancies for the two classes in such a way to allow filtering of PTWs through completely stopped cars traffic (Fan and Work, 2015). We distinguish the maximum total occupied area, which is the extreme total occupied areas corresponding to the null speed of a vehicle class, for the two classes in such a way that

$$V_2(a_{max}^2) = 0, V_1(a_{max}^2) > 0, V_2(a_{max}^1) = V_1(a_{max}^1) = 0, a_{max}^2 < a_{max}^1 \quad (3.15)$$

where V_2, V_1, a_{max}^2 and a_{max}^1 represent the speed of cars, the speed of PTWs, the maximum total occupied area of cars and the maximum total occupied area of PTWs, respectively. Accordingly, when the total area occupied by vehicles equals a_{max}^2 , while the average speed of PTWs is greater than zero, the cars completely stop. Due to this, PTWs can move through jammed car until the total area occupied by vehicles reaches to a_{max}^1 . On the grounds of the relation in equation (3.15) and some realistic conditions (see Appendix B.1), we approximate the jam area occupancy, i.e. $\rho_1 a_1 + \rho_2 a_2$, to 1 for PTWs and to 0.85 for cars, where ρ, a stand for density (veh/m^2) and projected area of vehicles (m^2), respectively.

Further modification is applied to the speed function in order to comply with triangular fundamental diagram theory, that is presence of two regimes, specifically, congestion and free flow regime (Gordon F Newell, 1993). In free flow there is no significant drop of average speed with the increase of density. However, beyond some critical density value, the average speed of vehicles decreases with density increase. Therefore, we



(A) Car speed at different density of PTWs. (B) PTWs speed at different cars density values.

FIGURE 3.10: Speed Vs total occupied area ($\sum \rho_1 A_1 + \sum \rho_2 A_2$), where $\rho_1 A_1$ and $\rho_2 A_2$ are area projected on the road by PTW and car, respectively.

adjust the speed functions to:

$$v_1 = \min \left\{ v_1^{max}, C v_1 v_1^{max} \left(1 - \frac{1}{N_1} \int_0^{r_1^{cr}} f_{pTN}(l) dl \right) \right\}, \quad (3.16)$$

$$v_2 = \min \left\{ v_2^{max}, C v_2 v_2^{max} \left(1 - \frac{1}{N_2} \int_0^{r_2^{cr}} f_{pTN}(l) dl \right) \right\}, \quad (3.17)$$

where N_i is a speed normalization factor and Cv is a scaling factor so that v_i equals the free flow speed at critical density in the presence of traffic of vehicle class i only.

The critical pore size depends on the traffic situation and the interacting vehicle classes (Ambarwati et al., 2014). The critical pore size accepted by vehicles when traveling at higher speed is larger than the critical pore size at lower speeds. To reproduce the critical pore size - speed proportionality (Minh, Sano, and Matsumoto, 2012), for example, we can formulate the critical pore size as:

$$r_i^{cr} = r_{min}^{cr} + r * (1 - (\rho_1 * a_1 + \rho_2 * a_2)),$$

where r_{min}^{cr} is the minimum critical pore size and r denotes the difference between the maximum and the minimum critical pore size. As such, the critical pore size increases with increasing speed or with decreasing vehicle class densities, which is in agreement with the gap acceptance theory.

To evaluate the impact of the critical pore on the speed function, we compare the result for a constant critical pore size, and a critical pore size scaled according to the actual traffic. As depicted in FIGURE 3.11, the critical pore size doesn't change the qualitative behavior of our fundamental diagram. Since the critical pore size does not have any qualitative implication, for simplicity we use a constant value.

After all the modifications, the speed-density relation look as shown in FIGURE 3.10. Different from the existing models which describe traffic composition in terms of total area/space occupancy (Nair, Mahmassani, and Miller-Hooks, 2012; Fan and Work, 2015; Benzoni-Gavage and Colombo, 2003), one of the key characteristics of our speed model is that it captures well the variation in traffic composition as the speed is expressed as a function of the density of each vehicle class. Specifically, for a given area occupancy, depending on the proportion of the vehicle classes, the speed value varies. For instance, for a given area occupancy, the higher the percentage of PTWs the higher becomes the number of vehicles, and the average pore size shrinks. In turn, the speed value decreases. The general properties of our speed model are summarized as follows:

1. A unique speed value is associated with a given total density and traffic composition.

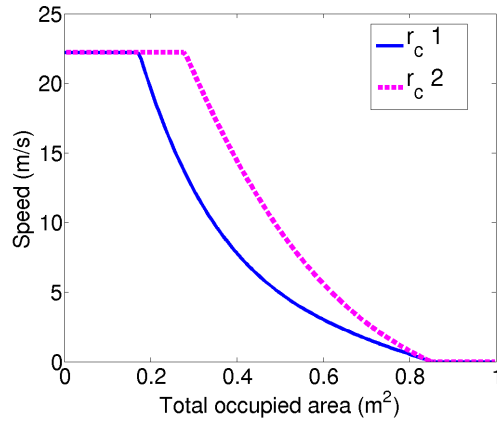


FIGURE 3.11: Speed vs total occupied area for constant critical pore size ($r_c^2 = 3m$) and a variable critical pore size (r_c^1) with the following parameters $r_c^{min} = 3m$ and $r = 2m$.

2. In free flow, vehicles move at constant (maximal) speed.
3. In congestion, speed decreases with increase of density.
4. Speed depends on the densities of the two vehicle classes and their proportion.
5. For the same occupancy area (total area occupied by vehicles) the more the share of PTWs is, the lower becomes the speed, which is the main property missed by multi-class models that define the speed function in terms of area occupancy.
6. Each class has a different fundamental relation
7. Each class has a distinctive critical and jam densities parameters.

None of the models known to us satisfies all the aforementioned properties, although there are models that satisfy a few of them. Property (3), (4) and (6) are common to most of multi-class LWR models. Nonetheless, models that describe speed as a function of total occupied space (Benzoni-Gavage and Colombo, 2003; Fan and Work, 2015; Chanut and Buisson, 2003; Nair, Mahmassani, and Miller-Hooks, 2012) do not satisfy property (1). While (J Van Lint, Serge Hoogendoorn, and Schreuder, 2008) satisfies property (1) and (Fan and Work, 2015) satisfies property (7), property (5) is unique to our model.

3.3 Flow equation

In the LWR model, traffic flow is assumed to be analogous to one-directional fluid motion. The motion of vehicles is governed by the conservation law, which is described using a system of differential equations. A Fixed or moving coordinate system is employed to describe the flow equation, which are named Eulerian or Lagrangian coordinates, respectively (see FIGURE 3.12). The two representations have different advantages. The Eulerian coordinate system is a simpler method. Yet, the Lagrangian representation has advantages in terms of computational efficiency and accuracy.

In regards to ITS applications, the the Lagrangian method follows vehicles, hence allows to study traffic phenomena at a finer detail. Moreover, with Lagrangian representation different traffic phenomena, which are difficult to study using the Eulerian method, can be studied, e.g., trajectory of vehicles. For the purpose of utilizing the benefits of both coordinate system, we formulate the flow equation in both representations.

3.3.1 Eulerian representation

The conservation law in Eulerian representation says that with no entering or leaving vehicles the number of vehicles between any two points is conserved. The variables

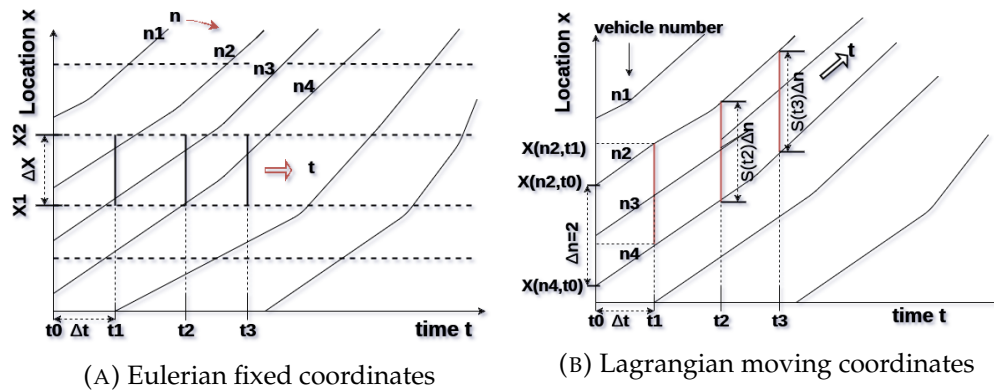


FIGURE 3.12: A schematic of Lagrangian and Eulerian approaches

are density, flow and average speed. In multi-class modeling, vehicles with identical characteristics are grouped into a class and a conservation law applies to each class. For two vehicle classes the conservation equation is written as

$$\frac{\partial \rho_i(x, t)}{\partial t} + \frac{\partial q_i(x, t)}{\partial x} = 0, \quad i = 1, 2, \quad (3.18)$$

where ρ_i and q_i denote density and flow of class i , respectively. The class specific flow, speed and density are related by the equation

$$q_i(x, t) = \rho_i(x, t)v_i(x, t), \quad i = 1, 2. \quad (3.19)$$

The equilibrium speed v_i for the individual vehicle class i is a function of the densities of both classes and satisfies the following conditions:

$$v_i = V_i(\rho_1, \rho_2), \quad \partial_1 V_i(\rho_1, \rho_2) \leq 0, \quad \partial_2 V_i(\rho_1, \rho_2) \leq 0, \quad (3.20)$$

where $\partial_1 V_i(\rho_1, \rho_2)$ and $\partial_2 V_i(\rho_1, \rho_2)$ denote $\frac{\partial V_i(\rho_1, \rho_2)}{\partial \rho_1}$ and $\frac{\partial V_i(\rho_1, \rho_2)}{\partial \rho_2}$, respectively. The interaction among vehicle classes is captured through the equilibrium speed. Moreover, the equilibrium speed is uniquely defined for all points of the space

$$S = \{(\rho_1, \rho_2) : \rho_1 \leq \rho_1^{jam}(\rho_1, \rho_2), \rho_2 \leq \rho_2^{jam}(\rho_1, \rho_2)\} \quad (3.21)$$

where $\rho_1^{jam}(\rho_1, \rho_2)$ and $\rho_2^{jam}(\rho_1, \rho_2)$ are the jam densities of vehicle class 1 (PTWs) and 2 (cars), respectively.

3.3.2 Lagrangian representation

In Lagrangian systems, the LWR model is formulated in (n, t) coordinate system (Leclercq, Jorge Andres Laval, and Chevallier, 2007). Cumulative vehicle count (n) is found to be more suitable for certain traffic flow analysis (Gordon F Newell, 1993; Ni, 2007), and also makes it easier to establish a connection between follow-the-leader and LWR models (Gordon Frank Newell, 2002). For a mixed traffic of cars and trucks, the Lagrangian formulation is given in (Leclercq and Jorge A Laval, 2009; Femke van Wageningen-Kessels, H. Van Lint, et al., 2010).

From an application standpoint, the Lagrangian representation is convenient to analyze vehicle-specific data such as trajectories and travel times. Using the spacing and speed data collected from probe vehicles together with the traffic flow model formulated in Lagrangian coordinate, traffic state can be estimated accurately (Yuan, JWC Van Lint, et al., 2012). Moreover, in hybrid traffic flow models, the Lagrangian representation is used in conjunction with the Eulerian representation (Leclercq, 2007).

The mathematical form of the conservation law in Lagrangian coordinates depends on the chosen coordinate system. Here, we take (n, t) coordinate system. Moreover,

there are two methods that are used to represent multi-class flows in Lagrangian coordinates.

In the first method, there are separate Lagrangian coordinates for each vehicles class (N-Lagrangian reference frames (N-LRFs)). On contrary, in the second method (1-Lagrangian reference frames (1-LRFs)) there is one Lagrangian reference frame that moves with one of the selected vehicle class. Thus, for the other vehicle classes the conservation equation is derived based on this Lagrangian reference frame. In a situations where tracking of each vehicle is needed (e.g for class specific controls (Yuan, FLM van Wageningen-Kessels, et al., 2011)) N-LRFs is suitable. Otherwise, 1-LRF is a computationally efficient approach, for instance to investigate the impact of PTWs on cars flow, or vice versa.

3.3.2.1 N-Lagrangian reference frames

Here, since we have two vehicle classes, there are two LRFs (i.e. N=2). By taking spacing and speed as state variables, the conservation equation in (n, t) coordinate system is written as (Leclercq, Jorge Andres Laval, and Chevallier, 2007):

$$\frac{\partial s_i(x(t), t)}{\partial t} + \frac{\partial v_i(n, t)}{\partial n} = 0 \quad i = 1, 2 \quad (3.22)$$

and

$$s = \frac{-\partial x}{\partial n}, \quad \rho = \frac{-\partial n}{\partial x} = 1/s \quad (3.23)$$

where s and v denote, respectively, the average spacing and the speed associated to a group of vehicle/s labeled n . The vehicle groups are labeled in time order. The conversation equation applies for each vehicle class. Moreover, the grouping of vehicle and the labeling of vehicle groups is done separately for each vehicle class. This representation also takes an assumption that vehicles in a group neither disband or merge with other groups. Class specific speed-spacing fundamental relation has the following form:

$$v_i = V_i(s_1, s_2) \quad (3.24)$$

The speed-spacing fundamental diagram (FD) for PTWs and cars are shown in FIGURE 3.13. As illustrated in the figures, the fundamental diagram for each class changes with the spacing/density of the other vehicle class.

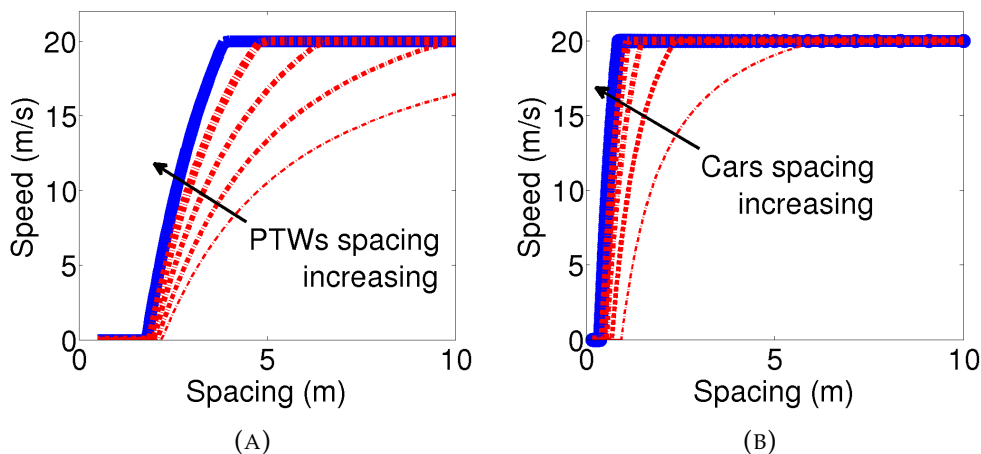


FIGURE 3.13: Speed-spacing fundamental diagram (a) for Cars (b) for PTWs, $V_{1,max} = V_{2,max} = 20 \text{ m/s}$

3.3.2.2 1-Lagrangian reference frame

In the above multi-class Lagrangian conservation equation, individual vehicle class has a separate labeling (cumulative vehicle count). (Femke van Wageningen-Kessels, H. Van Lint, et al., 2010) proposed an alternative formulation, where the Lagrangian coordinates move with a reference vehicle class and only vehicles of this class are counted. In other words, the evolution of traffic state variables of the carrier vehicle class and the other vehicle classes being carried inside is tracked.

The motion of the reference (carrier) class is governed by:

$$\frac{\partial s_r(x(t), t)}{\partial t} + \frac{\partial v_r(n, t)}{\partial n} = 0, \quad (3.25)$$

For the remaining vehicle classes:

$$\frac{\partial s_r/s_o}{\partial t} + \frac{\partial ((v_r - v_o)/s_o)}{\partial n} = 0, \quad (3.26)$$

or equivalently it can be formulated in non-conservative form

$$\frac{\partial s_o}{\partial t} + \frac{s_o}{s_r} \frac{\partial v_o}{\partial n} - \frac{v_o - v_r}{s_r} \frac{\partial s_o}{\partial n} = 0$$

where the subscript r and o refer to, respectively, the reference vehicle class and the other vehicle classes.

In the conservation equation given above, the traffic state variables are spacing (s) and speed (v). When density (ρ) is used instead of spacing, the flow equation takes the following form.

$$\frac{\partial (1/\rho_r)}{\partial t} + \frac{\partial v_r}{\partial n} = 0 \quad (3.27)$$

$$\frac{\partial (\rho_o/\rho_r)}{\partial t} + \frac{\partial (\rho_o(v_r - v_o))}{\partial n} = 0 \quad (3.28)$$

where $\rho_r > 0$ always.

3.4 Discretization scheme

A discretization (numerical) scheme is applied to approximate the solution of LWR model. That is, the continuity equations in equation (3.18), (3.22), (3.25) and (3.26), in conjunction with the fundamental relationship, need to be solved numerically. In the general discretization approach, the space (or vehicles) and time domain are divided into grid cells (or platoons) and time intervals, respectively.

The discretization schemes to solve the flow equation in the Eulerian and the Lagrangian representations are presented as follows.

3.4.1 Eulerian formulation

For the Eulerian representation, we apply a conservative finite volume method to approximate the numerical solution. In the approximation, the spatial domain is divided into equal grid cells of size Δx , and at each time interval Δt the density value in the domain is updated according to the conservation law. Rewriting in the integral form, it becomes

$$\frac{d}{dt} \int_{x_{i-1/2}}^{x_{i+1/2}} \rho(x, t) dx = q(\rho(x_{i-1/2}, t)) - q(\rho(x_{i+1/2}, t)) \quad (3.29)$$

Integrating equation (3.29) in time from t^n to $t^{n+1} = t^n + \Delta t$, we have

$$\int_{x_{i-1/2}}^{x_{i+1/2}} \rho(x, t^{n+1}) dx = \int_{x_{i-1/2}}^{x_{i+1/2}} \rho(x, t^n) dx + \int_{t^n}^{t^{n+1}} q(\rho(x_{i-1/2}, t)) dt - \int_{t^n}^{t^{n+1}} q(\rho(x_{i+1/2}, t)) dt. \quad (3.30)$$

After some rearrangement of equation (3.30), we obtain an equation that relates cell average density ρ_j^n update with average flux values at the cell interfaces.

$$\rho_i^{n+1} = \rho_i^n - \frac{\Delta t}{\Delta x} [F_{i+1/2}^n - F_{i-1/2}^n], \quad (3.31)$$

where $F_{i+1/2}^n$ is an average flux value at the cell interface $x = x_{i+1/2}$:

$$F_{i+1/2}^n = \mathcal{F}(\rho_i^n, \rho_{i+1}^n), \quad \text{where } \mathcal{F} \text{ is the numerical flux function.} \quad (3.32)$$

Accordingly, equation (3.31) rewrites

$$\rho_i^{n+1} = \rho_i^n - \frac{\Delta t}{\Delta x} [\mathcal{F}(\rho_i^n, \rho_{i+1}^n) - \mathcal{F}(\rho_{i-1}^n, \rho_i^n)]. \quad (3.33)$$

In the absence of a general Riemann solver, numerical methods for multi-class LWR model, based on a generalization of the cell transmission model (CTM), supply and demand functions for each vehicle class have been introduced in (FLM van Wageningen-Kessels, 2013; Fan and Work, 2015). However, these algorithms are computationally expensive to implement in our case due to the lack of an analytical expression for computing the numerical flux. Therefore, we have opted for the Lax-Friedrichs scheme (LeVeque, 1992), which is easier to implement and gives a good accuracy at sufficiently refined meshes. The numerical flux function is therefore given by

$$\mathcal{F}(\rho_i, \rho_{i+1}) = \frac{1}{2}(q(\rho_i) + q(\rho_{i+1})) + \frac{\alpha}{2}(\rho_i - \rho_{i+1}), \quad (3.34)$$

where α is the numerical viscosity satisfying the condition $\alpha \geq V_{max} = \max\{v_1^{max}, v_2^{max}\}$. The space and time steps Δx and Δt are selected to meet Courant, Friedrichs and Lewy (CFL) condition, which is a necessary condition for a numerical method to achieve stability and convergence. Therefore, Δt is chosen to satisfy $\Delta t \leq \Delta x / V_{max}$, due to the bounds on the eigenvalues derived in Section 4.1.

3.4.2 Lagrangian formulation

The discretization of the Lagrangian formulation is done by dividing the n (vehicle count) domain into platoons of size Δn . Then, the average spacing and the position of the platoons is updated at each time step Δt .

3.4.2.1 N-Lagrangian reference frames

To discretize the N-LRF formulation in equation (3.22), we apply the upwind method introduced by (Leclercq and Jorge A Laval, 2009). The n domain is subdivided into Δn sized clusters of vehicles (cells), which is done separately for each vehicle class. An approximation of the average spacing s over each cluster is updated at each time step Δt .

$$s_i^{t+\Delta t} = s_i^t - \frac{\Delta t}{\Delta n} (V_{i+1/2} - V_{i-1/2}) \quad (3.35)$$

where $V_{i+1/2}$ and $V_{i-1/2}$ are the fluxes (speeds) at the boundaries of cell i .

$$V_{i+1/2} = V(s_{1,i}, s_{2,i}, \dots), \quad V_{i-1/2} = V(s_{1,i-1}, s_{2,i-1}, \dots)$$

Therefore, equation (3.35) becomes

$$s_i^{t+\Delta t} = s_i^t - \frac{\Delta t}{\Delta n} (V(s_{1,i}, s_{2,i}, \dots) - V(s_{1,i-1}, s_{2,i}, \dots)) \quad (3.36)$$

which is similar to the direct difference approximation of the conservation equations. To obtain a stable solution Δt should be restricted to Courant-Friedrichs-Lewy (CFL) condition, i.e.

$$\Delta t \leq \frac{\Delta n}{\max(\lambda)}$$

where λ is the wave speed in vehicles per unit time.

For each vehicle class, clusters do not overlap each other. However, clusters of different vehicles class may overlap or occupy the same position. For example, in FIGURE 3.14 the second cluster of vehicle class 1 overlaps with two clusters (2 and 3) of the other vehicle class. To compute $V(s_{1,i}, s_{2,i})$, we need to approximate $s_{2,i}$ value in cluster i of vehicle class 1.

$$s_{2,i}^{(1)} = \frac{\Delta n_1 s_{1,i}}{\int_{X(i)}^{X(i-1)} \frac{1}{s_2(x)} dx}$$

where $s_2(x)$ is a function describing the average spacing s of class 2 as a function of location x . For the general case,

$$s_{c,i}^{(j)} = \frac{\Delta n_j s_{j,i}}{\int_{X(i)}^{X(i-1)} \frac{1}{s_c(x)} dx} \quad c = 1, 2, \dots \quad (3.37)$$

where j and c denote, respectively, the vehicle class cluster i belongs to and the other vehicle classes. For $j = c$, the integration is reduced to Δn_j , thus $s_{c,i}^{(j)} = \Delta s_{j,i}$.

Alternatively, each vehicle class can keep tracking the average spacing of the other vehicle classes inside the clusters of that vehicle class. In another words, a similar approach for 1-Lagrangian reference frame presented in Section 3.4.2.2 is applied.

For example, the average spacing of vehicle class 1 is updated according to the rule

$$s_{1,i}^{t+\Delta t} = s_{1,i}^t - \frac{\Delta t}{\Delta n} (V_{i+1/2} - V_{i-1/2}) \quad (3.38)$$

Then, the average spacing of class 2 vehicles inside the clusters of vehicle class 1 is updated following

$$\left(\frac{s_{1,i}}{s_{2,i}} \right)^{t+\Delta t} = \left(\frac{s_{1,i}}{s_{2,i}} \right)^t - \frac{\Delta t}{\Delta n} (V_{2,i+1/2} - V_{2,i-1/2}) \quad (3.39)$$

$$s_{2,i}^{t+\Delta t} = \frac{s_{1,i}^{t+\Delta t}}{\left(\frac{s_{1,i}}{s_{2,i}} \right)^{t+\Delta t}} \quad (3.40)$$

Similar procedures are employed for the other classes as well.

Following the definition of the flux (speed) at the boundary, the trajectory (position) X of each cluster can be updated using

$$X(i, t + \Delta t) = X(i, t) + \Delta t * V(s_{1,i}, s_{2,i}, \dots) \quad (3.41)$$

3.4.2.2 1-Lagrangian reference frame

In this approach, vehicles of the reference class are clustered into Δn sized groups. Then, the average spacing s of each vehicle class over the clusters of the reference class is updated at each time step Δt .

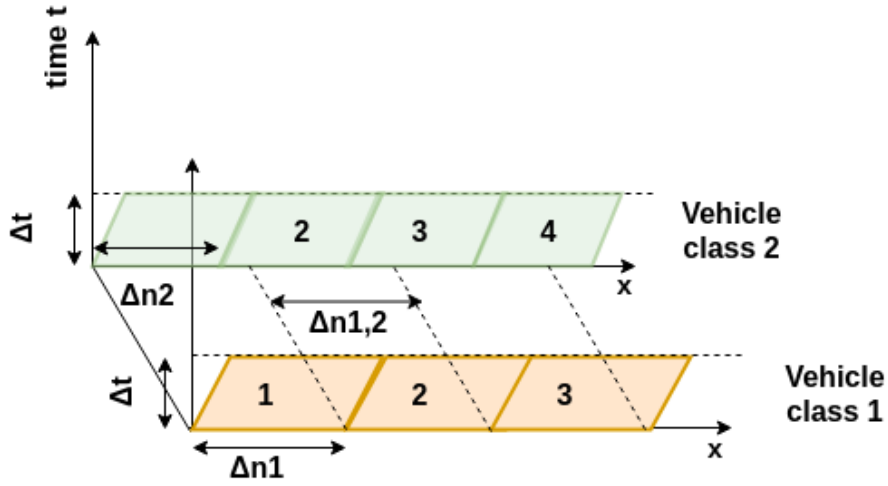


FIGURE 3.14: n-t domain discretization, separate coordinate for each vehicle class

For the reference class (r), the average spacing is updated following equation (3.36), and the trajectory is updated according to equation (3.41).

The average spacing of the other vehicle classes is updated according to:

$$\left(\frac{s_{r,i}}{s_{o,i}}\right)^{t+\Delta t} = \left(\frac{s_{r,i}}{s_{o,i}}\right)^t - \frac{\Delta t}{\Delta n} (V_{o,i+1/2} - V_{o,i-1/2}) \quad (3.42)$$

where $V_{o,i\pm 1/2}$ are the fluxes (speeds) at the cell boundaries. We give the definition of the fluxes based on the physical principle, which leads to the conservation law (see Appendix B.2).

When the speed of the reference class is always higher than the other classes ($v_r > v_o$), the direction of the fluxes is to the left. Thus,

$$\begin{aligned} V_{o,i+1/2} &= \frac{v_{r,i} - v_{o,i}}{s_{o,i}} \\ V_{o,i-1/2} &= \frac{v_{r,i-1} - v_{o,i-1}}{s_{o,i-1}} \end{aligned} \quad (3.43)$$

On the other hand, if ($v_r < v_o$), the direction of the fluxes is to the right (see FIGURE 3.15). This suggests that the fluxes should be defined as

$$\begin{aligned} V_{o,i+1/2} &= \frac{v_{r,i+1} - v_{o,i+1}}{s_{o,i+1}} \\ V_{o,i-1/2} &= \frac{v_{r,i} - v_{o,i}}{s_{o,i}} \end{aligned} \quad (3.44)$$

However, the flux definition in equation (3.44) is restricted to the situation where the fluxes through the edges are non-zero, i.e. $v_{o,i+1} > v_{r,i}$ and $v_{o,i} > v_{r,i-1}$.

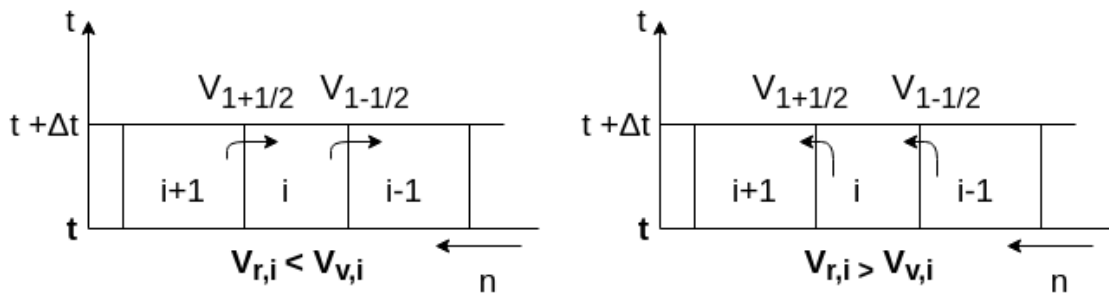


FIGURE 3.15: The direction of fluxes through the edges of the cluster

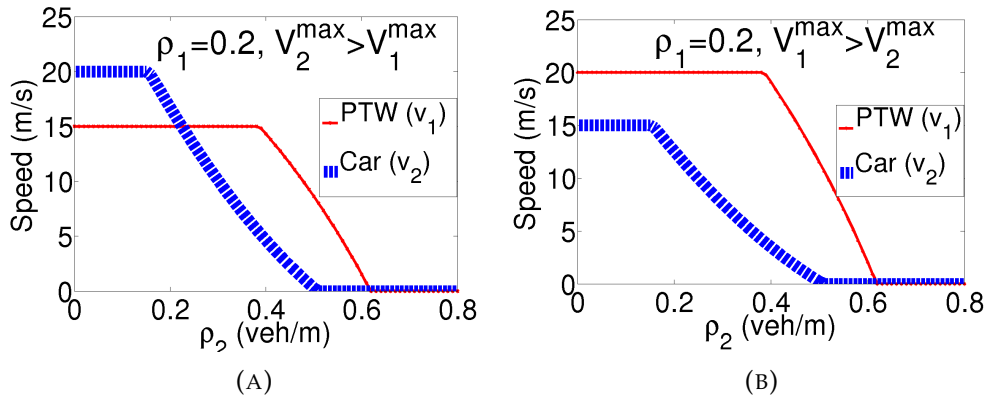


FIGURE 3.16: Speed-density relation for the case (a) maximum speed of Cars is greater than PTWs (b) maximum speed of PTWs is greater than cars, density of PTWs $\rho_1 = 0.2 \text{ veh/m}$

For traffic flow consisting of PTWs and cars, if the reference class is PTWs and PTWs have a higher free flow speed than cars (FIGURE 3.16(b)), the flux definition in equation (3.43) applies. Nonetheless, if the free flow speed of car is higher than PTWs (FIGURE 3.16(a)), whichever class is the reference class, we have both conditions, i.e. $v_r > v_o$ and $v_o > v_s$, depending on the traffic state. For this reason, we give a general definition for the fluxes, which applies irrespective of the order of the vehicle classes speeds.

Condition 1: If $v_{r,i} < v_{o,i}$,

Vehicles of class o can enter from cluster $i + 1$ to i , at the boundary $i + 1/2$, only if $v_{r,i} < v_{o,i+1}$. Vehicles of class o can enter from cluster i to $i - 1$, at the boundary $i - 1/2$, only if $v_{r,i-1} < v_{o,i}$. At the same time, class o vehicles in cluster $i - 1$ may enter to i if $v_{r,i-1} < v_{o,i-1}$. Accordingly, the flux at the boundaries are defined as:

$$\begin{aligned} V_{o,i+1/2} &= \min \left(0, \frac{(v_{r,i} - v_{o,i+1})}{s_{o,i+1}} \right) \\ V_{o,i-1/2} &= \min \left(0, \frac{(v_{r,i-1} - v_{o,i})}{s_{o,i}} \right) - \min \left(0, \frac{(v_{r,i-1} - v_{o,i-1})}{s_{o,i-1}} \right) \end{aligned} \quad (3.45)$$

Condition 2: If $v_{r,i} > v_{o,i}$,

At the boundary $i + 1/2$, class o vehicles leave cluster i with a flux of $\frac{(v_{r,i} - v_{o,i})}{s_{o,i}}$. In addition, class o vehicles from $i + 1$ may enter to i if $v_{o,i+1} > v_{r,i}$. At the boundary $i - 1/2$, class o vehicles from $i - 1$ can enter to i only if $v_{r,i-1} > v_{o,i-1}$. Accordingly, the flux at the boundaries are defined as:

$$\begin{aligned} V_{o,i+1/2} &= \frac{(v_{r,i} - v_{o,i})}{s_{o,i}} - \max \left(0, \frac{(v_{r,i} - v_{o,i+1})}{s_{o,i+1}} \right) \\ V_{o,i-1/2} &= \max \left(0, \frac{(v_{r,i-1} - v_{o,i-1})}{s_{o,i-1}} \right) \end{aligned} \quad (3.46)$$

Thus, equation (3.45) and (3.46) can be used to discretize equation (3.26).

3.5 Numerical Test

In this section, we evaluate the developed discretization schemes. To test the validity and accuracy of the discretization schemes, we compare the numerical results obtained with the Eulerian approach and the two Lagrangian methods.

3.5.1 Test setup

For the simulation experiment, the parameters in TABLE 3.2 are used.

TABLE 3.2: simulation settings

Maximum speed of cars	15m/s
Maximum speed of PTWs	20m/s
vehicle cluster size	7.5 vehicles
Time step	0.125 s
Space steps (Eulerian)	10m
Road length	3000m
lane width	3.5 m
Number of lanes	1
Simulation time	45s

Lax-friedrich discretization scheme is employed to solve the Eulerian conservation equations. We assume identical initial densities for the two vehicle classes, i.e. cars (ρ_2) and PTWs (ρ_1), where $\rho_1 = \rho_2 = 0.15 \text{ veh}/m$, for $x \in [0, 1400 \text{ m}]$ and $\rho_1 = \rho_2 = 0.3 \text{ veh}/m$, otherwise.

3.5.2 Results

The evolution of the initial density as described by the Eulerian and the Lagrangian approaches is presented in FIGURE 3.17. For the 1-LRF approach we consider two cases by changing the reference class. Lag. 1 stands for the result when PTWs are the reference class, and Lag. 2 stands for the results when cars are the reference class. Lag. 3 represents the result obtained from n-LRF approach. In these cases, the fundamental diagram takes the shape in FIGURE 3.16(b).

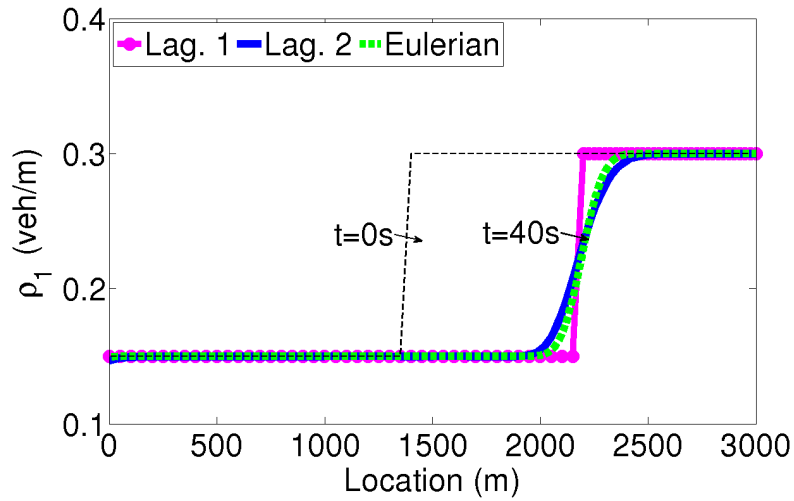
The density wave of PTWs and cars at time $t = 40 \text{ s}$ are depicted in FIGURE 3.17(a) and 3.17(b), respectively. As can be seen, the results are close to each other except the difference at the upstream and the downstream shock fronts. With this, we can prove the validity of the proposed discretization scheme for the case where the slower vehicle is the reference vehicle class (shown by Lag. 2).

Furthermore, the comparison of the two Lagrangian methods (1-LRF and N-LRFs) is presented in FIGURE 3.18. The density waves for cars and PTWs are shown in FIGURE 3.18(b) and 3.18(a). The figures illustrate that N-LRFs (Lag. 3) produces a more accurate result than 1-LRF (Lag. 1 and Lag. 2) approach. Specifically, at the high density to low density and low density to high density transition points numerical error are observed for the case of Lag. 1 and Lag. 2.

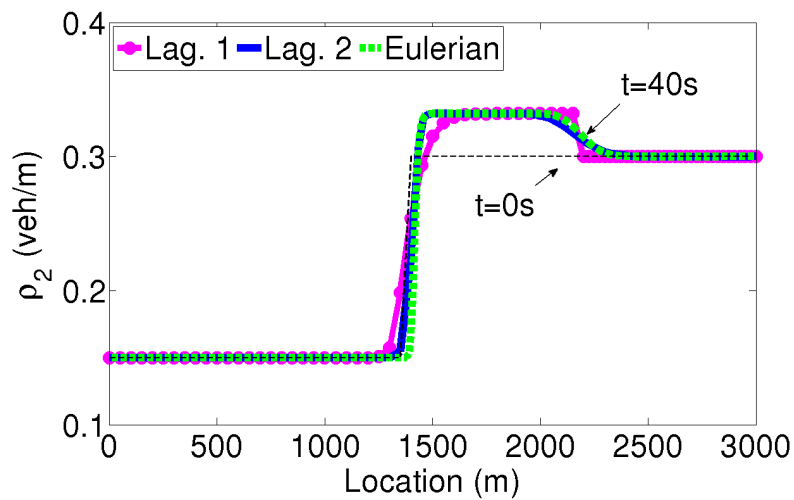
From the result one can deduce that, of the two multi-class Lagrangian representation methods, the N-LRFs approach produces a more accurate result than the 1-LRF approach. However, N-LRFs method is computationally less efficient. Because, beside updating the traffic state of the clusters of each vehicle class, it is also required to approximate the average spacing of the other vehicle class in the clusters of a given vehicle class.

We also test the proposed generic discretization scheme, for 1-LRF. For this experiment, we consider the fundamental digram in FIGURE 3.16(a), and the maximum speed of cars = $20 \text{ m}/s$ and the maximum speed of PTWs = $15 \text{ m}/s$. The rest simulation parameters and the initial density are identical to the the previous experiments. The evolution of cars and PTWs density waves is shown in FIGURE 3.19. According to the result obtained, the evolution is correctly described by the proposed scheme. This proves that the developed discretization scheme can produce the density evolution correctly.

The developed general discretization method for 1-LRF approach not only applies for a mixed flow of cars and PTWs, but also for any type of multi-class flow.

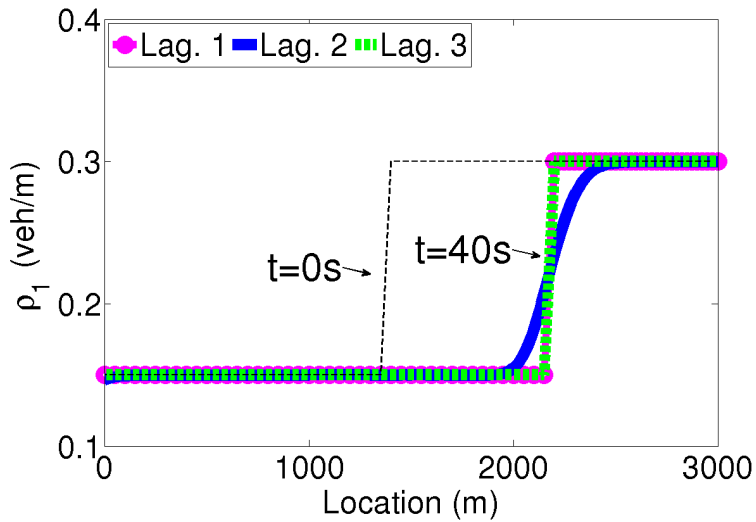


(A) PTW density wave

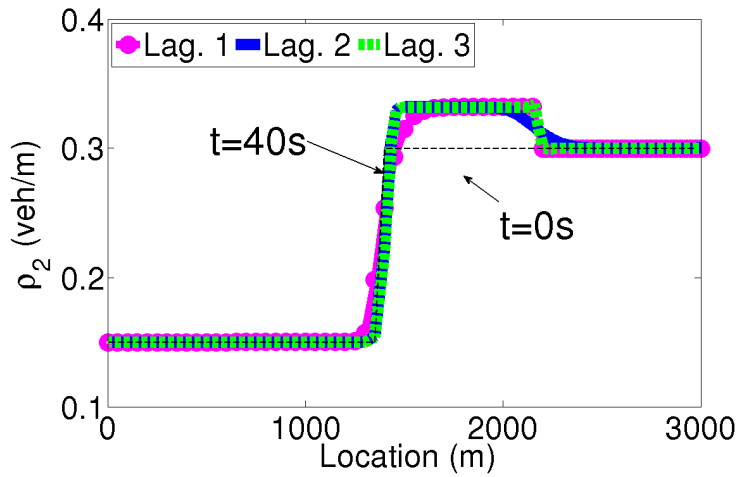


(B) Car density wave

FIGURE 3.17: The Lagrangian representations, when PTWs are the reference class (Lag. 1) and cars are the reference class (Lag. 2), vs. the Eulerian representation



(A) PTW density wave



(B) Car density wave

FIGURE 3.18: The comparison between the two Lagrangian methods, (Lag. 1, Lag.2) represent the 1-LRF approach and (Lag. 3) represent the n-LRF approach.

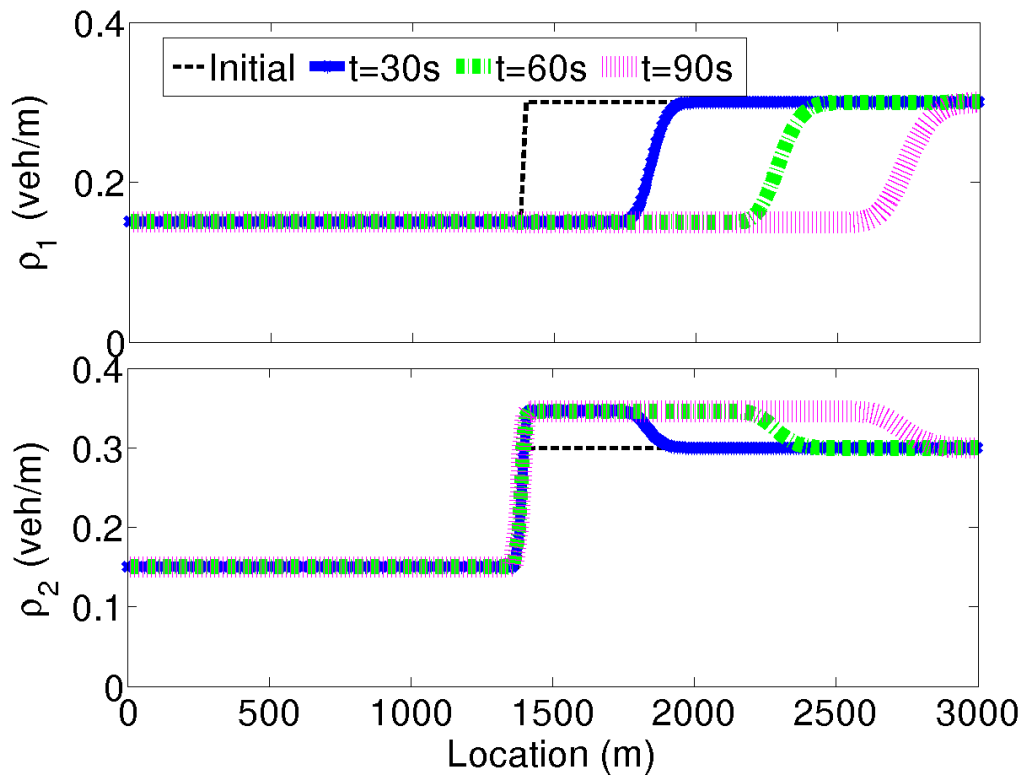


FIGURE 3.19: The density waves of PTWs (upper subplot) and cars (lower subplot), result produced using the general discretization scheme for 1-LRF approach

Microscopic description in Lagrangian representation

In this experiment, we apply the Lagrangian representation to track individual vehicle. The movement of vehicles is governed by the macroscopic rules.

In continuum flow model, Δn can take any positive value. However, a follow-the-leader type flow is observed when $\Delta n = 1$. In the discretization scheme, grouping is done per vehicle classes base, which perfectly works for traffic flows obeying lane discipline. However, when we have two-wheelers, which do not respect such an ordered flow, a special treatment is required. The reason is that, in the discretization, clusters of the same vehicle class are not allowed to overlap or occupy the same position. Consequently, the parallel movement of two-wheelers cannot be modeled properly. Thus, we integrate the side-by-side movement of two-wheelers by introducing sub-lanes. It is also assumed that, PTWs stay in the lane, i.e. there is no (sub-) lane change. Accordingly, two-wheelers in a sub-lane adhere to the follow-the-leader principle (see FIGURE 3.20).

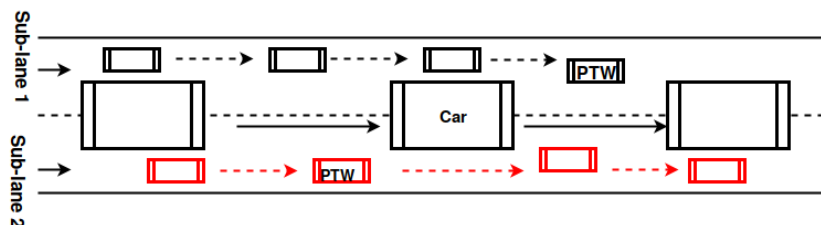


FIGURE 3.20: The schematic of sub-lane in Lagrangian representation, one-lane road and two sub-lanes for PTWs

$$X(i, t + \Delta t) = X(i, t) + \Delta t * V \quad (3.47)$$

The location of the vehicles is updated following equation (3.47). With this approach,

the behavior of each vehicle class can be analyzed at a fine-grained level. Further, additional vehicle (or vehicle class) specific rules also can be incorporated, making it a suitable and efficient solution for dealing with cooperative intelligent transport system (C-ITS) applications.

For the experiment, to track the interaction between vehicle classes at different traffic situations, a traffic light is located at 400 m, which stays red for the period $t \in [0, 40 \text{ s}]$. PTWs have two sub-groups (sub-lanes), and the clustering of each sub-groups is done separately. As can be observed from the overlapping trajectories of PTWs, by introducing sub-lanes the side by side movement of PTWs, in the same lane, can be reproduced (see the red and the black trajectory lines). Nevertheless, since the macroscopic laws are applied to define the microscopic movement of vehicles, some of the properties may not be described correctly. For example, PTWs are segregated into sub-lanes in order to avoid the overlap of vehicles in the same sub-lane. However, the macroscopic law allows the abreast movement of PTWs, thus the trajectory of PTWs in the same lane may overlap when the leader PTWs completely stops (see FIGURE 3.21, the two black trajectory line overlap around location $\approx 110 \text{ m}$, time $\approx 20 \text{ s}$). In fact, the required behavior can be produced by integrating new rules, beside the macroscopic law.

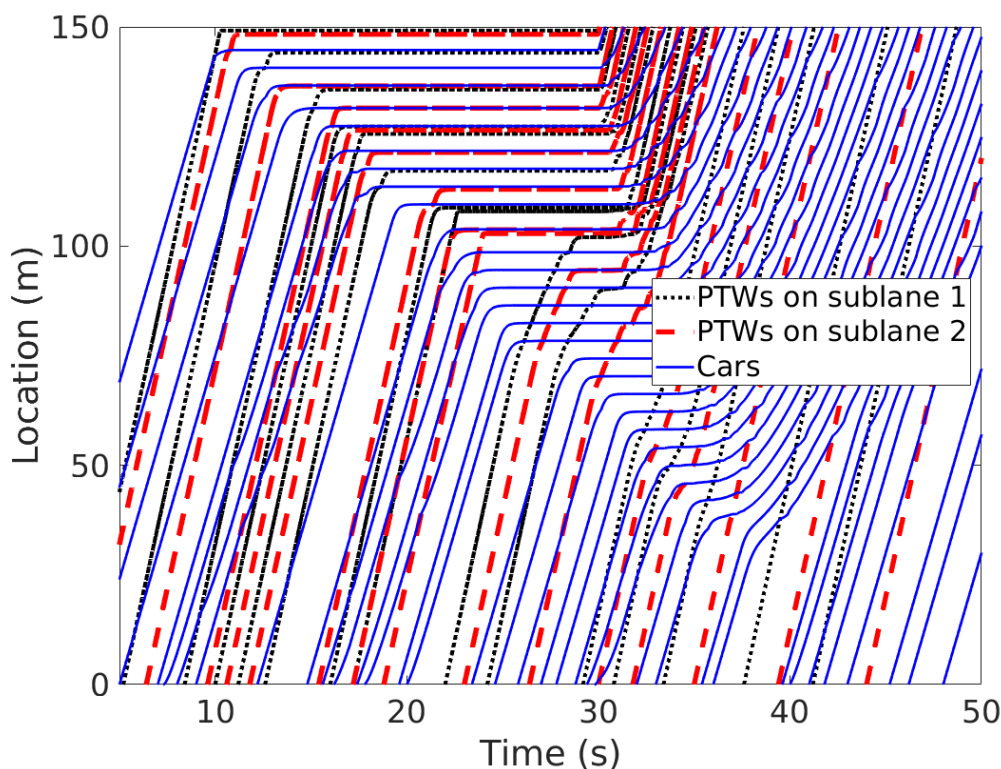


FIGURE 3.21: Trajectories of vehicles, two sub-lanes for PTWs

Tracking the trajectory of individual vehicle is one of the capabilities of the Lagrangian representation, which is impossible with the Eulerian method.

3.6 Summary and conclusion

In this chapter, a macroscopic model for traffic flow consisting of cars and PTWs is developed. The model follows the kinematic (LWR) theory, which treats traffic flow in analogy to the motion of fluid. The required model properties are set out. We apply an approach that leads to recreating the needed properties.

The interaction between the two vehicle types and the motion properties of each vehicle are modeled in the framework of fluid flow in porous medium. The road space is considered as a porous medium, wherein, intuitively, the vehicles are the solid particles that form the pores and the pores are the inter-vehicle spacing. We introduce

an approximation method to characterize the inter-vehicle spacing distribution. The distribution is determined by fitting the actual inter-vehicle spacing distribution with standard distributions. Truncated normal distribution is found to be best fitting distribution. We derive a formulation for the estimation of the distribution parameters. The parameters definition effectively captures the variation in traffic composition and road width or number of lanes.

The fundamental relation (speed-density) for each vehicle class is given by

$$v_i = \min \left\{ v_i^{max}, C v_i v_i^{max} \left(1 - \frac{1}{N_i} \int_0^{r_i^{cr}} f_{pTN}(l_p) dl_p \right) \right\},$$

Where f_{pTN} is the truncated normal distribution function, which represents the inter-vehicle spacing distribution.

$$f_{pTN}(l_p) = \begin{cases} 0 & l_p < 0 \\ \frac{f_p(l_p)}{\int_0^\infty f_p(l_p)} & l_p \geq 0 \end{cases} \quad \text{where } f_p = \frac{1}{\sqrt{2\pi}\sigma_c} \exp \frac{-(l_p - E(l_c))^2}{2\sigma_c^2}.$$

The parameter of the distribution function are defined as follows:

$$E(l_c) = \left(\frac{32}{9\pi\sqrt{\rho_1 + \rho_2}} - \frac{2(R_1\rho_1 + R_2\rho_2)}{\rho_1 + \rho_2} \right) \left(1 - \frac{1}{w^{\alpha_\rho}} \right) \quad \alpha_\rho = \frac{1}{1 - (\rho_1 a_1 + \rho_2 a_2)}$$

$$\sigma_c^2 = \frac{3}{\pi^2(\rho_1 + \rho_2)}.$$

To incorporate different vehicle types in the model, we apply the multi-class LWR modeling approach. The vehicles are grouped into classes based on their physical and maneuvering characteristics. The equation for the motion of vehicles is formulated with respect to a fixed reference frame, Eulerian, and a moving reference frame, Lagrangian.

The representation of the flow equation in the Eulerian coordinate system is written as:

$$\frac{\partial \rho_i(x, t)}{\partial t} + \frac{\partial q_i(x, t)}{\partial x} = 0, \quad i = 1, 2,$$

The representation of the flow equation in the Lagrangian coordinate system is written into two different forms.

- The N-LRF approach, wherein there is one reference frame for each vehicle class, writes as:

$$\frac{\partial s_i(x(t), t)}{\partial t} + \frac{\partial v_i(n, t)}{\partial n} = 0 \quad i = 1, 2$$

- The 1-LRF approach, wherein the flow equation is derived according to a reference frame that moves with the reference vehicle class, writes as:

$$\text{Reference vehicle class (r):- } \frac{\partial s_r(x(t), t)}{\partial t} + \frac{\partial v_r(n, t)}{\partial n} = 0,$$

$$\text{The rest vehicle classes (o):- } \frac{\partial s_r/s_o}{\partial t} + \frac{\partial ((v_r - v_o)/s_o)}{\partial n} = 0,$$

A discretization scheme to approximate the solution of the flow equation is developed. The scheme is established based on the physical principles. The developed numerical schemes are validated numerically. Furthermore, we show the microscopic description in the Lagrangian representation, based on the macroscopic behavioral laws.

The discretization method for the Eulerian representation has the following form:

$$\rho_i^{n+1} = \rho_i^n - \frac{\Delta t}{\Delta x} [\mathcal{F}(\rho_i^n, \rho_{i+1}^n) - \mathcal{F}(\rho_{i-1}^n, \rho_i^n)].$$

$$\mathcal{F}(\rho_i, \rho_{i+1}) = \frac{1}{2}(q(\rho_i) + q(\rho_{i+1})) + \frac{\alpha}{2}(\rho_i - \rho_{i+1}),$$

The discretization methods for the Lagrangian representation:

- The N-LRF approach is described by:

$$s_i^{t+\Delta t} = s_i^t - \frac{\Delta t}{\Delta n} (V(s_{1,i}, s_{2,i}, \dots) - V(s_{1,i-1}, s_{2,i-1}, \dots))$$

The average spacing of the other vehicle class (c) inside the cluster (i) of a given vehicle class j is approximated by:

$$s_{c,i}^{(j)} = \frac{\Delta n_j s_{j,i}}{\int_{X(i)}^{X(i-1)} \frac{1}{s_c(x)} dx} \quad c = 1, 2, \dots$$

- The discretization scheme for the 1-LRF approach is written as:

Reference vehicle class (r)-: $s_i^{t+\Delta t} = s_i^t - \frac{\Delta t}{\Delta n} (V(s_{1,i}, s_{2,i}, \dots) - V(s_{1,i-1}, s_{2,i}, \dots))$

The rest vehicle classes (o)-: $\left(\frac{s_{r,i}}{s_{o,i}}\right)^{t+\Delta t} = \left(\frac{s_{r,i}}{s_{o,i}}\right)^t - \frac{\Delta t}{\Delta n} (V_{o,i+1/2} - V_{o,i-1/2})$

If $v_{r,i} < v_{o,i}$,

$$V_{o,i+1/2} = \min\left(0, \frac{(v_{r,i} - v_{o,i+1})}{s_{o,i+1}}\right)$$

$$V_{o,i-1/2} = \min\left(0, \frac{(v_{r,i-1} - v_{o,i})}{s_{o,i}}\right) - \min\left(0, \frac{(v_{r,i-1} - v_{o,i-1})}{s_{o,i-1}}\right)$$

If $v_{r,i} > v_{o,i}$,

$$V_{o,i+1/2} = \frac{(v_{r,i} - v_{o,i})}{s_{o,i}} - \max\left(0, \frac{(v_{r,i} - v_{o,i+1})}{s_{o,i+1}}\right)$$

$$V_{o,i-1/2} = \max\left(0, \frac{(v_{r,i-1} - v_{o,i-1})}{s_{o,i-1}}\right)$$

In the next chapter (Chapter 4), we analyze the model properties. Furthermore, the qualitative behavior of the model is assessed against the realistic traffic phenomena. The model parameters are refined and the model is validated.

Chapter 4

Model analysis and comparison

This chapter presents the analysis of the model properties. The developed model is evaluated against the requirements set out in Chapter 3. Furthermore, the mathematical property of the model is analyzed. To verify the qualitative characteristics of the model, we compare the model with similar models, as well as we test the model behavior against the known real-world traffic phenomena.

For the model development different assumptions and approximation methods are introduced. In order to validate the assumption and improve the descriptive capability of the model, the model is calibrated and validated. Due to the lack of real data that can be used for the calibration and validation of the model, we utilize synthetic data obtained from Vissim. In the calibration process, the model parameters are adapted to represent the observed traffic characteristics. The validation phase is intended to investigate the validity of the assumptions and the applicability of the model. For the validation, the model parameters optimized in the calibration phase are employed. We use different data for the calibration and the validation of the model.

The chapter is organized as follows. In the first section (Section 4.1), the mathematical properties of the model is presented. Then, in the next section (Section 4.2), the property of the fundamental diagrams in relation to the model requirements in Chapter 3 is analyzed. Section 4.3 describes the verification of the model, as well as the comparison with other models. The calibration and validation of the model is discussed in Section 4.4. Finally, Section 4.5 concludes the chapter.

4.1 Mathematical properties of the model

To describe the solution of the system equations (3.18)-(3.20) in terms of wave motion, the jacobian matrix Dq of $q = (q_1, q_2)$ should be diagonalizable with real eigenvalues, in another words, the system has to be hyperbolic. We can prove the hyperbolicity by showing that the system is symmetrizable, i.e. there exists a positive-definite matrix S such that SDq is symmetric (see (Benzoni-Gavage and Colombo, 2003)).

Re-writing the system in the form:

$$\frac{\partial \rho}{\partial t} + Dq(\rho) \frac{\partial \rho}{\partial x} = 0,$$

where

$$\rho = \begin{bmatrix} \rho_1 \\ \rho_2 \end{bmatrix} \quad \text{and} \quad q(\rho) = \begin{bmatrix} \rho_1 v_1(\rho) \\ \rho_2 v_2(\rho) \end{bmatrix},$$

the Jacobian matrix of $q(\rho)$ is given by:

$$Dq(\rho) = \begin{bmatrix} \frac{\partial(\rho_1 v_1)}{\partial \rho_1} & \frac{\partial(\rho_1 v_1)}{\partial \rho_2} \\ \frac{\partial(\rho_2 v_2)}{\partial \rho_2} & \frac{\partial(\rho_2 v_2)}{\partial \rho_1} \end{bmatrix} = \begin{bmatrix} \rho_1 \partial_1(v_1) + v_1 & \rho_1 \partial_2(v_1) \\ \rho_2 \partial_1(v_2) & \rho_2 \partial_2(v_2) + v_2 \end{bmatrix}$$

For $\rho_1 > 0, \rho_2 > 0$,

$$S = \begin{bmatrix} \frac{1}{\rho_1 \partial_2(v_1)} & 0 \\ 0 & \frac{1}{\rho_2 \partial_1(v_2)} \end{bmatrix} \quad (4.1)$$

is a symmetrizer of Dq , thus the system satisfies the hyperbolicity condition.

The eigenvalues of the Jacobian representing information propagation (characteristic) speed are given by:

$$\lambda_{1,2} = \frac{1}{2} \left[\alpha_1 + \alpha_2 \pm \sqrt{(\alpha_1 - \alpha_2)^2 + 4\rho_1 \rho_2 \partial_2(v_1) \partial_1(v_2)} \right],$$

where

$$\alpha_1 = \rho_1 \partial_1(v_1) + v_1, \quad \alpha_2 = \rho_2 \partial_2(v_2) + v_2.$$

Following (Benzoni-Gavage and Colombo, 2003, Proposition 3.1) it is possible to show that

$$\lambda_1 \leq \min\{\alpha_1, \alpha_2\} \leq \min\{v_1, v_2\} \text{ and } \min\{v_1, v_2\} \leq \lambda_2 \leq \max\{v_1, v_2\}, \quad (4.2)$$

where, we have taken $\lambda_1 \leq \lambda_2$.

The proof in (Benzoni-Gavage and Colombo, 2003) assumes that $V_1 > V_2$ to exclude the degenerate case, when $V_1 = V_2$. However, Zhang et al. (P. Zhang et al., 2006) also studied the properties of a similar model as in (Benzoni-Gavage and Colombo, 2003), but here for a generic speed function which is expressed as a function of total density, i.e. $v_i = v_i(\rho)$, where $\rho = \sum_i \rho_i$. Accordingly, it is proved that for $v_1 < v_2 < v_3 \dots < v_m$, the eigenvalues are bounded such that $\lambda_1 < v_1 < \lambda_2 < v_2 < \lambda_3 < \dots < v_m - 1 < \lambda_m < v_m$ (refer (P. Zhang et al., 2006, Theorem 3.1, Lemma 2.2, Lemma 2.3)).

Due to the complexity of the dependency of the speed function on vehicle class densities, we could not follow a similar analytical approach. Nonetheless, we have checked the validity of this relationship, i.e. $\lambda_1 < v_1 < \lambda_2 < v_2 < \lambda_3 < \dots < v_m - 1 < \lambda_m < v_m$, using a graphical analysis, by taking a specific case where $v_1 > v_2$ is not true in all permissible traffic states. In our model, $v_1 > v_2$ is not always satisfied when the maximum speed of cars is higher than PTWs'. Hence, for the test, the maximum speed of cars is set to be greater than the maximum speed of PTWs.

Let $\lambda_1 = \min\{\lambda_1, \lambda_2\}$ and $\lambda_2 = \max\{\lambda_1, \lambda_2\}$, if the relation $\lambda_1 < \min\{v_1, v_2\} < \lambda_2 < \max\{v_1, v_2\}$ holds, then $\max\{v_1, v_2\} - \lambda_2 > 0$, $\min\{v_1, v_2\} - \lambda_2 < 0$ and $\min\{v_1, v_2\} - \lambda_1 > 0$.

FIGURE 4.1(a) shows that $\max(v_1, v_2) - \lambda_2 > 0$, implying $\lambda_2 < \max(v_1, v_2)$. From FIGURE 4.1(b) it can be learned that $\min(v_1, v_2) - \lambda_2 < 0$, thus $\min(v_1, v_2) < \lambda_2$. FIGURE 4.2 shows that $\min(v_1, v_2) - \lambda_1 > 0$ over all point in $S = \{\rho_1, \rho_2\}$, thus $\lambda_1 < \min(v_1, v_2)$.

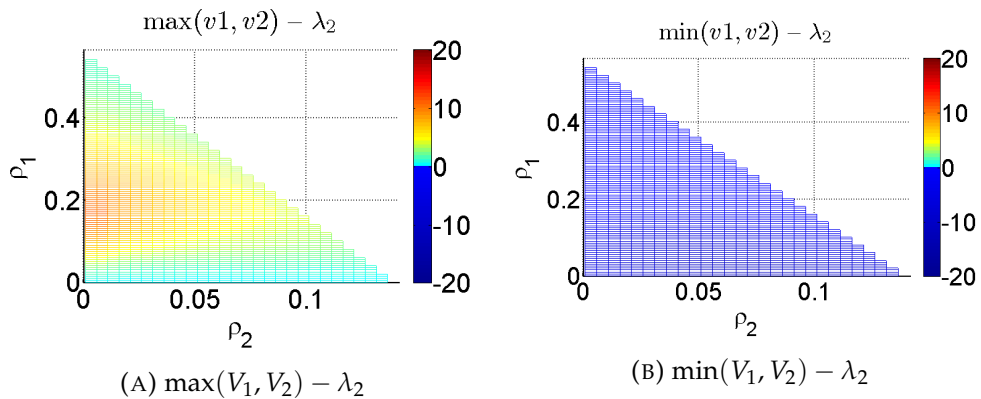


FIGURE 4.1: Evaluation of the maximum characteristics speed over a point in $S = \{\rho_1, \rho_2\}$, Here $V_1 = 22m/s$ and $V_2 = 27m/s$

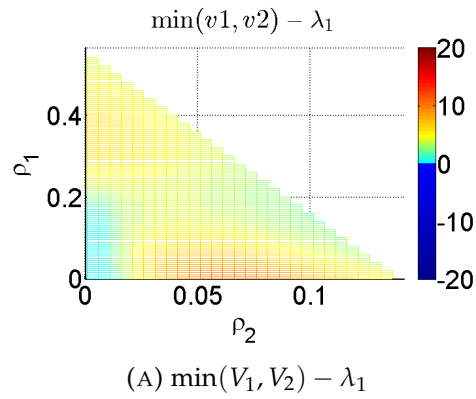


FIGURE 4.2: Evaluation of minimum characteristics speed over a point in $S = \{\rho_1, \rho_2\}$, Here $V_1 = 22m/s$ and $V_2 = 27m/s$

The results from the graphical analysis strongly suggest that the relation in equation (4.2) is valid for our model, which confirms that in the model no wave travels at a higher speed than the traffic and thus the wave propagation speed is finite.

4.2 Fundamental relation

In the formulation of the mode, Chapter 3, list of model requirements are specified. Here, we assess the model, specifically the fundamental relation, with respect to these requirements.

The first requirement states that there should be four traffic regimes, i.e. free-flow, semi-congested, congested and creeping. This requirement is satisfied by the model, since different jam and critical densities are specified for PTWs and cars (refer FIGURES 4.3).

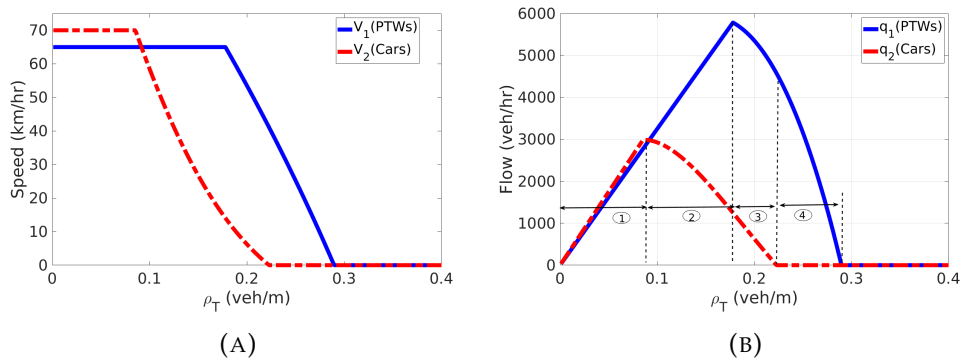


FIGURE 4.3: The four traffic regimes , (A) Speed-density relation (B) Flow-density relation, where $\rho_T = \rho_1 + \rho_2$

The other requirement of the fundamental relation can be restated as: the model should be able to describe the variation in vehicles classes maximum speed and physical dimension (length and projected area). These variations are included in the speed-density relation (see equation (3.14)). Thusly, this requirement is also satisfied.

Requirement 5 relates to the relation of speed of vehicles and road width. In the speed-density relationship, the density of vehicles is expressed in vehicles per unit square since in situation where vehicles do not respect lane discipline the 'areal density' is more descriptive than the 'linear density'. Therefore, the road section is considered as a single unit. The fundamental relations are often established on a per-lane bases. However, we explicitly integrate the road width (see equation (3.12)). The reason is that, for instance vehicles filtering between rows of traffic find more space in multi-lane scenarios than single lane cases. This requirement is also satisfied by the model (Figure

4.4). Unlike the ordered flow, for N lane scenarios the jam densities (ρ_j^N) have the following relation with the one-lane (ρ_j^1) case: $\rho_j^N > N\rho_j^1$. The same applies for the critical densities.

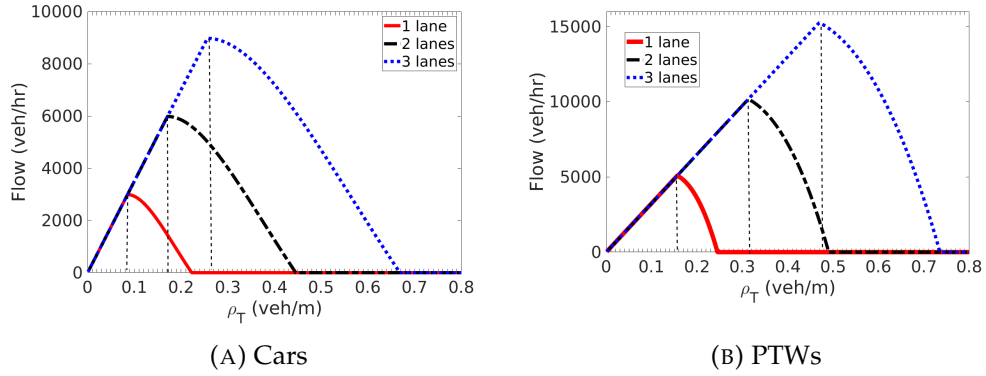


FIGURE 4.4: The variation of the fundamental relation with road width

The other requirement states that the equilibrium speed should be defined uniquely for each traffic composition. This requirement is also satisfied as the speed depends on each class density. FIGURE 4.5 shows the variation in speed-density and flow-density with traffic composition, i.e. with the change of the density of vehicle class 1 (ρ_1). The models that describe the speed-density relation as a function of area occupancy can not capture these properties (e.g., (Nair, Mahmassani, and Miller-Hooks, 2012; Fan and Work, 2015))

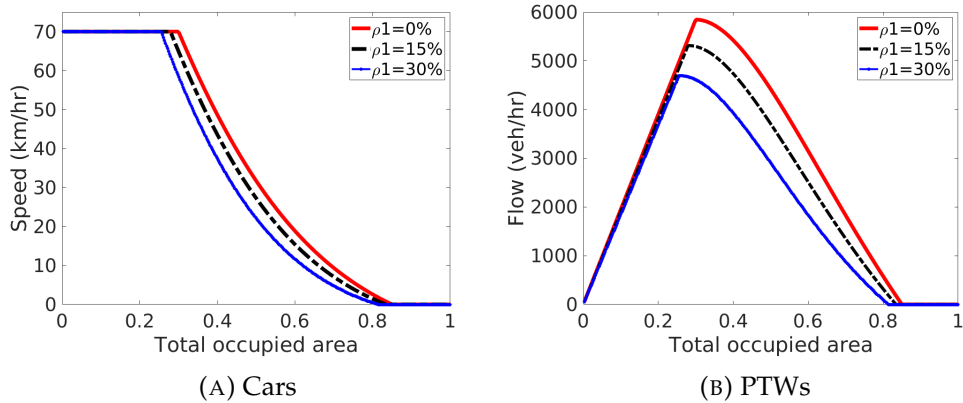


FIGURE 4.5: Speed versus total occupied area for cars at different traffic composition

4.3 Model comparison and verification

The verification experiments are intended to evaluate the developed model against the model in (Nair, Mahmassani, and Miller-Hooks, 2011), which follows the same approach, and the required qualitative behaviors.

4.3.1 Pore size distribution verification

Here, we verify the pore size distribution against the results in (Nair, Mahmassani, and Miller-Hooks, 2011), which are produced by determining the cumulative distribution of the pore size from the average of multiple simulation outcomes. We expect that the

vehicle spacing distribution we propose yields qualitatively the same result as the result obtained from the multiple simulation runs. To derive the pore size distribution, we have introduced simplification assumptions which are not used in (Nair, Mahmassani, and Miller-Hooks, 2011). The impact of these assumptions on the model behavior can be grasped through the qualitative comparison between the results from our model and (Nair, Mahmassani, and Miller-Hooks, 2011).

Therefore, we reproduce the result in (Nair, Mahmassani, and Miller-Hooks, 2011) following the same approach used in the paper. In Nair's approach, for each configuration, the fraction of accessible pores is determined by running multiple simulation run, where vehicles are randomly placed in the domain (without overlapping), and then the probability of finding a pore greater than the critical pore size is determined from this configuration. However, at high density it may not be possible to find a solution within a reasonable amount of time. In these cases, the author proposed to adjust the pore space distribution to reflect 'unplaced vehicles'. But, nothing is mentioned in the paper the way the pore space distribution can be adjusted. Thus, we applied our own method for adjusting the pore size distribution. For a given total number of vehicles, first the fraction of accessible pores (F_c) is determined according to the 'placed vehicles'. If all the vehicles cannot be placed within the time limit set, F_c will be reduced by a ratio of total number of 'placed vehicles' to total number of vehicles (see FIGURE 4.6).

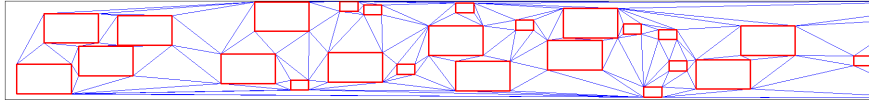


FIGURE 4.6: The setting used for the extraction of the inter-vehicle spacing distribution

For the sake of comparison, we use similar loading profile and simulation parameters. With *normal profile*, the interaction of the two classes under uninterrupted flow conditions is studied, while a traffic flow with disruption is studied in *queue profile*. The maximum speed is set to $V_1 = 80 \text{ km/hr}$ for PTWs and $V_2 = 100 \text{ Km/hr}$ for cars. The simulation is done for 300 s on the space domain $x \in [0, 3000 \text{ m}]$, and with homogeneous initial density of $\rho_1(x, 0) = 0, \rho_2(x, 0) = 0$. We also set $\Delta x = 100 \text{ m}$ and $\Delta t = 2.5 \text{ sec}$. For both experiments the upstream inflow is set to:

$$F_1(0, t) = \begin{cases} 0.5 \text{ veh/sec} & \text{for } t \in [100 \text{ s}, 200 \text{ s}], \\ 0 & \text{otherwise,} \end{cases}$$

$$F_2(0, t) = \begin{cases} 0.5 \text{ veh/sec} & \text{for } x \in [0 \text{ s}, 200 \text{ s}], \\ 0 & \text{otherwise,} \end{cases}$$

and we give absorbing boundary conditions downstream, so that the vehicles leave freely.

From FIGURE 4.7, it can be observed that PTWs traffic density wave moves faster than cars. Due to this, although PTWs start behind, they move past cars traffic and leave the simulation domain faster. At $t = 250 \text{ s}$, all PTWs have overtaken cars. Both models behave similarly except small quantitative changes.

The result in FIGURE 4.8 represents the interrupted scenario, where for $t \in [0 \text{ s}, 250 \text{ s}]$ the flow is blocked at the mid of roadway (at 1500 m). Important properties observed from the results are: PTWs are able to move to the front of the queue passing stationary cars (from $t = 200 \text{ s}$ to $t = 250 \text{ s}$), thus, when the blockage is removed, PTWs clear first. In this scenario, a big quantitative divergence is observed between the two models, particularly when the queue is formed. In our model, we defined jam densities for each class and the speed function is scaled to reach zero at the jam densities (Section 3.2.2, FIGURE 3.10). But, this modification is not applied to the speed function in Nair's

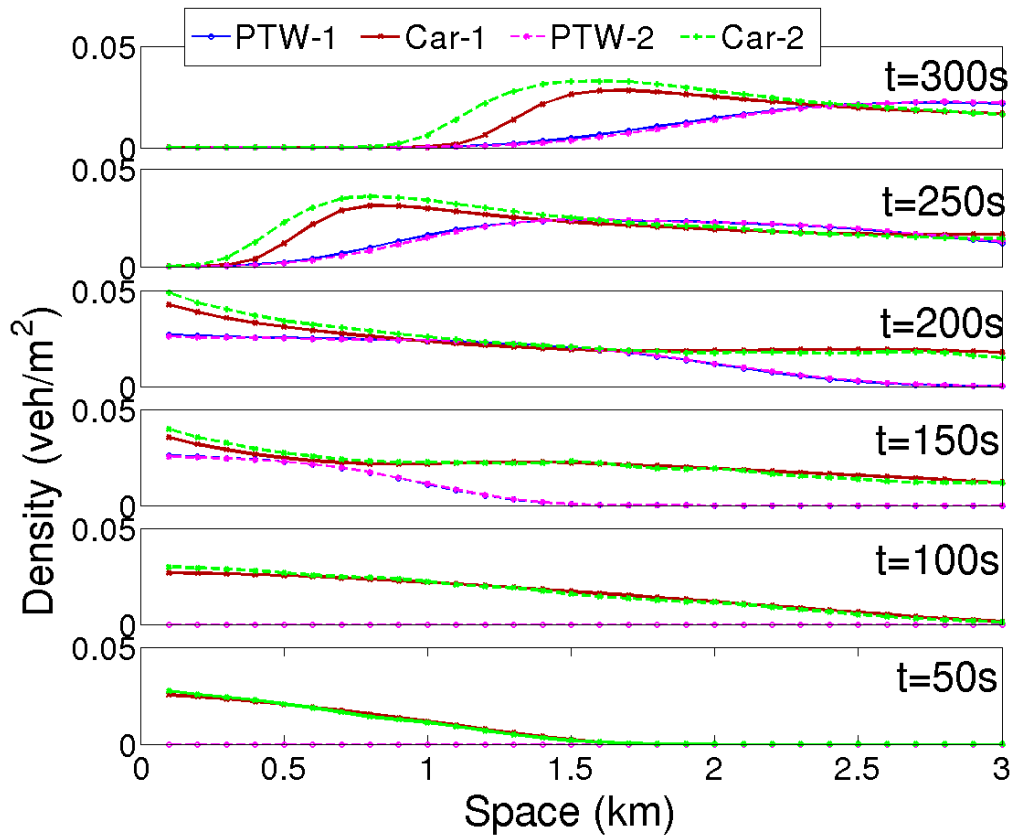


FIGURE 4.7: Normal profile, traffic density waves of cars and PTWs at different time steps. (PTW-1, Car-1) and (PTW-2, Car-2) represent result from our model and Nair's model, respectively.

model, see FIGURE 4.9. The difference between the speed values becomes more significant at the higher densities. The resulting quantitative change mainly happens because of the speed difference. Otherwise, both models are quantitatively similar.

The results in figures 4.7 and 4.8, have almost the same qualitative properties as the results in (Nair, Mahmassani, and Miller-Hooks, 2011), confirming the validity of the assumptions made to establish the distribution function of inter-vehicle spacing.

4.3.2 Verifying model properties

In this section, the capability of our model to reproduce the observed macroscopic phenomena of a mixed flow of PTWs and cars is evaluated. The following two well-known features (Fan and Work, 2015) are used as a benchmark to evaluate our model.

- **Overtaking-** when the traffic volume is high, cars start to slow down. However, PTWs remain unaffected or less affected by the change in traffic situation, as they can ride between traffic lanes. As a consequence, PTWs travel at higher speed, and overtake slow moving cars.
- **Creeping-** when cars are stopped at traffic signals or because of traffic jams, PTWs can find a space to filter (creep) through stationary cars and move ahead.

In addition, a comparison with the models in (Benzoni-Gavage and Colombo, 2003) and (Fan and Work, 2015), hereafter referred as *N-pop* and *creeping* respectively, is presented along with the verification of our model, *porous G*. The two models are chosen for the comparison because the *creeping* model is proved to reproduce these phenomena and the *N-pop* applies a similar modeling approach with *creeping*.

For creeping and overtaking experiments, the parameters in TABLE 4.1 are chosen.

The jam density refers to the maximum area occupancy, which equals to $\rho_1 a_1 + \rho_2 a_2$ for *porous G* model and $\rho_1 l_1 + \rho_2 l_2$ for the other models, where vehicles come to a

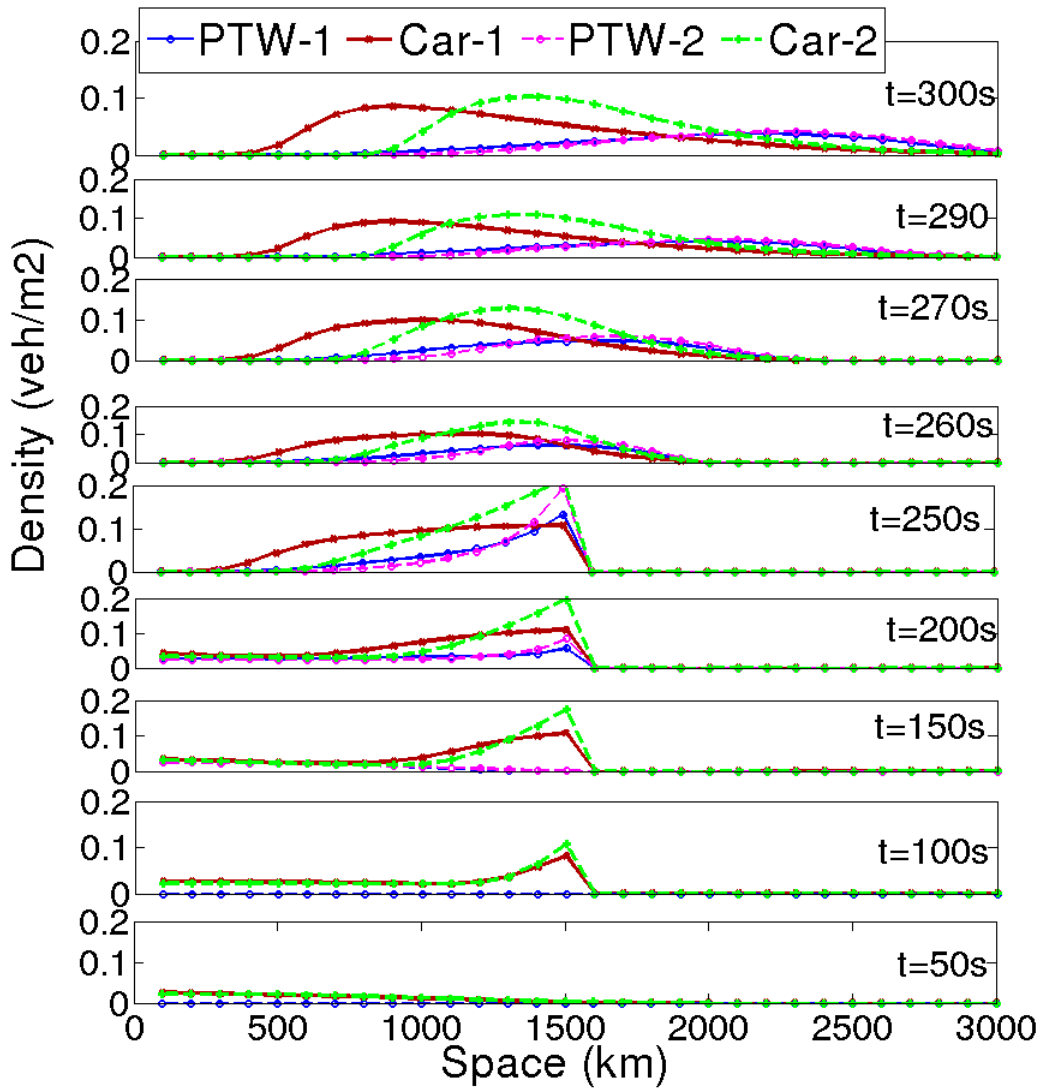
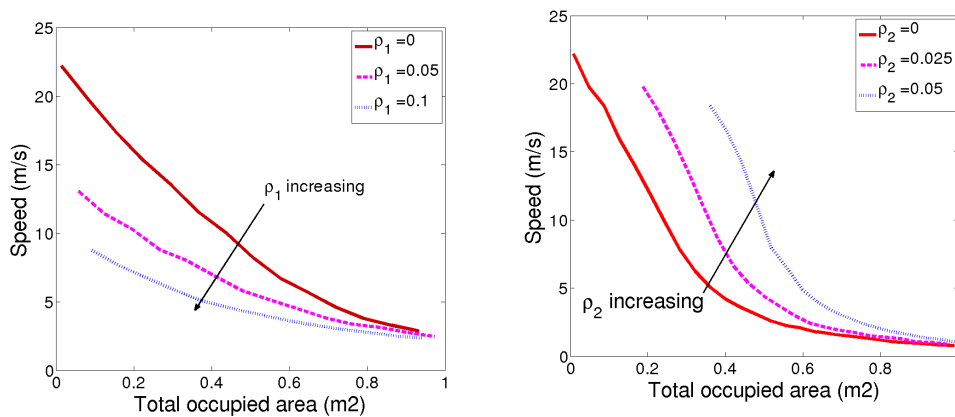


FIGURE 4.8: Queue profile, traffic density waves of cars and PTWs at different time steps. (PTW-1, Car-1) and (PTW-2, Car-2) represent result from our model and Nair’s model, respectively.



(A) Car speed at different density of PTWs (B) PTWs speed at different cars density values.

FIGURE 4.9: Speed Vs total occupied area ($\sum \rho_1 A_1 + \sum \rho_2 A_2$) Nair’s model (Nair, Mahmassani, and Miller-Hooks, 2011), where $\rho_1 A_1$ and $\rho_2 A_2$ are area projected on the road by PTW and car, respectively.

complete stop state. The simulation is done on a road of length 50 m and $\Delta x = 0.05$ m and Δt is selected according to CFL condition.

	PTW	Car
Vehicle length (m)	1.5	3
Vehicle radius (m)	0.75	1.5
Max. speed (m/s)	1.8	1
Jam density <i>porous G</i>	1	0.85
Jam density <i>creeping</i>	1.8	1
Jam density <i>N-pop</i>	1	1

TABLE 4.1: Simulation Parameters

4.3.2.1 Creeping experiment

A signalized intersection is employed for testing creeping. In the simulation, PTWs start behind the cars traffic and cars traffic have concentrated close to the traffic signal, so that PTWs arrive after most of the cars reached a complete stop. The simulation is done for 200 s and starts with initial densities

$$\rho_1(x,0) = \begin{cases} 0.25 & \text{for } x \in [1 \text{ m}, 21 \text{ m}], \\ 0 & \text{otherwise,} \end{cases} \quad \rho_2(x,0) = \begin{cases} 0.25 & \text{for } x \in [31 \text{ m}, 50 \text{ m}], \\ 0 & \text{otherwise.} \end{cases}$$

The inflow and the outflow at the boundaries are set to zero. At the time PTWs start catching up cars traffic (FIGURE 4.10(a)), most of the cars are at stationary state (see FIGURE 4.10(a) lower subplot space location 45 – 50 m). However, as shown in FIGURE 4.10(b), PTWs maneuver through those stationary cars and reach the front of the queue for the case of *creeping* and *Porous G* models. For the *N-pop* model, the PTWs traffic stays behind the cars since both classes have the same jam density. Table 4.2 shows the average speeds of PTWs and cars in a particular location at time $t = 50$ s. As can be observed from the speed values, unlike *N-pop* model, in the other two models PTWs have a non-zero speed value even though cars are at a complete stop state. The results

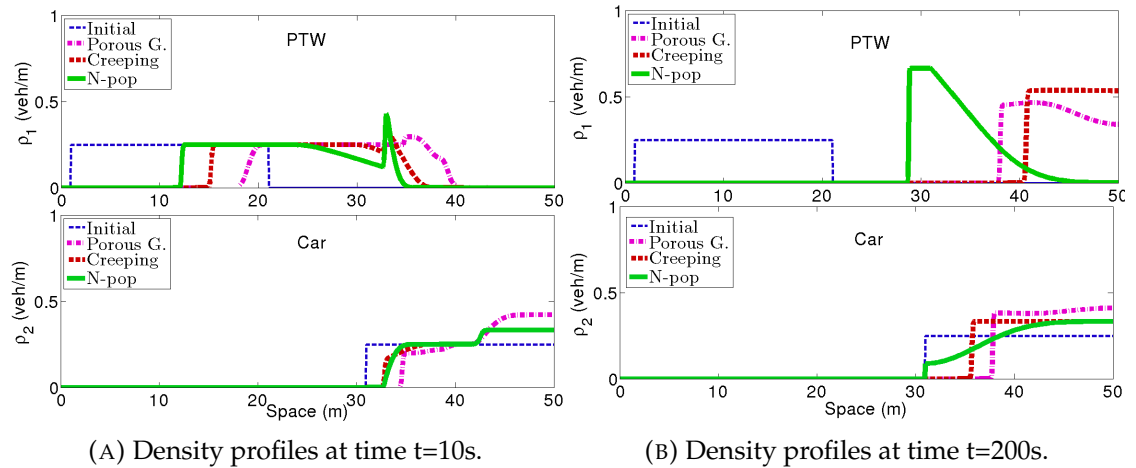


FIGURE 4.10: Creeping experiment density-space diagram, upper subplot for PTWs and lower subplot for cars.

	<i>Creeping</i>	<i>Porous G</i>	<i>N-pop</i>
V_1	0.2179	0.6349	0
V_2	0	0	0

TABLE 4.2: Speed values extracted at time $t = 50$ sec and position $x = 39.15$ m

from the creeping experiment show similar behavior to the situation we may observe in real scenarios, i.e. PTWs seep through cars queue to reach the head the queue, both for *Porous G* and *Creeping* models. However, for the *N-pop* model, PTWs remain behind car

traffic queue. Thus, only the first two models are able to produce this predominantly observed phenomenon of mixed traffic flow of cars and PTWs.

4.3.2.2 Overtaking experiment

For the overtaking scenario, the cars traffic is placed ahead of PTWs.

The simulation starts with the initial state where:

$$\rho_1(x,0) = \begin{cases} 0.3 & \text{for } x \in [1 \text{ m}, 20 \text{ m}], \\ 0 & \text{otherwise,} \end{cases} \quad \rho_2(x,0) = \begin{cases} 0.3 & \text{for } x \in [15 \text{ m}, 34 \text{ m}], \\ 0 & \text{otherwise.} \end{cases}$$

The inflow at the upstream boundary is set to zero, and vehicles are allowed to leave freely at the downstream boundary. For this experiment, we consider two cases one when free flow speed of PTWs is higher than cars and the other when cars take the higher free flow speed. The occurrence of overtaking is evaluated by inspecting the evolution of traffic densities of the two classes. Overtaking is said to happen when the density waves of the two classes come to the same level in space and one of the two go past the other, i.e the tail end of one class is before the other.

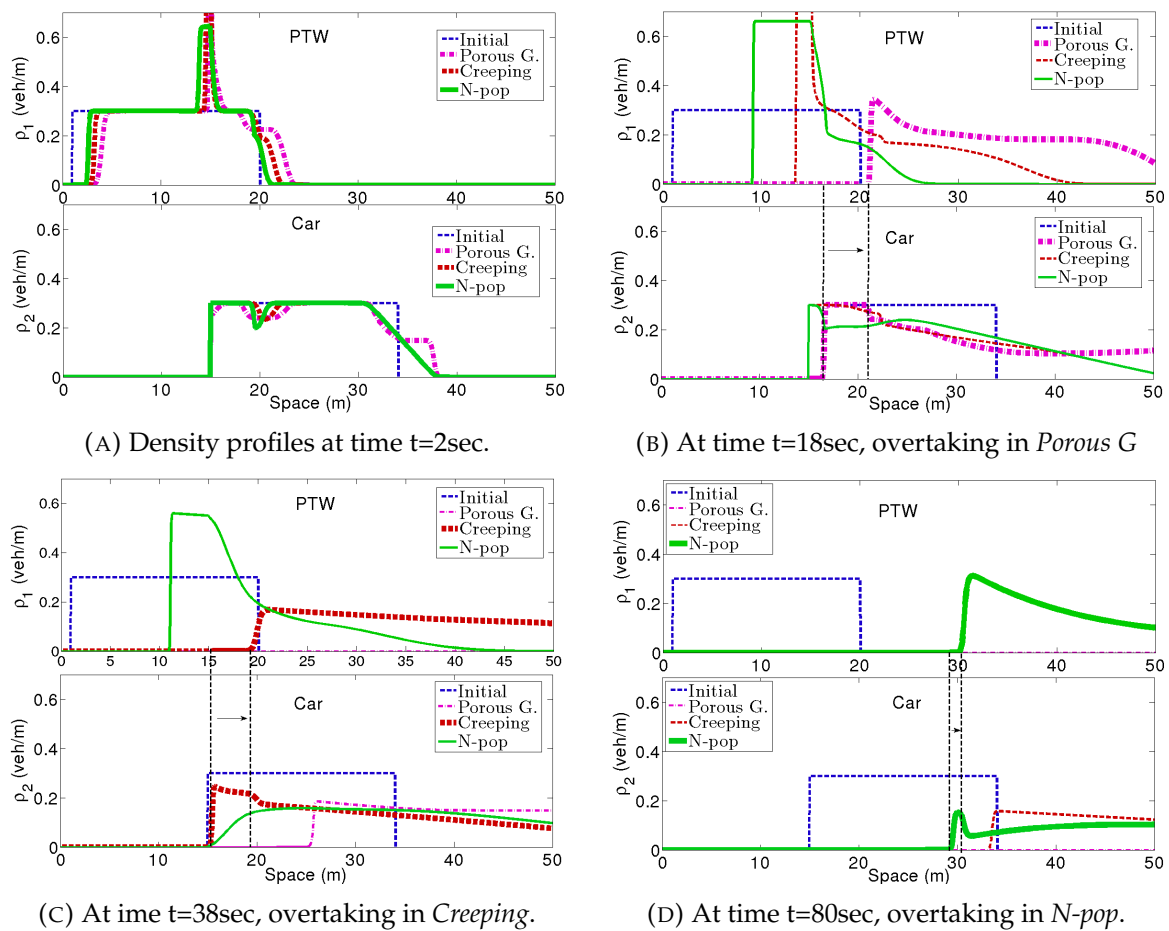


FIGURE 4.11: Overtaking experiment density-space diagrams, upper subplot for PTWs and lower subplot for cars, free flow speed of $V_1 = 1.8\text{m/s}$ greater than $V_2 = 1\text{m/s}$. The dashed lines stretching from upper subplot to the lower connect the tail of the density profiles for cars and PTWs' traffic and the spacing between the two lines indicates the distance gap after PTWs overtake.

As FIGURE 4.11 depicts, when free flow speed of PTWs is greater than cars, PTWs overtake cars in all the three models. In *Porous G* model overtaking is observed at around time $t = 18 \text{ s}$ (FIGURE 4.11(b)), and for *Creeping* and *N-pop* models overtaking happens at $t = 38 \text{ s}$ (FIGURE 4.11(c)) and $t = 80 \text{ s}$ (FIGURE 4.11(d)), respectively.

The simulation results in FIGURE 4.12 correspond to the case where free flow speed of cars ($V_2 = 1.8$) is greater than free flow speed of PTWs ($V_1 = 1.5$). As shown, in the

two models, *Porous G* and *Creeping*, overtaking is observed. In *Porous G* model overtaking happens around time $t = 26$ s (FIGURE 4.12(b)) and at time $t = 40$ s (FIGURE 4.12(c)) for *Creeping*. Nonetheless, *N-pop* model fails to reproduce overtaking. At time $t = 52$ s for *N-pop* the tail end of PTWs traffic is around location $x = 26$ m whereas for cars traffic it is around $x = 41$ m (FIGURE 4.12(d)), which is far behind.

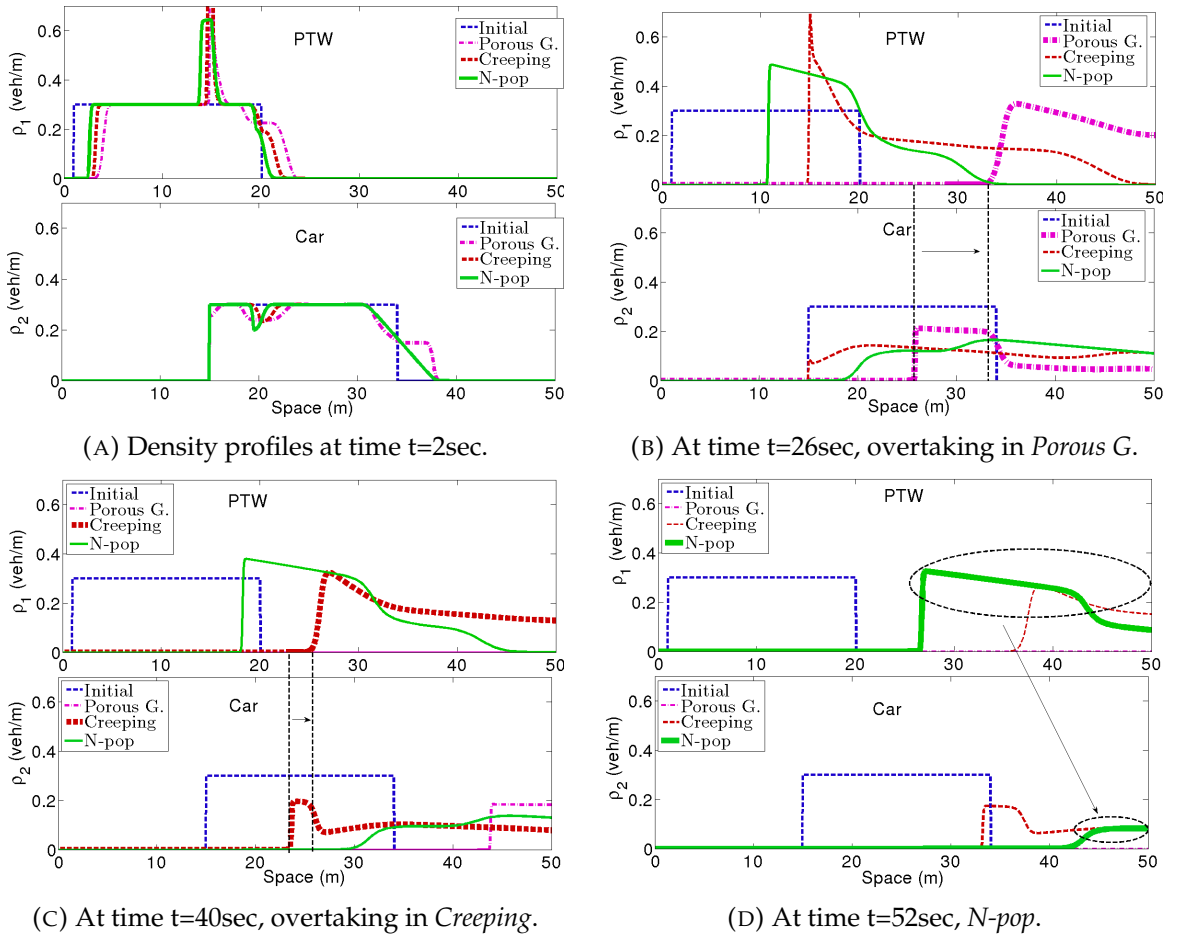


FIGURE 4.12: Overtaking experiment density-space diagrams, upper subplot for PTWs and lower subplot for cars, free flow speed of $V_2 = 1.8$ m/s greater than $V_1 = 1.5$ m/s.

According to what is illustrated in figures (FIGURE 4.11 and 4.12), all the three models are able to show the overtaking phenomenon when PTWs free flow speed is higher than cars. Further, for *Porous G* and *Creeping* models overtaking happens in the case where free flow speed of cars is higher than PTWs' as well.

In *N-pop* model, unlike the other two models, overtaking never happens unless car free flow speed is higher. This can be explained using a particular instance in FIGURE 4.13. As shown in the figure, in *Creeping* and *Porous G* models there exist a region where the speed of PTWs is greater than cars despite the free flow speed choice.

In conclusion, the model verification results validate that our model (*Porous G*) can reproduce the required creeping and overtaking phenomena. The *Creeping* model also satisfies all these properties. Yet, this model has a limitation, as occupied space is a mere factor that determines the speed and the variation in the composition of vehicles has no influence as long as the occupied space is the same (see Section 3.2.2, FIGURE 3.10). The *N-pop* model, however, lacks the creeping behavior and overtaking is conditioned by the free flow speed of PTWs.

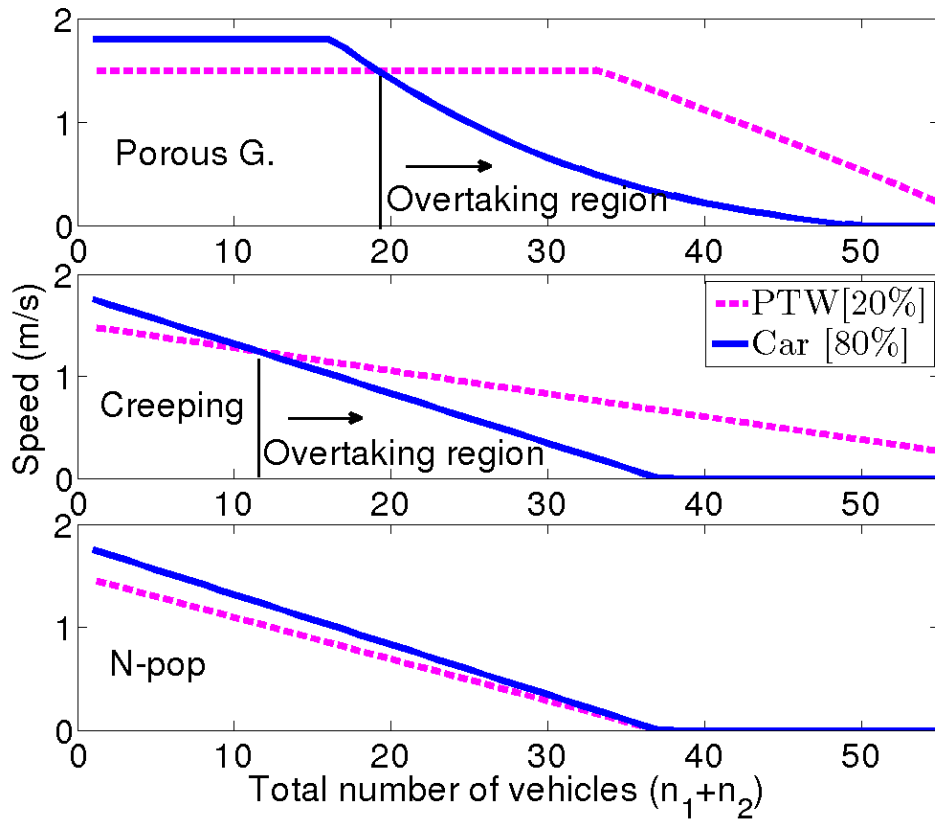


FIGURE 4.13: Speed vs. total number of vehicles plot, when free flow speed of PTWs less than cars and cars account to 80% of the total traffic, upper subplot *Porous G.*, middle subplot *Creeping*, lower subplot *N-pop*.

4.4 Model calibration and validation

The model is validated against the desired qualitative behaviors. Yet, to accurately reproduce the real traffic situation, adjusting the model parameters is imperative. For the calibration and validation process, trajectory data for each vehicle class at different ranges of traffic densities is required. In addition, for non-lane based traffic the influence of the road geometry is significant, thus information about the roadway such as lane width, number of lanes, etc is necessary. Although there are widely available methods to collect vehicles' trajectory data, only a few of them are applicable for the required calibration and validation experiments. The challenge is mainly in getting the required traffic parameters and accurate geo-location of vehicles, specifically for PTWs. For example, data collected from sensors like inductive loops are not sufficient as extrapolation of vehicles spatial location is very difficult, if not impossible. Floating Car Data (FCD) could be an efficient method for collecting vehicles' trajectory data, where smartphones or GPS devices in vehicles continuously send location, speed, etc. information. However, the inefficiency of smartphone GPS to produce the true location of PTWs (Koyama and Tanaka, 2011) and the low penetration rate of vehicles equipped with an accurate GPS receiver make FCD method less applicable. Another potential alternative is to use video cameras and to extract the required traffic data (vehicle number, vehicle type, location, etc.) utilizing image processing techniques (Ch Mallikarjuna, Phanindra, and Rao, 2009). Given the complexity of data collection, calibrated commercial simulators like Vissim can serve as a means of model calibration. We therefore utilize the data from Vissim simulation model for the model calibration and validation process.

4.4.1 Vissim simulation

Vissim is a microscopic simulation platform that can reproduce a realistic traffic flows and operations (Fellendorf and Vortisch, 2010). With Vissim, the movement of different types of vehicles (e.g., cars, trucks, powered two-wheelers, etc.) and pedestrians can be studied. The car-following behavior of vehicles is modeled according to Wiedemann model. There are also model for the lateral and the lane-changing behaviors. Vissim can also model the lane sharing or same lane overtaking behaviors found in non-lane bound traffic flow. Moreover, the models are calibrated. In addition, Vissim can generate various aggregated or raw data evaluation results, such as floating car data, travel time information, delay.

To generate the data required for the model calibration and validation, we apply the following simulation settings. Two vehicle types are defined, motorcycle (PTWs) and cars. Vissim allows to define vehicle type dependent driving behaviors and model parameters. In our case, PTWs and cars have different car-following parameters and driving behaviors. PTWs can overtake in the same lane but not cars. Cars are not overtake in the same lane but can take any lateral position within the lane.

The data is collected on a two-lane road network of length 1.5 km and the width of the traffic lanes are 3.5 m. There are three links, but the data collection is carried out at link 2. The schematic representation of the road network is shown in FIGURE 4.14. The vehicle specific parameters used for the simulation are presented in Appendix C.

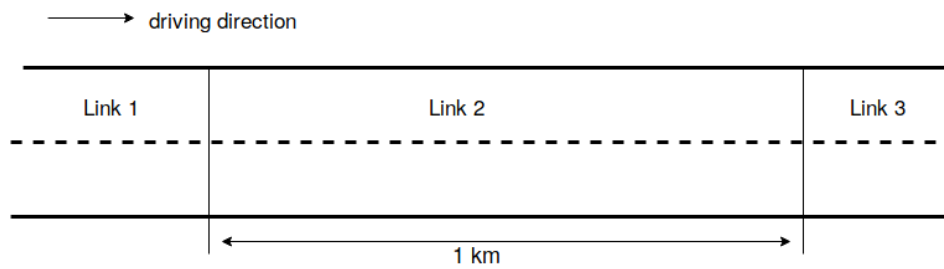


FIGURE 4.14: Schematic representation of the road network

The simulations are carried out for one hour period, however the data collection starts at 300 s.

4.4.2 Analyzing the data

The collected floating car data contains the following information: time step, vehicle ID, vehicle type, rear and front coordinates, speed, link and lane number, etc. To use the data for the calibration of the fundamental diagrams, the density, flow and average speed information has to be extracted from the data.

To derive the density we use the following equation.

$$\rho = \frac{\sum_i n_i t_i}{lT} = \frac{\sum_{n=1}^N t_n}{lT} \quad (4.3)$$

where l , t_n and T are, respectively, the length of the road section, the time spent by a vehicle in the section and the observation period, which in our case equals 6 min

The average speed, which is the space mean, is derived as follows:

$$v = \frac{\sum_{n=1}^N d_n}{\sum_{n=1}^N t_n} \quad (4.4)$$

where t_n is time spent by a vehicle in the section and d_n is the distance traveled in the duration of t_n .

The flow can be derived from the flow, density and speed relationship. Thus, the flow becomes:

$$q = \frac{\sum_{n=1}^N d_n}{lT} \quad (4.5)$$

The speed-density and flow-density relations, for different ratio of PTWs, obtained from the simulation data are shown in FIGURE 4.15.

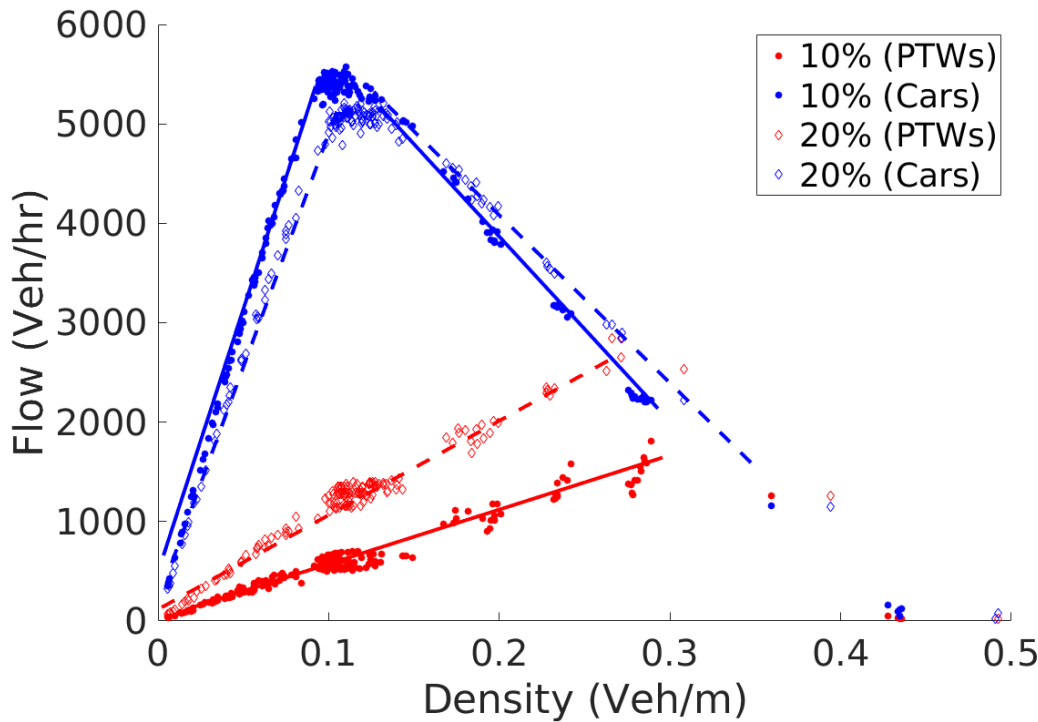


FIGURE 4.15: The Flow-density curve for PTWs and cars, at the traffic composition of [10% PTWs – 90% cars] and [20% PTWs – 80% cars]

Furthermore, to extract the inter-vehicle spacing or pore size information from the data, we apply the following procedure. First, the coordinates of the center of vehicles is computed from the rear and front coordinates. Then, using Delaunay triangulation the distance between vehicles is measured. Note that, since the Delaunay triangulation is performed based on the center coordinates, the triangle edges may cross more than two vehicles. In this case the triangle edge is removed. FIGURE 4.16 shows the schematic representation of the pore size measurement.

4.4.3 Model calibration

The purpose of the calibration procedure is to adjust the fundamental diagrams parameters for the two vehicle classes. In particular, the searched parameters are the jam

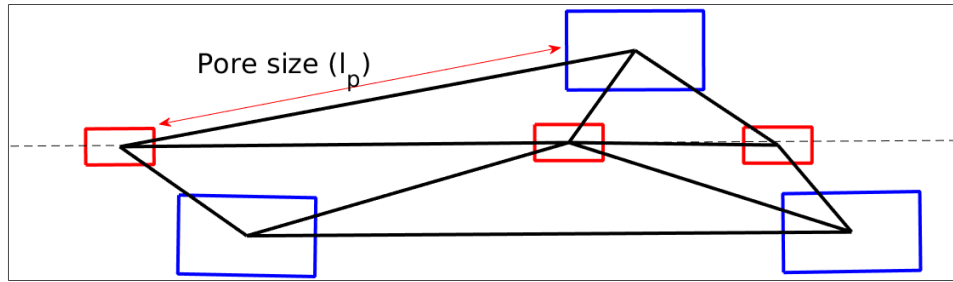


FIGURE 4.16: Schematic representation of the pore size measurement method

densities, the critical pore size and the scaling factor of the model. For the jam densities, curve fitting is utilized while the other parameter are calibrated by employing an iterative search of the parameters until a good fitting curve to the observation is obtained.

The jam densities are dependent on the traffic composition. Therefore, it is necessary to establish relationship between the jam and critical density parameters, and the traffic state. Hence, we first establish a relation between the jam density of each class and the traffic composition. Matlab curve fitting is employed to find an equation that relate the jam densities and the traffic composition. Accordingly, we obtain the following equation.

$$\rho_{jam,n} = \rho_{jam,n}^0 - 0.33\rho_o \quad (4.6)$$

where $\rho_{jam,n}^0$ is the jam density of vehicle class n when the density of the other vehicle class is zero. This value is determined for each vehicle class based on the fundamental relation in FIGURE 4.18. The obtained $\rho_{jam,n}^0$ values for cars and PTWs are, respectively, 400 *veh/km* and 2000 *veh/km*.

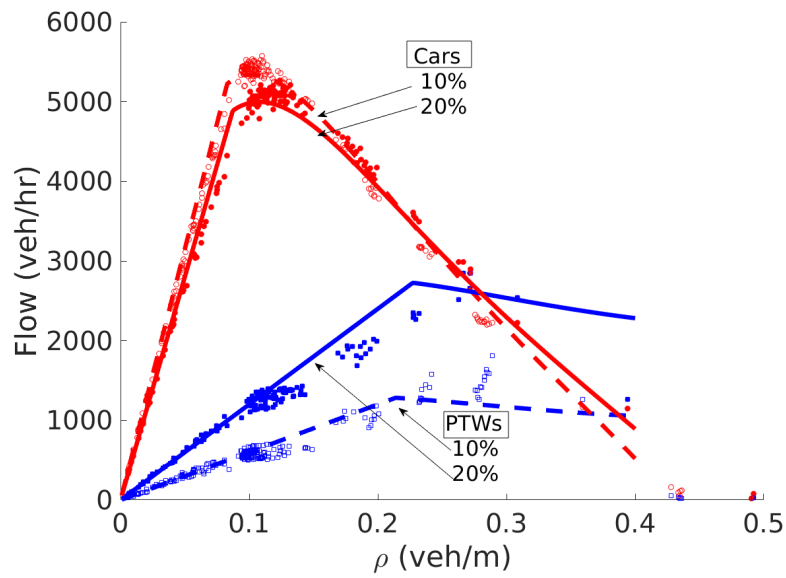
For the critical pore size, we start with the equation that relates the critical pore size with the traffic state.

$$r_n^{cr} = w_n + \alpha * (1 - (\rho_1 * a_1 + \rho_2 * a_2)) \quad (4.7)$$

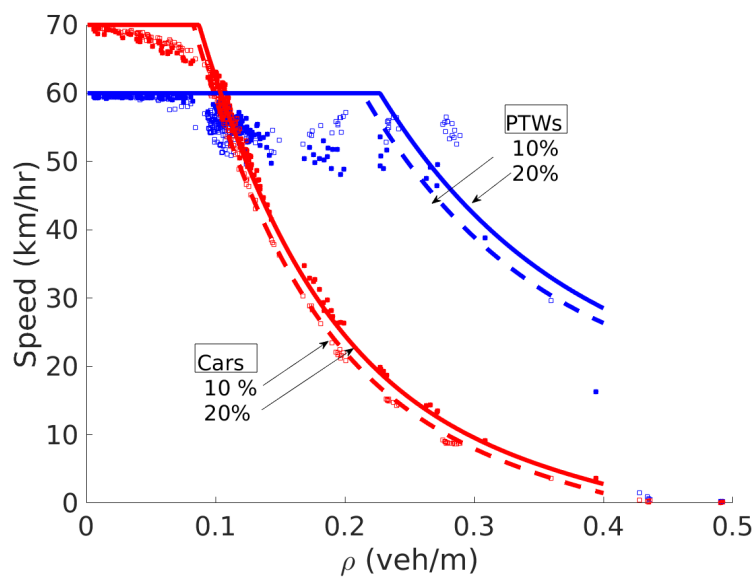
where w_n is the width of the vehicles and $\rho_1 * a_1 + \rho_2 * a_2$ is the total sum of the projected area of class 1 and class 2 vehicles. From the iterative search, $\alpha = 4$ and $\alpha = 4.5$ for PTWs and cars, respectively, are accepted for all tested cases. Similarly, the scaling factors are also determined, which equal 3.5 for PTWs and 2 for cars.

The Fundamental relation curves obtained from the Vissim simulation data and the fitted curves after calibrating the model parameters are shown in FIGURE 4.17 and FIGURE 4.18.

The calibrated parameters are used in the next model validation procedure.

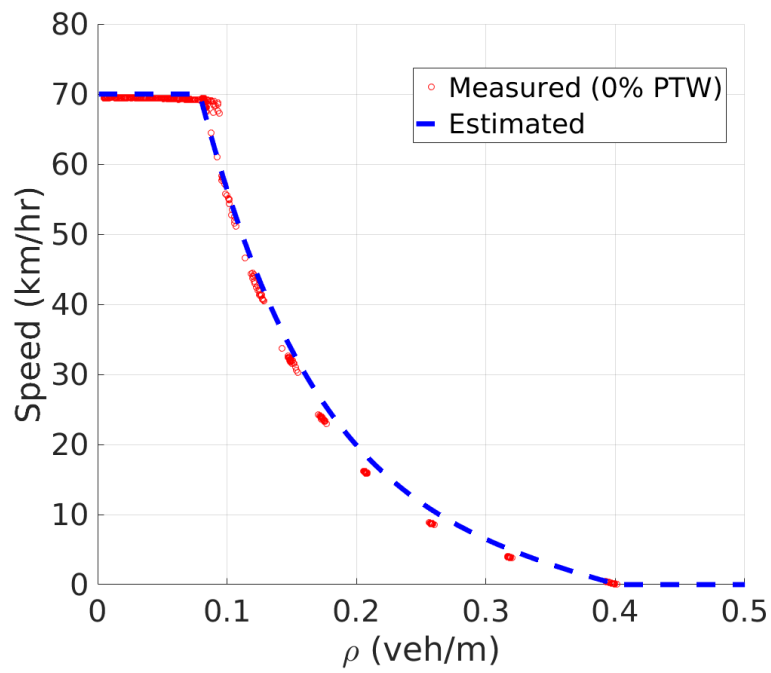


(A)

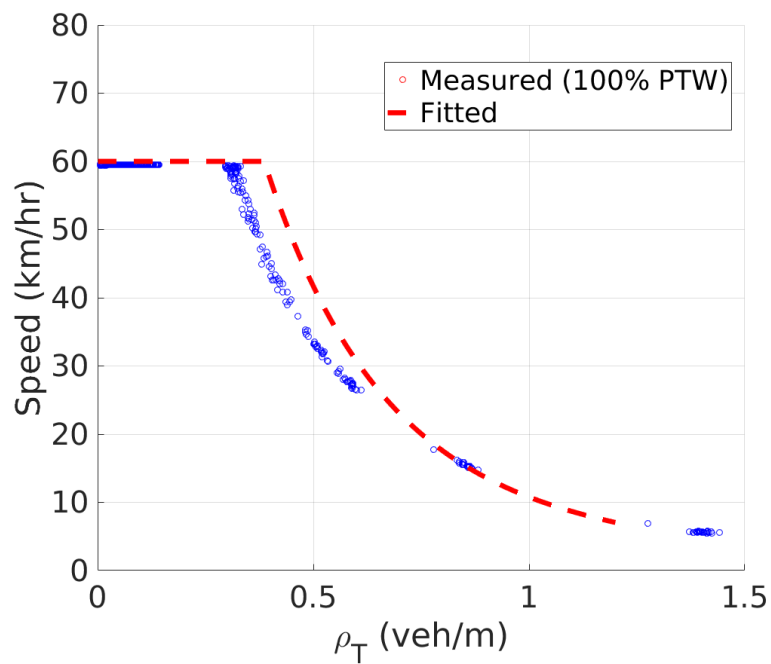


(B)

FIGURE 4.17: The estimated and measured (A) flow–density relationship (B) speed–density relationship



(A)



(B)

FIGURE 4.18: The estimated and measured speed–density relationship (A) for cars (B) for PTWs, when the fraction of the other vehicle class is zero

4.4.4 Validation

In this section, we validate the pore size distribution. Further, by using the calibrated parameters, the applicability of the model is validated.

Spacing distribution

The model is founded on the assumption that the traffic flow behavior can be characterized using the inter-vehicle spacing distribution. Thus, the accuracy of the model highly depends on how precisely the inter-vehicle spacing distribution is estimated. The inter-vehicle spacing distribution, therefore, has to be validated. The validation of the spacing distribution process involves, for different traffic compositions and densities, collecting position information of vehicles, measuring spacing between vehicles, estimating statistical parameters of inter-spacing (mean, variance) and curve fitting experiments.

Inter vehicle spacing distribution is analyzed for different traffic compositions. Three distributions, namely exponential, log-normal and truncated normal, are tested. The goodness of the fit measurements and the fitting curves are shown in TABLE 4.3 and FIGURE 4.19, respectively.

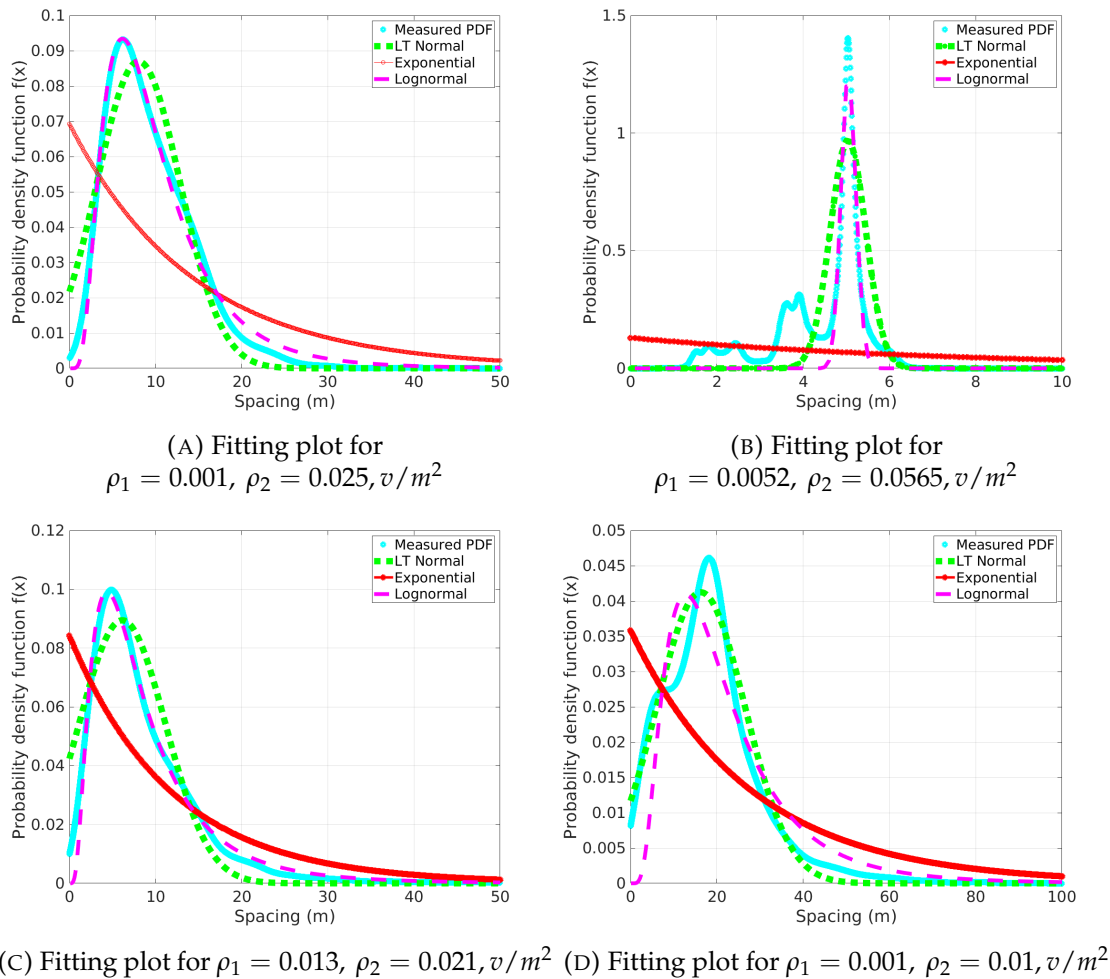


FIGURE 4.19: Fitting of theoretical distributions with the observed distribution, for different vehicles composition

According to the results, log-normal fits better in the three of cases studied. However, truncated normal distribution fits better for the case $\rho_1 = 0.1 \text{ veh}/m^2, \rho_2 = 0.01 \text{ veh}/m^2$. Although, log-normal fits better in most of the cases, the goodness of fit measure for truncated normal is close to log-normal. From these observations, we can see that truncated-normal distribution can give a good estimate in most of the cases, but at higher traffic densities log-normal gives a better estimate.

	SSE	R-square	RMSE	SSE	R-square	RMSE
	$\rho_1 = 0.001, \rho_2 = 0.025$			$\rho_1 = 0.0052, \rho_2 = 0.057$		
LT-normal	0.217	0.9584	0.0047	19.5	0.641	0.0442
Log-normal	0.0413	0.9921	0.0020	7.89	0.854	0.0281
Exponential	2.068	0.605	0.0144	47.15	0.1324	0.068
	$\rho_1 = 0.013, \rho_2 = 0.021$			$\rho_1 = 0.1, \rho_2 = 0.01$		
LT-normal	0.303	0.942	0.0055	0.0586	0.9688	0.0024
Log-normal	0.051	0.99	0.0023	0.250	0.866	0.005
Exponential	1.4	0.732	0.012	0.756	0.597	0.0087

TABLE 4.3: Goodness of the fit measurements for different theoretical distributions.

We check also the formulation used to estimate the parameters of the distribution. It appears that the formulation for the estimation of the distribution parameters gives a good approximate of the observed parameters.

Applicability of the model

This section presents the validation of the applicability of the developed model. The calibrated parameters are applied in the model. We use different simulation data for the validation, but obtained from similar simulation setting. The measured average speed is computed over 30 s period. The applicability of the model to correctly predict the observed average speed is evaluated.

Figures 4.20 and 4.21 show the observed and the estimated average speed. The first one represents the result for light traffic condition and the later one is for higher traffic densities. As can be seen, there is a good matching between the curves representing the estimated and observed average speed. However, there are also wider gaps between the two observations around 5 min, 19 min and 40 min.

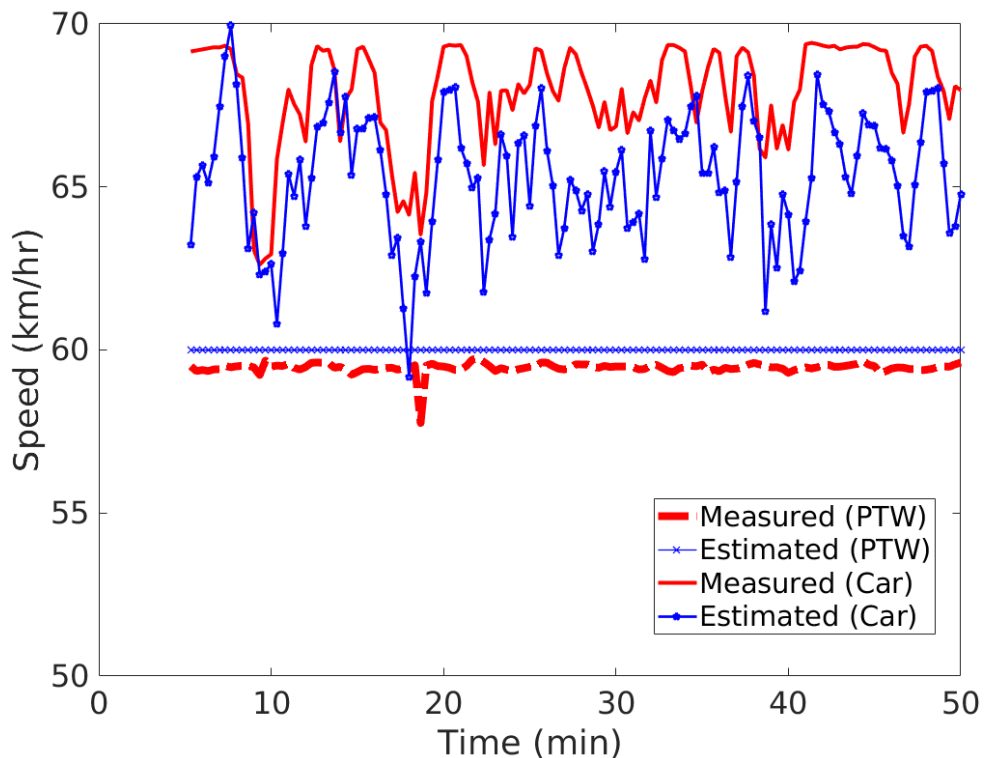


FIGURE 4.20: The observed and estimated average speed over a time

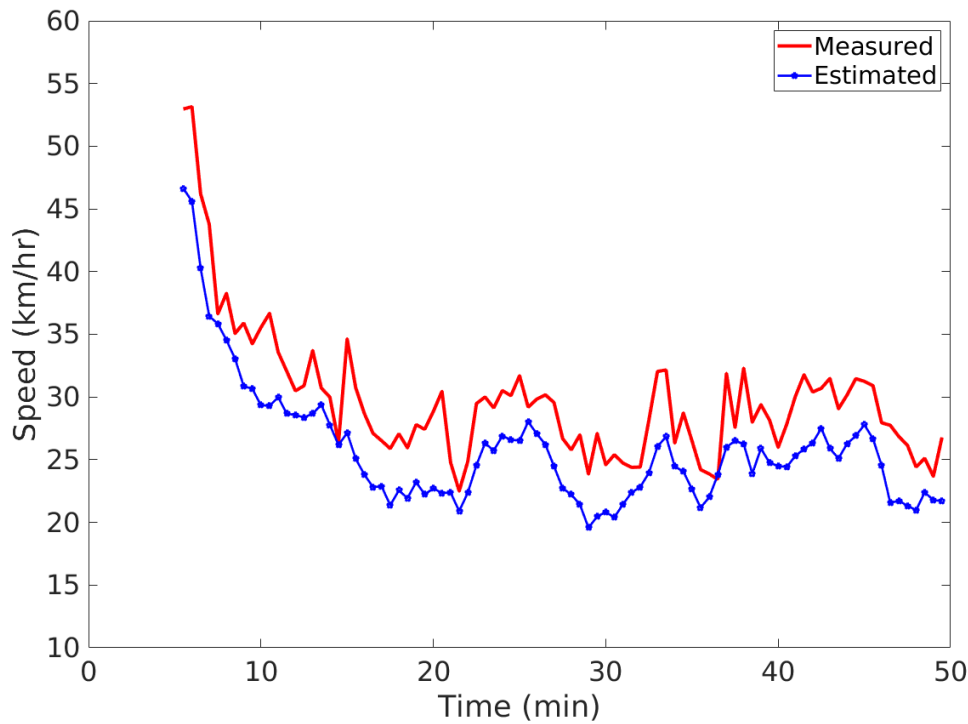


FIGURE 4.21: The observed and estimated average speed at higher traffic densities (cars average speed)

4.5 Summary and conclusion

In this chapter, we study the qualitative and quantitative behaviors of the developed heterogeneous traffic flow model. The mathematical properties of the model, which is related to the characteristics speed, is analyzed. The characteristics speed are proved, analytically and numerically, to be bounded by the vehicles speed.

Furthermore, the model is assessed with respect to the following required features of the fundamental relation. The first requirement is the speed-density and flow density relations should be uniquely defined for each permissible vehicle class density. There should also exist four traffic regimes that describe the total traffic flow state. At free flow state, both vehicle classes are in free flow state. In semi-congested state, PTWs are in free flow state but cars are congested. In congested state, both vehicle classes are congested but travel at different speeds. The fourth traffic regime, which is the creeping phase, describes the traffic situation where PTWs can travel at non-zero speed while cars are completely stopped.

The fundamental relation is derived in Chapter 3 based on the porous flow approach. The pore size distribution is one of the important feature of the model, which we determine by applying different approximation methods. We compare our model with Nair's model (Nair, Mahmassani, and Miller-Hooks, 2011), which follows the same approach but obtains the pore size distribution from multiple simulation runs. In a mixed cars and PTWs flow, overtaking and creeping are the commonly observed traffic phenomena. We evaluate our model, also compare with other two models, with respect to these two traffic features.

Moreover, the calibration and validation of the model is performed using the traffic data obtained from a micro-simulation model Vissim. The fundamental curves are derived from the traffic data, and the model parameters are adjusted to fit the curves. Accordingly, we establish a relation between the traffic composition and the jam densities of the vehicle classes. Further, the acceptable critical gap is described as a function of the traffic state. In the validation phase, first the validity of the proposed inter-vehicle

spacing or pore size distribution is checked. The results show that the proposed distribution, i.e. truncated normal distribution, fits well in most of the cases but log-normal fits better at higher traffic densities. Further, the applicability of the model is evaluated by comparing the estimated and the measured average speed. The model is able to reproduce the evolution of the average speed correctly. However, the model should be further analyzed using wide ranges of traffic conditions.

In the following section, the model is applied to analyze the traffic characteristics that are important for ITS application development.

Chapter 5

Perspectives for future ITS applications

ITS applications have contributed a lot in creating a safe and efficient transportation system. However, for the effectiveness of the applications, all types of transport modes have to be incorporated.

The use of PTW is growing world wide, due to the many advantages they offer. To benefit from the mobility opportunities offered by the shift to PTWs, it is necessary to make the transportation system adapted to PTWs. The specific behaviors of PTWs have to be considered during the development of ITS applications. For example, traffic management strategies in response to certain conditions, such as traffic jams and incidents, have to be optimized to PTWs. Otherwise, it might become counterproductive to ensuring efficient road use. Moreover, traffic information systems, like jam ahead indication and routing information, have to be adapted to vehicle types as a congested road for cars may not be necessarily congested to PTWs. The benefit of optimizing ITS applications to PTWs specific behaviors is two fold. It not only results in a safe and efficient road use but also encourages the use of PTWs, which in turn improves mobility.

In some cities, electrical scooter sharing initiatives are proposed, e.g., scoot (Cohen and Shaheen, 2018), for drivers to switch transportation modes when reaching city centers. Yet, major user acceptance of PTWs in future traffic will not success unless PTW-aware Cooperative Intelligent Transport Systems (C-ITS) technologies are available. First and foremost, safety technologies, such as cooperative lane merging or PTWs approach indications, are required, considering the high vulnerability level of PTW. But also, emerging traffic efficiency technologies, such as PTW-aware traffic monitoring, traffic light management, adaptive speed limits and advanced navigation technologies, are expected to provide a major impact on future urban and suburban traffic congestion. Despite the advancement of ITS systems and applications for cars, little has done to integrate PTWs into the systems (Barmounakis, Vlahogianni, and Golias, 2016). Understanding the mobility characteristics and the impact of PTWs is the first step toward the integration of PTWs to the ITS systems.

In this chapter, we use the model developed in Chapter 3 to study the impact of PTWs and to assess the existing traffic management trends from the context of traffic flow containing PTWs. More specifically, in Section 5.1 the impact of PTWs on road capacity and travel time is presented. Section 5.2 describes traffic control systems and the adaptation to the specific needs and behaviors of PTWs.

5.1 Traffic impact analysis

The traffic impact analysis targets to assess the potential improvements in traffic mobility obtained from growing use of PTWs. Identifying the opportunities leads to the introduction of new innovative smart city applications. Furthermore, it gives the necessary information on how transport policies, mobility plan, traffic management, etc. should be shaped to benefit from the opportunities. Thus, the section here explores the impact of PTWs on traffic flow and road capacity. First, we analyze the role of PTWs, at different penetration rates, in minimizing congestion by substituting some of the cars

with PTWs. Then, we investigate the benefit of the mode shift to PTWs in the reduction of travel time.

5.1.1 Road capacity

Road capacity, which is also called critical density, is defined as the maximum volume of traffic that corresponds to the maximum flow rate. Above the road capacity, traffic flow enters congestion state and the flow of vehicles decreases with the increase in traffic volume. In mixed traffic flow, the road capacity varies depending on the total density and the traffic composition. Here, the role of PTWs in reducing congestion is evaluated. For the comparison, the flow-density plot for different ratios of PTWs is presented in FIGURE 5.1. The following simulation parameters are used to produce the results. The maximum speed of cars is $V_2 = 100 \text{ km/hr}$, maximum speed of PTWs is $V_1 = 80 \text{ km/hr}$, and we consider a single lane one-way road with a carriage width of 3.5 m .

PTWs stay in free flow state for longer ranges of densities than cars, because of their ability to ride in between other vehicles. The flow-density diagram, which is depicted in FIGURE 5.1(b), shows the variation of the maximum flow rate and the critical density of the two classes. FIGURE 5.1(a) shows the total flow rate against the total volume of vehicles. The total flow rate describes the number of vehicles that leave a given point per unit time, which is equal to the sum of the flow rates of PTWs and cars. As FIGURE 5.1(a) illustrates, increasing the fraction of PTWs from 0% to 10% results in a 9.3% improvement of the road capacity and 2.74% increase of the maximum flow rate.

% of PTWs	Critical density (veh/km)	Maximum flow (veh/hr)
0	43.1	4248
10	47.1	4320
25	58.1	4608
35	72.1	4896
50	116.1	6084

TABLE 5.1: The change in critical density (*veh/km* per unit lane width) and the maximum flow rate (*veh/hr/lane*) at different ratios of PTWs

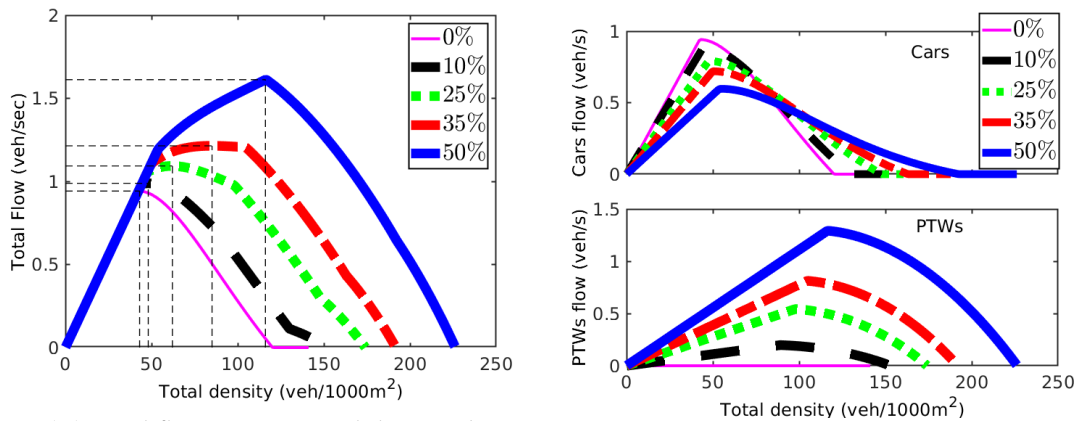
The results in FIGURE 5.1 and TABLE 5.1 point up that the shift to PTWs indeed helps to improve road capacity. Besides, the variation in the reaction of the two vehicle classes for a given traffic situation calls new methods for traffic management and monitoring.

5.1.2 Travel time

Here, we analyze how replacing some of the cars with PTWs improves travel time, based on the instantaneous travel time analysis. The instantaneous travel time (iTT) is computed on the assumption that vehicles travel through the considered road section at a speed profile identical to that of the present local speed, and it is formulated as:

$$t_{inst} = \sum_{i=1}^n \frac{\Delta x}{v(x_i, t)}, \quad (5.1)$$

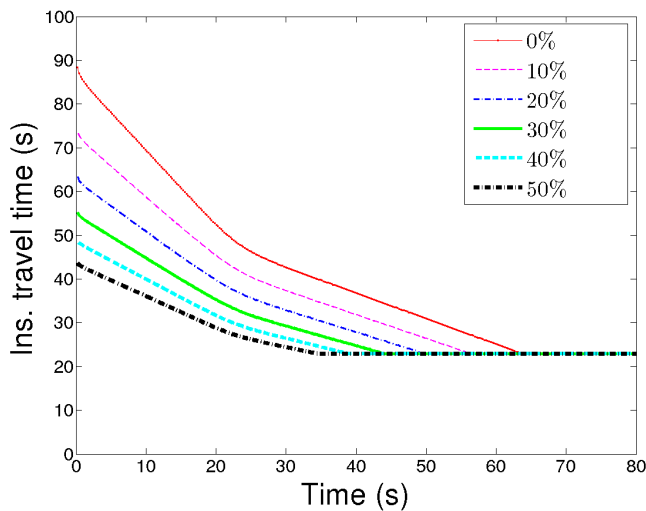
where n is the number of cells and Δx is the mesh size. The experiment is done under the following simulation setup: road length of 500 m , $\Delta x = 10 \text{ m}$, free flow speeds $V_1 = V_2 = 80 \text{ km/hr}$ and the simulation is run for 80 s . A homogeneous initial total density of $\rho_1(x, 0) + \rho_2(x, 0) = 0.1$ for $x \in [0, 500 \text{ m}]$ is set. The result in FIGURE 5.2 is produced by computing the instantaneous travel time every 0.02 s . According to the result, a 12.4% reduction in the average travel time is obtained even at the lowest penetration of PTWs (10%). The table in FIGURE 5.2 below presents the iTT values



(A) Total flow rate vs. total density, the connecting dashed lines show the maximum flow rate and the corresponding road capacity. (B) Flow-total density diagram, upper subplot for cars and lower subplot for PTWs.

FIGURE 5.1: Flow-density diagram, for different penetration rates of PTWs.

averaged over the whole simulation period, for different traffic compositions, and the improvement in the average travel time. According to these results, in addition to the reduction in the average travel times, with the increase in modal shift to PTWs, cars travel at a high speed for longer time. Certainly, the results show that PTWs help in maintaining reliable and reduced travel times.



% of PTWs	cars average travel time	Improv. (%)
0	41.6	
10	36.45	12.4
20	32.74	21.3
30	30	27.9
40	28	32.7
50	26.68	35.9

FIGURE 5.2: The change in travel time of cars for different penetration rate of PTWs.

5.2 Assessing traffic control systems

This section assess the ITS traffic control strategies with respect to the traffic characteristics in cars and PTWs mixed flow. For the study, two traffic control methods, namely adaptive traffic light control and variable speed limit control, are selected.

5.2.1 Adaptive traffic light control

An adaptive signal control (ASC) approach dynamically optimizes traffic signal plan according to the traffic condition in real time. Constantly gathered data is used to detect traffic demand variation, and to determine the appropriate offset, green split and cycle

length. Due to its traffic responsive nature, ASC surpasses the limitation of the conventional pre-calculated signal control methods, which rely on historical data. However, the efficiency of adaptive control scheme is limited by the way the traffic flow characteristics is interpreted. Traffic flow characteristics such as traffic arrival, queue formation and dissipation patterns are the main factors that regulate ASC operation.

Most of the existing adaptive signal controllers are designed for lane-disciplined cars traffic flows. Thus, the operation of ASC is adapted to the traffic characteristics of the lane disciplined flows. This assumption is challenged by the unique traffic flow behaviors appearing as a consequence of the growing use of PTWs. The queue formation and dissipation pattern of PTWs significantly differs from cars. For instance, during queue formations in mixed traffic conditions, PTWs tend to move to the head of the queue by filtering through the queue of other vehicles, giving them the opportunity to leave the queue before other vehicles. Besides, thanks to their high maneuverability, PTWs altogether depart from the queue in a very short time. Therefore, ASC operations based on the knowledge of cars traffic flow can not anticipate this early departure and thus produce a sub-optimal signal plan.

In this section, we analyze the queue build-up and dissipation process in mixed traffic flows consisting of PTWs and cars, and devise an effective adaptive signal control techniques to integrate PTWs in ASC signal plans. We consider adaptive traffic light controllers which allocate green phase lengths according to the variation of traffic volumes (Zhou et al., 2010; Faye, Chaudet, and Demeure, 2012). That is, the green time length is determined based on the volume (number) of vehicles in the queue. Adjusting the green phase length according to the traffic demand (i.e. traffic volume) allows to avoid over/under-allocation of green periods. As pointed earlier, the existing adaptive traffic controllers determine the green length on the knowledge of cars traffic flow, thus the effectiveness of the control scheme is affected by the presence of vehicles with divergent moving behaviors, like PTWs. We show the effect of neglecting the unique characteristics of PTWs on the effectiveness of ASC operation. Further, the benefit of accommodating these unique properties is illustrated.

5.2.1.1 Queue dynamics

Understanding the queue dynamics is a basic procedure for the optimization of traffic signal plan in adaptive schemes. The queue dynamics describes the behavior of vehicles in the queuing process and the pattern they leave the queue. In the mixed flow of PTWs and cars, PTWs lane-sharing behaviors allow them to advance to the front of the queue. In consequence, PTWs dissipate from the queue before other vehicles. The queue dissipation pattern can be illustrated considering the maximum flow rate at which vehicles leave the stop line, called saturation flow rate. For the case of homogeneous traffic flow, the reached saturation flow rate is fairly constant. However, in mixed flow the property is different.

To study the queue dynamics and identify the possible influences on the existing traffic signal operation, we perform simulation experiments. We consider the following simulation scenario: a single-lane isolated intersection with road segment length of 510 m and width of 3.5 m, and a free flow speed of 80 km/hr is chosen for both cars and PTWs. The road segment is divided into cells of size $\Delta x = 5$ m, and the solution is updated at each time step Δt , which is chosen according to the CFL condition $\Delta t \leq \Delta x / \max(V_i)$. The traffic light is located at 500 m, and the red light is active between $t \in [0, 60]$ s]. A fixed total arrival rate of 2 veh/s is set for time $t \in [0, 50]$ s], and the arrival rate is zero for the rest of the simulation times. The arrival rate for each vehicle class is determined from their proportion. Accordingly, the queue dissipation behavior is studied with a gradual increase of PTWs ratio as well as the queue clearance time is analyzed with respect to the traffic composition.

TABLE 5.2 shows the clearance time (CT), denoting the time needed to clear vehicles from the queue. The influence of PTWs on intersection clearance time is illustrated by varying the fraction of PTWs. According to the results, the intersection clearance

time, which is the maximum of the clearance times of the two vehicle classes, decreases with the increase of the ratio of PTWs. This is further shown by examining the queue formation and discharging behaviors. FIGURE 5.3 shows the queue dynamics, for each vehicle class, when the ratio of PTWs is 25%. The lane sharing capability of PTWs grants them to concentrate close to the stop line (FIGURE. 5.3(a)) and dissipate from the queue at higher saturation flow rate (see FIGURE. 5.3(c)).

Ration of PTWs(%)	CT of Cars	CT of PTWs	Relative Error
0	34.74	-	-
15	30.99	13.57	+10.8%
25	28.13	14.02	+19.01%
35	25.43	14.17	+26.79%
50	21.23	14.47	+38.89%
75	14.47	14.77	+57.47%
100	-	14.92	+57.04%

TABLE 5.2: The change in the clearance time with the ration of PTWs

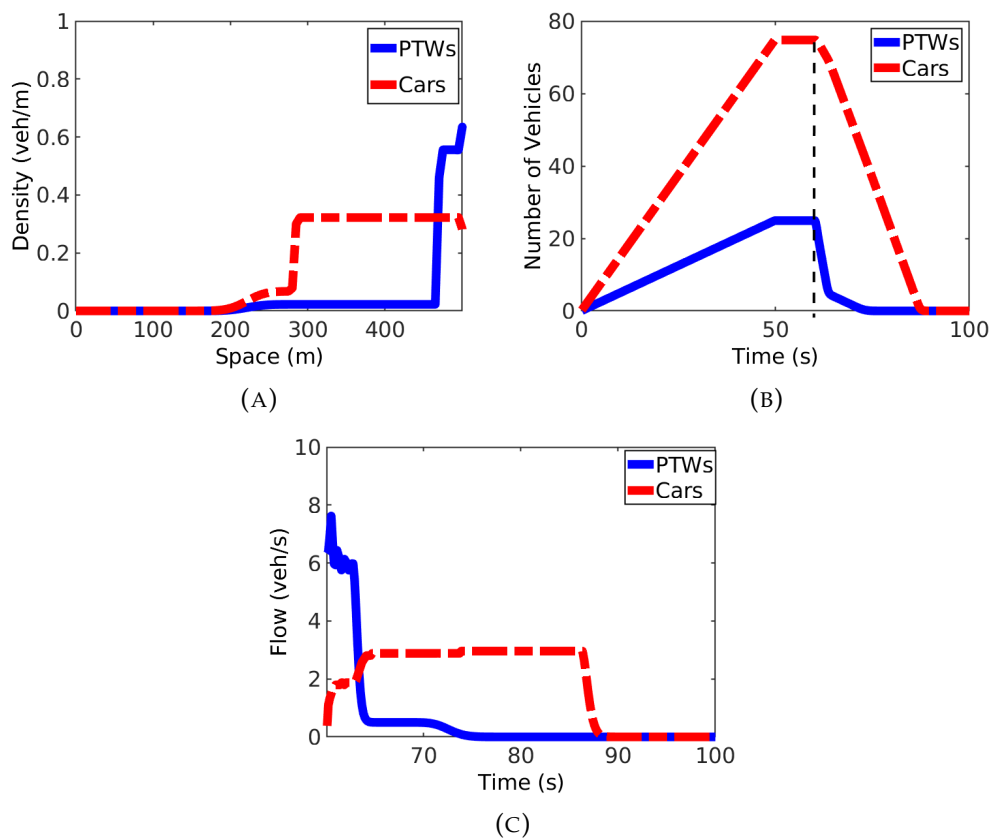


FIGURE 5.3: (A) The density profile immediately before traffic light turns red, (B) The evolution of queue length, and (C) The saturation flow rate, traffic proportion [25% PTWs, 75% Cars]

To explain this from the context of adaptive traffic light operation, let's consider an ASC that counts the number of vehicles in the queue and estimates the queue clearance time correspondingly. Thus, regardless of the proportion of PTWs, the clearance time would be estimated to 34.74 s (see TABLE 5.2) on the assumption of pure cars traffic, resulting in overestimation of clearance time. Moreover, the relative change of the actual CT and estimated CT, i.e. $\frac{\text{Estimated CT} - \text{Actual CT}}{\text{Actual CT}}$, shown in TABLE 5.2 depicts that the estimation error increases with the increase of PTWs ratio. Due to CT overestimation, a longer green time is assigned, which causes unnecessary delay on vehicles waiting in the queue of the adjacent intersections.

The introduction of an advanced stop line for PTWs has been proposed as a strategy to facilitate PTWs mobility at traffic signals (Allen, Bygrave, and Harper, 2005). For traffic lights with advanced stops, we evaluate the clearance time and the discharging behavior, by performing similar experiments. In the simulation, the stop line for cars is located 10 m upstream from the traffic light. The results in FIGURE 5.4 and TABLE 5.3 illustrate that the measured relative CT error is higher than the case for the intersection without advanced stop line.

Ration of PTWs(%)	CT of Cars	CT of PTWs	Relative Error
0	35.34	-	-
15	31.14	13.57	+11.89%
25	28.43	14.02	+19.54%
35	25.73	14.17	+27.18%
50	21.53	14.47	+39.08%
75	14.62	14.77	+58.63%

TABLE 5.3: The change in clearance time with ration of PTW, at traffic light with advanced stop line

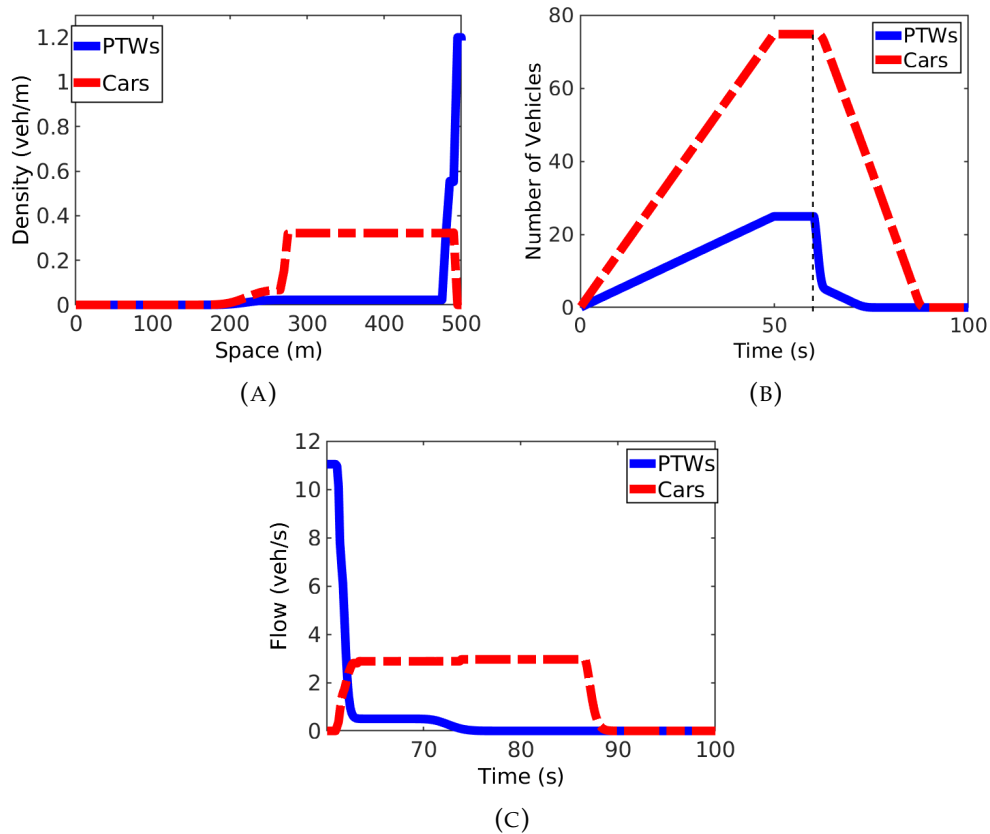


FIGURE 5.4: Traffic light with advanced stop line (A) The density profile immediately before the traffic light turns red (B) The evolution of queue length (C) saturation flow rate, traffic proportion [25% PTWs, 75% Cars]

Given the queue formation and dissipation patterns of PTWs, another alternative to estimate the CT is by excluding PTWs, i.e. considering only the number of cars in the queue to determine the clearance time. Obviously, the estimated CT is below the actual CT. Yet, the divergence from actual CT is lower than the case where all vehicles in the queue are counted (TABLE 5.4).

Both counting all the vehicles and counting only cars in the queue result in the clearance time estimation errors. However, the estimation error for the latter case is smaller, particularly for low PTW penetration rates. Nevertheless, either way the performance

of the ASC is affected as vehicles in the adjacent intersection are forced to wait for more time due to over estimation of the green time in the first case or some vehicles are forced to wait for more than one cycle to clear from the queue in the latter case.

Ration of PTWs(%)	Estimated CT	Actual CT	Relative Error (%)
0	34.74	34.74	0%
15	29.63	30.99	-4.58%
25	26.33	28.13	-5.69%
35	22.88	25.43	-11.18%
50	17.77	21.23	-19.47%

TABLE 5.4: The estimated and the actual clearance time, when PTWs are excluded from CT computation

5.2.1.2 Optimization approach

We consider an adaptive signal control in an isolated intersection that adjusts the green time duration according to the upstream traffic demand. The ASC is assumed to measure queue length in number of vehicles queued at the intersection. The information of queue length can be gathered using connected vehicle technologies or detectors. The green time duration is set for a time sufficient to clear all queued vehicles. Accordingly, the queue clearance time or the green time is computed from the number of queued vehicles and the saturation flow rate (SF), ignoring the start-up loss time at the very beginning of the green time.

However, for the mixed flow of cars and PTWs, the individual vehicle class saturation flow rate is subjected to change, depending on the traffic composition. The variation in the saturation flow rate can be seen in FIGURE 5.3(c). As can be seen, the saturation flow rate of cars at the former green time period is lower than the latter period. The flow-density relation shown in FIGURE 5.5 also explains the dependency of the maximum flow rate or saturation flow rate on the density of the other vehicle class. Therefore, the saturation flow rate for each vehicle class varies with the traffic composition.

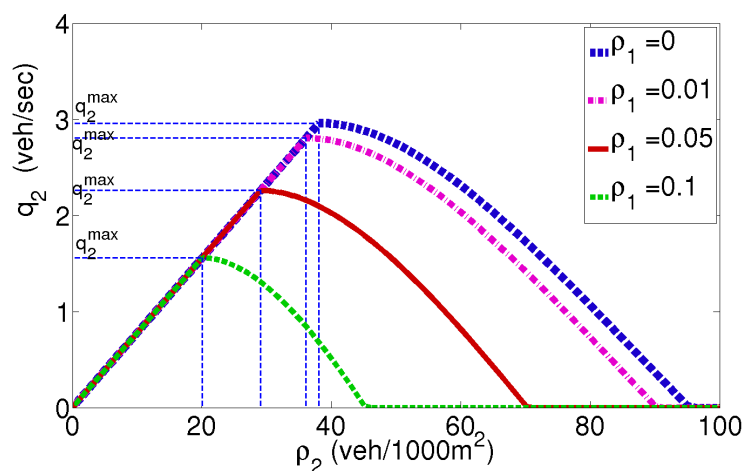


FIGURE 5.5: The variation in flow-density and the maximum flow of cars with PTWs density (veh/m^2).

For the purpose of estimating the saturation flow rate in a less complex way, we develop a passenger car unit (PCU) for PTWs. The total SF rate is, therefore, expressed in PCU. The objective here is to find the PCU values for PTWs so that the total saturation flow rate can be expressed with a constant value regardless of the traffic composition.

Hence, the PCU value of PTWs is expressed according to the following equation.

$$PCU_{PTWs} = \frac{SF_0 - SF_{car}}{SF_{PTW}} \quad (5.2)$$

where SF_0 is the maximum flow rate for pure cars traffic, and SF_{cars} and SF_{PTWs} are the current saturation flow rate of cars and PTWs, respectively.

The results from the simulation runs with different PTWs ratio is used to estimate PCU_{PTWs} (hereafter referred as PCU) values. A result from one example scenario, where we have a similar simulation setting as the previous experiments except here the red time is set to 80 s, is shown in FIGURE 5.6. As depicted in the figure, the PCU values for the first 1 s of the green time decrease sharply and remain constant (≈ 0.19) until the saturation phase ends. The later sharp increases are related to the end of saturation phase, which is not important for our analysis. The result shows that when the ration of PTWs is less than 100%, the PCU value is more or less constant regardless of PTWs proportion, except the fluctuations for very short period at the very beginning of the green time. FIGURE 5.7(b) shows the flow of individual class (veh/s) and the total saturation flow rate in PCU/s. As illustrated, by using the PCU value the variation in the total saturation flow rate is hidden, making it easier for queue clearance time prediction.

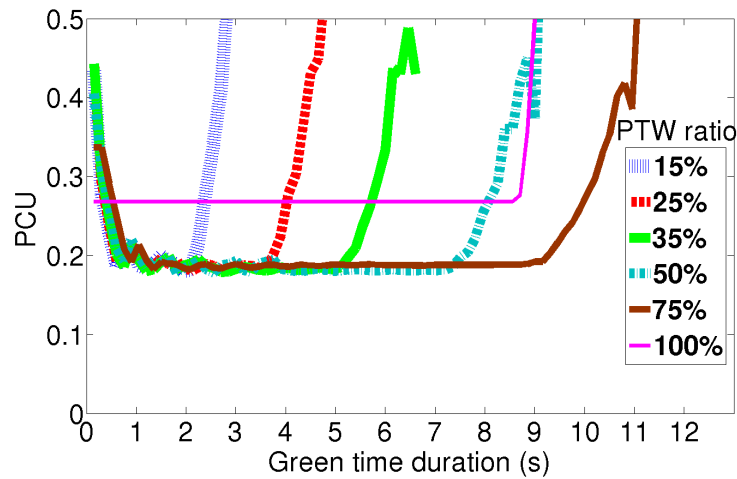


FIGURE 5.6: The change in passenger PCU value of PTWs over the green time duration

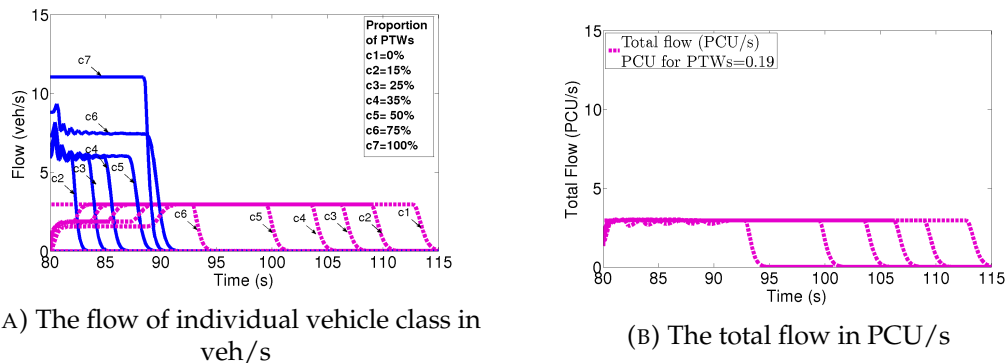


FIGURE 5.7: The saturation flow rate when vehicles discharge from the queue

Therefore, we can use the estimated saturation flow rate expressed in PCU per unit time to determine the green time duration. On the assumption of instantaneous transition to SF state, the green time needed to clear the vehicles in the queue is formulated

as follows:

$$T_{cl} = \frac{PCU * N_1 + N_2}{SF_b} \quad (5.3)$$

where N_1 and N_2 represent the number of PTWs and cars in the queue, respectively. With this formulation we integrate the flow behavior of PTWs and minimize the over / under estimation of the green time.

5.2.1.3 Evaluation

The performance of the proposed green time optimization method is evaluated by comparing with the no-optimized approach. For the simulation, we use the scenario shown in FIGURE 5.8. The length of each intersection approach is 505 m and the stop lines are located at a distance of 5 m upstream. Vehicles inflow rate of 1.3 veh/s and 0.7 veh/s is set for cars and PTWs, respectively. The evolution of the total number of vehicles at the two intersection approaches is assessed and the average delay is measured accordingly. The average delay is determined from the average number of vehicles unable to move to the next cell in one simulation step (Pohlmann and Friedrich, 2010). The green time duration for each approach is decided based on the traffic situation. However, for the first signal phase, intersection approach 1 (R_1) and intersection approach 2 (R_2) starts with green phase and red phase, respectively, where this state lasts for 60 s.

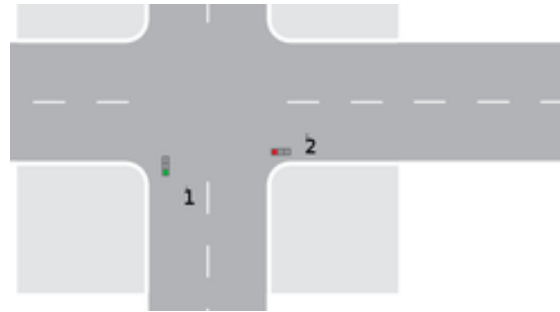


FIGURE 5.8: Simulation experiment scenario

The evolution of the number of vehicles at the first intersection approach is presented in FIGURE 5.9. From the results, it can be observed that the queue length for the non-optimized approach is higher than the optimized approach, which is resulted from the long green time duration. The delay averaged over the simulation time is shown in TABLE 5.5. According to the results, our proposed green time computation method gives a better output in terms of the average delay.

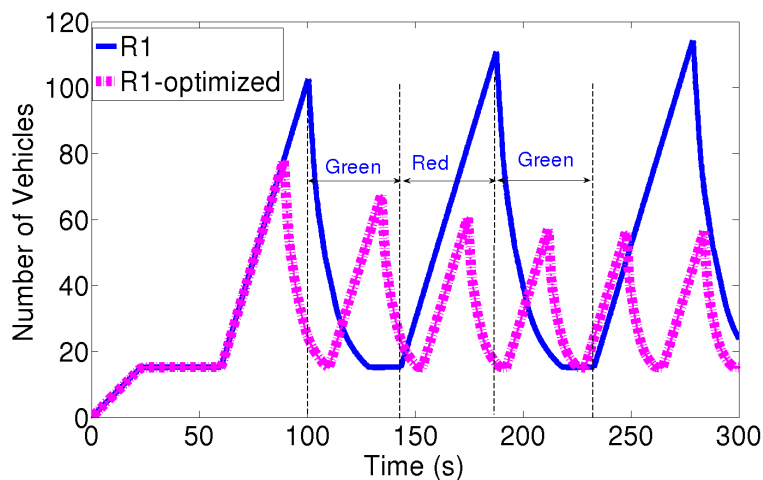


FIGURE 5.9: The evolution of the total number of vehicles in the queue over the simulation time, at the 1st intersection approach

	Non-optimized	Optimized
R_1	42.59	29.36
R_2	46.34	34.8

TABLE 5.5

5.2.2 Variable speed limit control

Variable Speed Limit (VSL) control is one of the widely implemented traffic control strategies (Carlson et al., 2010), and it has showed a promising potential in creating stable flow (Lin, Kang, and G.-L. Chang, 2004), improving safety (Abdel-Aty, Dilmore, and Dhindsa, 2006; C. Lee, Hellinga, and Saccomanno, 2004) and mitigating pollution (Zeg-eye et al., 2009). Depending on the objectives, VSL can be applied in different ways. A VSL intended to reduce speed variations aims at avoiding the occurrence of congestion (Smulders, 1990) or traffic safety issues (Abdel-Aty, Cunningham, et al., 2008) due to speed inhomogeneity. Another application of VSL is to manage congestion at freeway bottlenecks, for example at lane merge locations or lane blocking incidents. By regulating the flow rate upstream of the bottleneck with VSL, traffic delay can be reduced (Lin, Kang, and G.-L. Chang, 2004; Hadiuzzaman, Qiu, and Lu, 2012). Similarly, VSL is implemented to control the upstream propagation of shock wave (Andreas Hegyi, De Schutter, and J. Hellendoorn, 2005; A Hegyi and SP Hoogendoorn, 2010). In essence, the speed is controlled in such a way to reduce inflow to the congestion area so that the congestion dissolves rapidly.

Most of the existing VSL control systems are designed for homogeneous traffic, i.e. the traffic flow is assumed to be composed of vehicles with identical characteristics. In reality, traffics comprise vehicles with varied physical and maneuvering characteristics. The collective traffic flow dynamics is the result of the property of the individual vehicle class and the interaction among the classes. Moreover, each class has a different effect on the traffic flow characteristics. Thus, applying indistinguishable control and management actions in such heterogeneous conditions limits the efficiency of the control system because, first, the system fails to predict the traffic state accurately. Second, identical control action is applied irrespective of the impact the vehicle classes have on the traffic flow. There are only very few studies addressing control strategies for heterogeneous traffic flows.

For traffic flows consisting of cars and trucks, attempts have been made to incorporate the difference between vehicle types. To take into account the heterogeneity of traffic flow, mutli-class model-based freeway traffic control is introduced in (S. Liu, H. Hellendoorn, and De Schutter, 2017; Pasquale et al., 2016). Similarly, Deo, De Schutter, and Andreas Hegyi (Deo, De Schutter, and Andreas Hegyi, 2009) propose a model predictive (MPC) ramp metering and VSL control that utilizes a multi-class model and show the performance improvement obtained by incorporating the heterogeneity in the prediction model. A multi-class model based route guidance presented in (Schreiter et al., 2012) further shows the advantage of adapting a class specific controls.

The aforementioned studies address the multi-class aspect in the context of slow moving trucks and fast moving cars. Despite having different length and speed, cars and truck have similar driving characteristics. The driving dynamics and characteristics of PTWs are however largely different, as they may share the same lane or filter through rows of traffic. Although lane filtering by PTWs is not legally accepted everywhere due to safety concerns, it is a common practice on most of the European roads. Because of these unique maneuvering behaviors, PTWs uniquely impact traffic flows and also have a fully different perception of traffic conditions from cars (e.g. a road jammed for cars may not be necessarily jammed for PTWs (see FIGURE 5.10(a))).

PTWs represent a growing class of traffic, between the year 2002 and 2011 the fleet

of PTWs increased by 17% in Europe (OECD/ITF, 2015). The ability of PTWs to ride between lanes of traffic contributes to congestion reduction and cutting travel time (Yperman, 2011; Wigan, 2002). Nonetheless, unless PTWs are included in VSL and other traffic control systems, the control action could impair the potential benefits. Besides, given the high vulnerability of PTWs, safety issues should be taken into account. For instance, VSL control is often implemented to manage congested or close to congestion traffic situations. In moderate to high traffic levels, PTWs highly engage in lane filtering (Ouellet, 2012; Sperley, Pietz, et al., 2010), which is one of the factors that increase the risk of accident. PTWs appear to be traveling faster than other vehicles (Ouellet, 2012) while accidents occur during lane filtering events. For this reason, the speed control decisions have to be adjusted in order not to further escalate accidents that arise from the speed difference. To ensure efficient and safe operation accordingly, it is important to integrate PTWs in the control systems.

In this section, we propose a VSL control for PTW and cars, following a Model Predictive Control (MPC) approach. The VSL system determines the speed limit for each vehicle type based on traffic efficiency and safety objectives, namely minimizing the total travel time, and minimizing the speed difference between PTWs and cars. The proposed control system uses the Lagrangian representation of the developed model as a traffic state prediction model. We choose the Lagrangian representation because of the flexibility it gives to apply vehicle group/platoon based speed limitation. We analyze the vehicle class specific control approach with simulation experiments. The advantage of class-specific control is discussed by comparing with no-control and single control cases.

5.2.2.1 Methodology

We consider a VSL system that regulates the incoming traffic to minimize congestion. The system predicts the onset of congestion and a proper speed limit is selected to avoid the occurrence of congestion. In an inevitable situation, the propagation of congestion to the upstream direction is suppressed through VSL.

The traffic flow is composed of two vehicle classes, PTWs and cars. The two vehicle classes have different maneuvering behaviors, e.g. PTWs filter between lanes, maintain smaller gaps, etc. Hence, the two classes perceive the traffic conditions differently, the speed-density relation of the two classes shown in FIGURE 5.10(a) illustrates this. Furthermore, the traffic properties, like the capacity flow, the critical and jam density, for each vehicle class vary with the traffic composition (see FIGURE 5.10(b)).

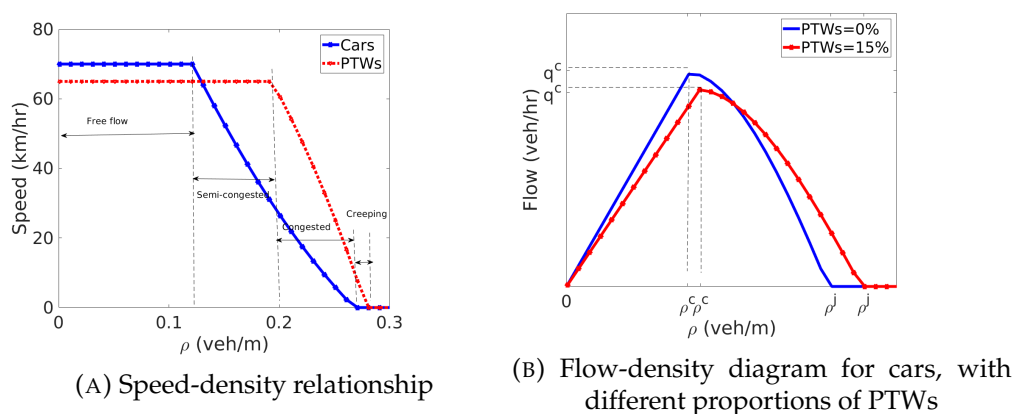


FIGURE 5.10: The fundamental properties of the traffic flow

Under this kind of traffic flow applying identical speed limit for each vehicle class may impact the traffic flow efficiency. As there may be conditions where PTWs should be controlled, at certain traffic conditions the impact of two-wheeler is minimal and imposing a speed limit is unnecessary (FIGURE 5.11(a)). Depending on the proportion of PTWs, the impact they have on escalating congestion varies. For example, when there is

a high number of PTWs, in the event of congestion, PTWs can filter between slow moving cars and enter to the congested area (FIGURE 5.11(b)). Thereby, the outflow from the congested area for cars decreases, which in consequence prolongs the time required to resolve the traffic jam. Nevertheless, at low proportions of PTWs, imposing a speed limit on PTWs has an insignificant impact to the congestion clearance/minimization, rather it may increase travel time of PTWs and apparently PTW riders less like be obedient to the speed limit. Moreover, the decision of the speed limit should take into account safety issues since the speed difference between the two vehicle classes could possibly increase the risk of accident.

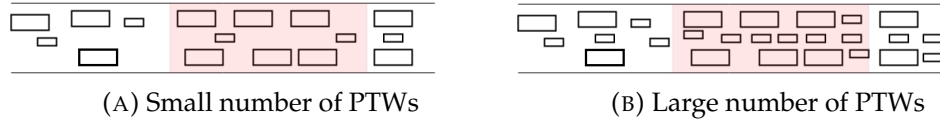


FIGURE 5.11: An illustrative example of traffic conditions at different PTWs proportion

Therefore, we apply vehicle class specific variable speed limit that takes into account traffic efficiency and safety objectives. Different from the common link-based controls, we implement a platoon-based speed limit.

The proposed MPC based variable speed control has two basic building blocks, a multi-class prediction model, and a multi-objective and class specific control algorithm. The control action produced by the control algorithm depends on the measured current traffic state and the future traffic state anticipated by the prediction model.

5.2.2.2 Lagrangian Prediction Model

The Lagrangian representation of the developed model is used to describe the dynamics of the traffic flow. We recall the model discussed in Chapter 3. In one-reference frame Lagrangian representation, the flow equation for the reference class is given by:

$$\frac{\partial s_r(x(t), t)}{\partial t} + \frac{\partial v_r(n, t)}{\partial n} = 0 \quad (5.4)$$

The flow equation for the other vehicle class is written

$$\frac{\partial s_r(x(t), t)/s_o(x(t), t)}{\partial t} + \frac{\partial ((v_r(n, t) - v_o(n, t))/s_o(n, t))}{\partial n} = 0, \quad (5.5)$$

where s and v represent, respectively, the average spacing and the average speed of vehicle group n . The fundamental speed-spacing (density) relation (FIGURE 5.10(a)) is expressed as a function of the density of each vehicle class, i.e.

$$v_i = V_i(s_1, s_2, \dots) = V_u^{max}(1 - F_i(s_1^*, s_2^*, \dots)) \quad (5.6)$$

where V^{max} is the free flow speed and $F_i(\rho_1, \rho_2, \dots)$ represents the proportion of inaccessible free space for vehicle class i . The detailed description of the speed function can be found in Section 3.2.2.

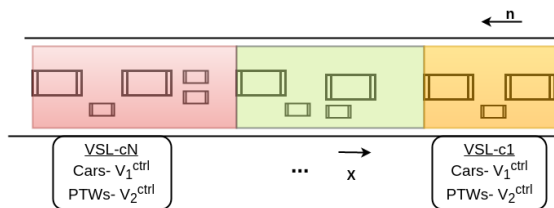


FIGURE 5.12: The representation of the proposed VSL control

In Lagrangian discretization, rather than dividing the road stretch into segments, the vehicles are grouped into $i = 1, \dots, N$ clusters (see FIGURE 5.12). Since the one-reference frame Lagrangian representation is applied here, the cluster is formed according to one of the vehicle class (the reference vehicle class). We takes cars as a reference vehicle class.

Assuming number of vehicles in the clusters remains unchanged, i.e there are no on and off ramps, the evolution of the traffic flow for cars is formulated in Lagrangian coordinates as follows (Hereafter, unless specified, index 1 and 2 denote car and PTWs vehicle classes, respectively).

$$s_{1,i}(k+1) = s_{1,i}(k) - \frac{\Delta t}{\Delta n} (v_{1,i}(s_{1,i}(k), s_{2,i}(k)) - v_{1,i-1}(s_{1,i-1}(k), s_{2,i-1}(k))) \quad (5.7)$$

Where i , Δn , respectively, denote the cluster index, the number of cars in a cluster. k denotes the time step counter and it has the following relation with the simulation time t and the model update time step Δt , $t = k\Delta t$.

The average spacing (s) of PTWs inside the clusters of cars is written as.

$$\left(\frac{s_{1,i}}{s_{2,i}} \right) (k+1) = \left(\frac{s_{1,i}}{s_{2,i}} \right) (k) - \frac{\Delta t}{\Delta n} (f_{2,i+1/2}(k) - f_{2,i-1/2}(k)) \quad (5.8)$$

where $f_{2,i+1/2}$ and $f_{2,i-1/2}$ are the flow rates of PTWs at cluster i boundaries. $\frac{1}{s_{2,i}} = \frac{n_2}{s_{1,i}\Delta n}$, substituting this into equation (5.8), we obtain

$$n_{2,i}(k+1) = n_{2,i}(k) - \Delta t (f_{2,i+1/2}(k) - f_{2,i-1/2}(k)) \quad (5.9)$$

The flows at the boundaries are defined as follows:

If $v_{1,i} < v_{2,i}$,

$$f_{2,i+1/2} = \min \left(0, \frac{(v_{r,i} - v_{o,i+1})}{s_{o,i+1}} \right)$$

$$f_{2,i-1/2} = \min \left(0, \frac{(v_{r,i-1} - v_{o,i})}{s_{o,i}} \right) - \min \left(0, \frac{(v_{r,i-1} - v_{o,i-1})}{s_{o,i-1}} \right)$$

If $v_{1,i} > v_{2,i}$,

$$f_{2,i+1/2} = \frac{(v_{r,i} - v_{o,i})}{s_{o,i}} - \max \left(0, \frac{(v_{r,i} - v_{o,i+1})}{s_{o,i+1}} \right)$$

$$f_{2,i-1/2} = \max \left(0, \frac{(v_{r,i-1} - v_{o,i-1})}{s_{o,i-1}} \right)$$

The simulation time step Δt should be restricted to Courant-Friedrichs-Lewy (CFL) condition, i.e.

$$\Delta t \leq \frac{\Delta n}{\max(\lambda_1, \lambda_2)} \quad (5.10)$$

where λ stands for information propagation speeds (vehicle per second).

In the presence of on and off ramps, the equations for the reference class can be formulated following (Femke van Wageningen-Kessels, Yuan, et al., 2013). For PTWs, vehicle class equation (5.8) is rewritten as:

$$\left(\frac{s_{1,i}}{s_{2,i}} \right) (k+1) = \left(\frac{s_{1,i}}{s_{2,i}} \right) (k) - \frac{\Delta t}{\Delta n} (f_{2,i+1/2}(k) - f_{2,i-1/2}(k) - r_2(x(i), k) + l_2(x(i), k)) \quad (5.11)$$

$r_2(x(i))$ and $l_2(x(i))$ are the the on ramp and off ramp PTWs' flows rate at the location x of cluster i , respectively.

5.2.2.3 MPC-based VSL Controller

The variable speed limit control problem is solved in model predictive control (MPC) scheme. The MPC approach implements a receding optimization strategy. At each time instant, an optimal control sequence is solved over the prediction interval $[k_c T_c, T_c(N_p + k_c - 1)]$, where N_p is the Prediction horizon.

For the sake of minimizing the computation complexity, a control horizon $N_c \leq N_p$ is selected. Consequently, from the control horizon onward the control variable becomes constant. Then, only the first values of the control sequences is applied to the system, and the horizon is moved to the future by T_c step.

We implement a general control frame work similar to (Caligaris, Sacone, and Siri, 2007), where vehicle class specific speed control is applied.

The control variables for N number of clusters and two vehicle classes is written as:

$$v_1^{ctrl}(k) = [v_{1,1}^{ctrl}(k), \dots, v_{1,N}^{ctrl}(k)]$$

$$v_2^{ctrl}(k) = [v_{2,1}^{ctrl}(k), \dots, v_{2,N}^{ctrl}(k)]$$

$$u^{ctrl}(k) = [v_1^{ctrl}(k), v_2^{ctrl}(k)]^T$$

and the state variables, i.e. the spacing and the speed

$$s_1(k) = [s_{1,1}(k), \dots, s_{1,N}(k)]$$

$$s_2(k) = [s_{2,1}(k), \dots, s_{2,N}(k)]$$

$$v_1(k) = [v_{1,1}(k), \dots, v_{1,N}(k)]$$

$$v_2(k) = [v_{2,1}(k), \dots, v_{2,N}(k)]$$

Then, the state equation becomes

$$x(k) = [s_1(k), s_2(k), v_1(k), v_2(k)]^T$$

$$x(k+1) = f(x(k), u^{ctrl}(k))$$

In other words, the traffic state at time $k+1$ is a function of the traffic state and the control input, which is the speed limit, at time k . When the speed limit control is applied, the speed for each vehicle class becomes

$$V_{u,i} = \min\{v_{u,i}, (1 + \alpha_i)v_{u,i}^{ctrl}\} \quad (5.12)$$

$v_{u,i}$ is the desired speed derived from the fundamental relation and α_i is the driver non-compliance factor, i.e. the disobedience of drivers to the speed limit. The equation in equation (5.12) implies that at 100% compliance, vehicles may drive lower than the speed limit due to the traffic condition, but the maximum speed is limited to $v_{u,i}^{ctrl}$.

Objective function

Given the initial conditions, the control objective is to minimize the total time spent (TTS) by all vehicle classes in the freeway mainline via the adjustment of the speed limit. Moreover, we include a safety objective that minimizes the speed difference (SD) between vehicle classes. Thus, our objective function has the following form.

$$J = \alpha_{TTS} \sum_{k_c=1}^{N_p} \sum_{i=1}^N (n_{1,i}(k_c) + n_{2,i}(k_c)) \Delta t + \alpha_{SD} \sum_{k_c=1}^{N_c} \sum_{i=1}^N \left(\frac{v_{1,i}^{ctrl}(k_c) - v_{2,i}^{ctrl}(k_c)}{v_1^f - v_2^f} \right)^2, \quad v_1^f - v_2^f \neq 0 \quad (5.13)$$

Where $n_{1,i}$ and $n_{2,i}$ are number of class 1 and class 2 vehicles, respectively. Correspondingly, $v_{1,i}^{ctrl}(k_c)$, $v_{2,i}^{ctrl}$ stands for the speed limit of class 1 and 2. The weighting factors for TTS, α_{TTS} , and SD, α_{SD} , are tuned depending on the the control policy.

Constraints

The control variable is constrained by the following conditions: The difference between the speed limits in a consecutive control steps should be less than the maximum allowed speed change, which is related to the deceleration/acceleration capability of the vehicle class and safety.

$$\Delta v_{u,i}^{ctr} \leq v_u^{maxdiff} \quad (5.14)$$

The control speed for each class u should be bounded by the minimum speed limit and the free flow speed of the respective class.

$$v_{u,i}^{ctrl} \in [v_u^{min}, v_u^{max}] \quad (5.15)$$

5.2.2.4 Evaluation

In order to evaluate the performance of the proposed VSL control, we compare results from the following three approaches. No control: no speed limit is imposed on any of the two vehicle classes; Single control (1-VSL): the speed limit applies only for cars; Class specific control (2-VSL): separate speed limit for cars and PTWs, which is the proposed approach.

Simulation setup



FIGURE 5.13: Simulation scenario, freeway link

The proposed vehicle class specific VSL control scheme is evaluated in the following simulation scenario. We consider a 3 km long freeway link with no off-ramp and on-ramp. At the initial state, congestion is created at the middle section of the freeway segment and we have a free flow condition in the upstream and the downstream directions (FIGURE 5.13). The VSL is applied to control the flow in the upstream of the congested section. The initial densities are given in TABLE 5.6. The initial densities are chosen such that free-flow conditions are created upstream and downstream of the central location, where we create congestion. The value of the initial densities at the upstream free-flow region are changed so that to increase PTWs proportions and thereby have a significant effect.

TABLE 5.6: Initial densities (veh/m), ρ_1 for cars and ρ_2 for PTWs

Location	[0-1500 m]	[1500-2500 m]	[2500-3000 m]
ρ_1	0.18	0.45	0.2
ρ_2	0.14	0.2	0.1

In the optimization, the control speeds ($v_{1,i}^{ctrl}$ and $v_{2,i}^{ctrl}$) are chosen from the discrete set of VSLs specified for each vehicle class, where $v_{1,i}^{ctrl} \in \{15, 12, 9, 6\}$ and $v_{2,i}^{ctrl} \in \{20, 17, 14, 11\}$. Furthermore, the speed difference between two consecutive speed limits is constrained to 3 m/s (≈ 10 km/hr). For the traffic simulation, the Lagrangian coordinate moves with cars and the platoon/cluster size equals $\Delta n = 50$. The MPC parameters are set to the following values, $N_c = 3$ (1.5 min), $N_p = 5$ (2.5 min), $T_c = 30s$ ($T_c = 36(\Delta t)$). The value of N_p is to the time needed by cars to cross the road segment in free-flow condition. The implemented MPC generates possible sequences of

$v_{1,i}^{ctrl}, v_{2,i}^{ctrl}$ combinations from the discrete speed sets, which conform to the constraints specified, and search for the sequence that optimize the objective function.

The performance of the proposed VSL is investigated by comparing results from the three different VSL control scenarios. First, no VSL control is applied, and the improvement obtained from the VSL control is evaluated with respect to this uncontrolled case. Total time spent (TTS) by vehicles is used as a metric for the evaluation. Furthermore, we study two VSL control cases. In the first case, the control speed is derived and applied only for cars (Hereafter we call it *1-VSL*), whereas in the second case a specific VSL is applied for the individual vehicle class (Hereafter we call it *2-VSLs*). The first case answers the question whether we need to have VSL control for PTWs or not. On the other hand, the later case provides an insight on the benefit/need of having VSL control for PTWs.

Simulation results

Uncontrolled case

The evolution of cars densities and speed in uncontrolled case is presented in FIGURE 5.14(a) and FIGURE 5.14(b), respectively. As illustrated by the figures, the congestion propagates backward (from 1500 m to 500 m) and the effect linger for long time. We show the results for cars only because they are more affected by the congestion and the backward propagation of the congestion is more visible.

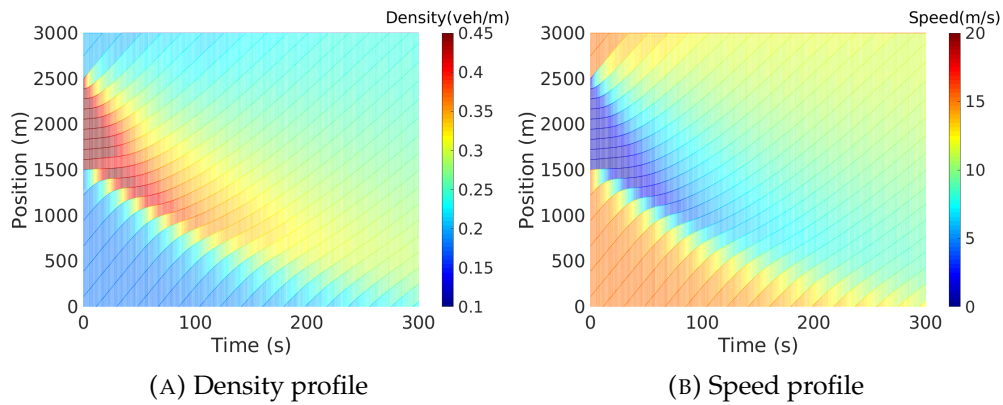


FIGURE 5.14: Evolution of the traffic densities and speed for cars under uncontrolled case

Single control (*1-VSL*)

In this case, we apply a VSL control for cars only. The speed limitation applies only to the platoon upstream of the congested area. The density and speed evolution of cars are shown in FIGURE 5.15. In addition, the speed limits over the simulation period are shown in FIGURE 5.16, no speed limit is imposed on PTWs. As reported by the result, the backward congestion propagation is suppressed. Furthermore, a 3.01% (relative change) improvement in the TTS is obtained. However, as illustrated on FIGURE 5.18, a speed difference between 10-14 m/s is created between cars and PTWs, which creates dangerous overtaking situations.

Class specific control (*2-VSLs*)

In this experiment, similar to the previous ones, the VSL is imposed only to the vehicles upstream of the congested area. But, we have a VSL specific to each vehicle class. The speed and densities evolution cars are shown in FIGURE 5.17 and FIGURE 5.19 respectively. In addition to the TTS minimization, we add the minimization of the speed difference in the objective function, the weighting factors $\alpha_{TTS}, \alpha_{SD}$ set to 1. From the figures in FIGURE 5.17, it can be seen that the congestion propagation is suppressed. We

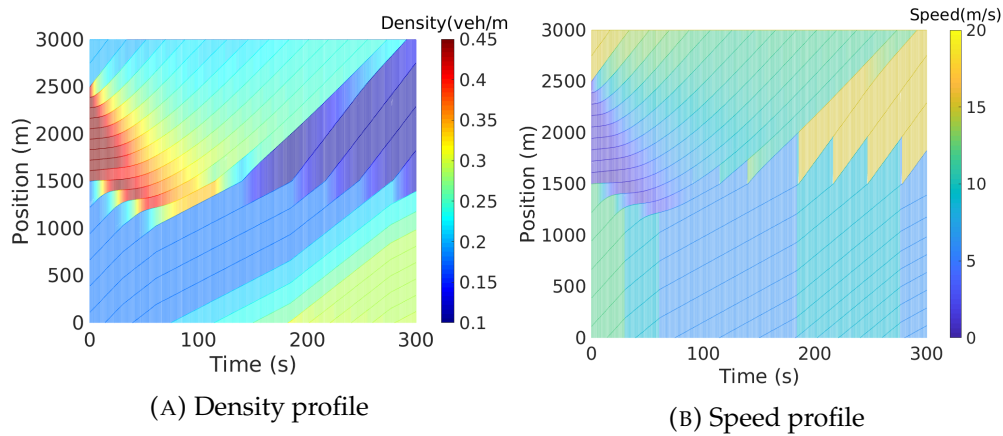


FIGURE 5.15: Evolution of the traffic densities and speed for cars under 1-VSLs

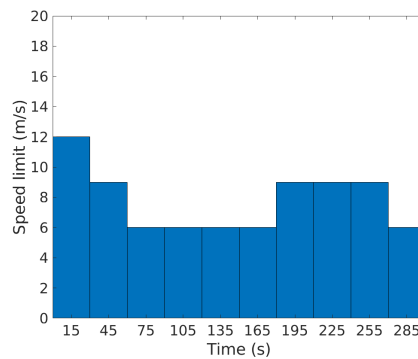


FIGURE 5.16: Time evolution of the speed limit for cars (1-VSL)

achieve 3.12% improvement on the TTS, compared to the uncontrolled case. Compared to 1-VSLs , the TTS is reduced by 0.115%. However, a major improvement is obtained in terms of minimizing the speed difference between cars and PTWs. FIGURE 5.18 depicts the speed difference between PTWs and cars during 1-VSLs and 2-VSLs controls. What we can observe is that the speed difference between cars and PTWs is minimized in the 2-VSLs since the speed limits are optimized considering the speed difference.

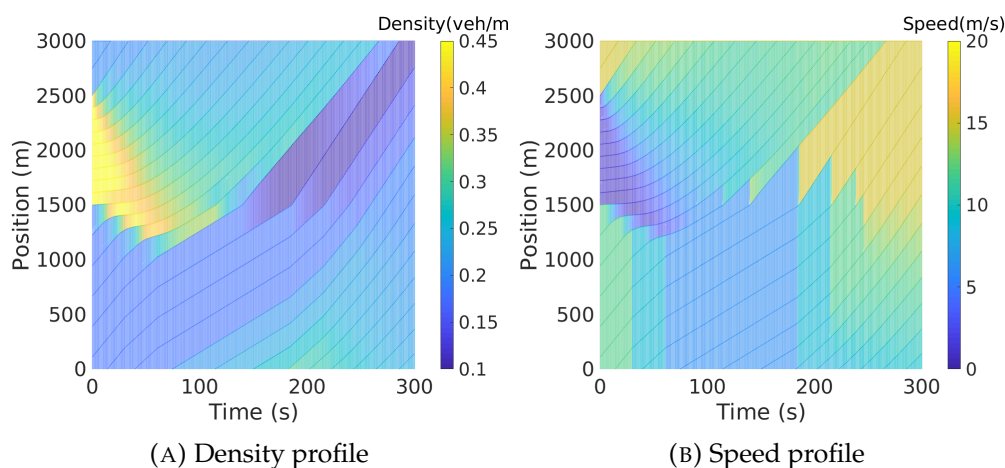


FIGURE 5.17: Evolution of the traffic densities and speed for cars under 2-VSLs

The results represent what we observe at the selected traffic proportion and condition. However, we have noticed also for lower proportions of PTWs, if the speed limit is optimized to minimize TTS only, 1-VSLs and 2-VSLs produce identical results. The reason for this is that PTWs have insignificant impact and imposing speed limit on PTWs

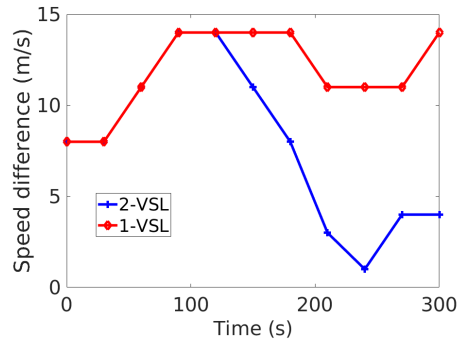


FIGURE 5.18: Speed difference incurred by VSLs for cars and PTWs in (1-VSL) and 2-VSLs controls

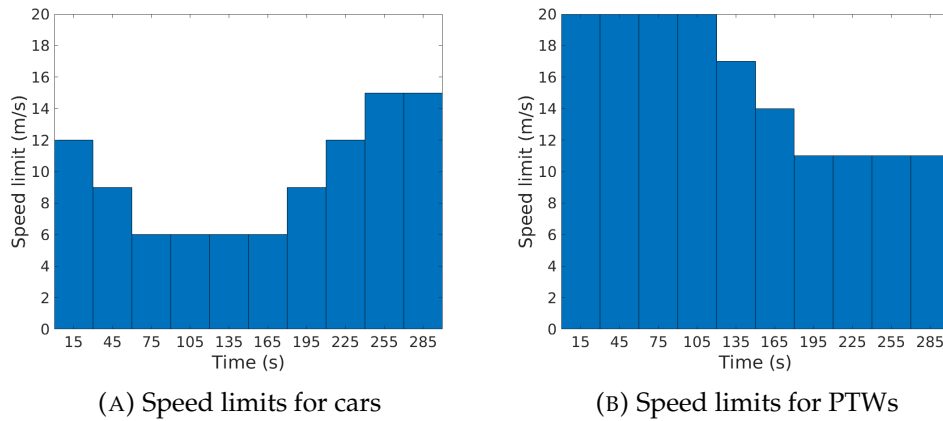


FIGURE 5.19: Speed limits evolution over the simulation time -2-VSLs

neither improve the TTS of cars nor the TTS of the collective traffic. In this case, the advantage with 2-VSLs is the possibility to control the speed difference between cars and PTWs, and thereby to minimize accident risks.

In general, the results show 1-VSLs and 2-VSLs control have almost the same effect in regards to minimizing TTS. Nonetheless, the 2-VSLs is able to minimize the speed difference between PTWs and cars, thus potential accident situations, and this at no impact on TTS compared to 1-VSLs. Implementing a VSL control for both cars and PTWs creates a more efficient mobility and conjointly reduce accident opportunities. Therefore, vehicle-class based optimization is beneficial from both traffic efficiency and safety aspects.

The proposed variable speed limit control strategy notably illustrates the need to optimize speed differences in a multi-class VSL between PTW and cars to keep the peculiar advantage of PTWs and yet to mitigate safety risks between the two vehicle types.

5.3 Summary and conclusion

The growing use of PTWs has brought opportunities and at the same time challenges. The shift to PTWs can help in easing congestion. However, the peculiar maneuvering feature of PTWs pose a challenge on the integration of PTWs into the transport system. Despite the advancement of smart traffic management and control systems, little has done to integrate PTWs to these systems. The growing penetration of PTWs added to their vulnerability and unique maneuverability demands for the integration of PTWs to C-ITS systems. In this chapter, the developed heterogeneous traffic flow model is applied to study the traffic characteristics that are important to integrate PTWs into the ITS.

In heterogeneous traffic flow the road capacity depends on traffic composition. We analyzed the variation of the capacity with the ratio of PTWs. It appears that with increase of the ratio of PTWs the road capacity increases. This emphasizes the advantage of the shift to PTWs in minimizing traffic congestion. The travel time of PTWs and cars is also assessed. The results show that PTWs have shorter travel time than cars in all the times. The capability of PTWs to filter between traffic lanes grants them an advantage to experience a shorter travel time. This is important properties that should be considered in the development ITS applications for PTWs, e.g., in multi-modal transport and optimal route planning. Furthermore, PTWs have a different perception of the traffic state than cars, for example a congested state for cars does not necessarily implies the same for PTWs. Traffic information systems, such as traffic jam indication, should also take into account this variation.

Moreover, the existing traffic control approaches are evaluated taking adaptive traffic light and variable speed limit control systems as an examples. We develop a method to integrate PTWs into the systems. The integration of PTWs is found to improve the efficiency of the systems. The implication of the variable speed limit control approach to traffic safety is also pointed out.

Chapter 6

Conclusion

This dissertation focuses on the development and analysis of a traffic flow model that can accurately capture the traffic features in a mixed flow of cars and PTWs. The objective is to develop a model that can be applied in a wide range of ITS applications. We find out that multi-class LWR approach is suitable for our purpose. LWR models are efficient for analytical and theoretical analysis of traffic phenomena at large-scale. Their computational efficiency makes LWR models also preferable for real-time ITS applications. Moreover, the possibility to represent the traffic flow in Eulerian and Lagrangian frameworks allows to study the traffic flow from two different observation points. In the Eulerian representation, the flow is analyzed with respect to a fixed reference point. On the other hand, the Lagrangian representation tracks the trajectory of vehicles, which permits to study the traffic flow at a finer level of detail, but still using the macroscopic laws.

This chapter summarizes the main research contributions of the dissertation and suggests future research directions.

6.1 Research contributions

Model development

The Multi-class LWR modeling approach decomposes the heterogeneous traffic flow into homogeneous sub-flows or vehicle classes. Different approximation methods and analogies are introduced to represent the interaction between the vehicle classes. In this dissertation, the porous flow method is employed, which treats the flow of vehicles in analogy with the flow of a fluid in a porous medium. Transforming the concept to traffic flow modeling, the road space is considered as the porous medium where the pores represent the inter-vehicle spacing. This approach reflects the maneuvering behavior of disordered traffic flows, such as mixed cars and PTWs flow.

In order to use the porous flow approach for traffic flow modeling, it is essential to characterize the inter-vehicle spacing (or the pore size) distribution. Here, we introduce a new method for the determination of the pore size distribution (Chapter 3). Furthermore, it is also important to derive the parameters of the distribution. For this reason, we estimate the parameters of the distribution by approximating the spatial distribution of vehicles with a planar Poisson point process. We find out that the pore size distribution better fits with truncated normal distribution. The parameters of the truncated distribution are defined uniquely for each vehicle class density. The relation of the distribution parameters and the road width is also included in the parameters definition.

The flow equation is described in Lagrangian and Eulerian frameworks. In the Eulerian representation, the movement of vehicles is expressed with respect to a fixed reference frame. Whereas, the Lagrangian representation describes the flow equation with respect to a reference frame that moves with vehicles. The two representations provide different views of the traffic phenomena. For applications that use traffic data collected along the trajectory of vehicles, e.g, floating car data, the Lagrangian model is more convenient. The Eulerian model is suitable for application developed to utilize Eulerian measurements, e.g, data from loop detectors and cameras.

Discretization scheme

We developed a numerical scheme to solve the flow equations represented in the Lagrangian and the Eulerian frameworks. The Lax-Friedrichs discretization scheme is applied for the Eulerian representation (Chapter 3). For the Lagrangian representation, we develop a new discretization scheme. The scheme is derived based on the underlying traffic characteristics in traffic flow consisting of cars and PTWs, particularly we look at the average speeds of the vehicle classes at different traffic states. We prove that the discretization method leads to the conservation equation. Further, the developed discretization method is evaluated numerically. We compare the result from the Eulerian and the Lagrangian discretization methods. The results show that the Lagrangian method produces an accurate description.

Model validation and calibration

The developed model is calibrated and validated using synthetic data obtained from a micro-simulation tool. In the calibration process, the parameters of the fundamental diagrams are adjusted to fit the observation. For the calibration, a trial-error method is applied. We calibrate the jam density of each vehicle class, which is expressed as a function of the traffic composition. Further, the critical pore-size (gap) is calibrated. The critical pore size is expressed as a function of the traffic state and the width of vehicles. In the validation process, the inter-vehicle spacing (or pore size) distribution is validated. Using the calibrated parameters, the applicability of the developed model is validated. The simulation results closely replicate the observed average speed.

Model application

ITS has a potential to benefit PTWs in so many ways. However, the effort made to integrate PTWs into the intelligent transportation systems is relatively insufficient, and the existing ITS applications for PTWs are designed mainly to mitigate safety issues. Indeed, addressing safety challenges is essential, but solving other traffic problems is also important. The developed model can contribute as enabler for PTWs-aware ITS application and traffic regulations. In general, the model can be utilized for the following purposes:

- For analyzing the traffic characteristics in a mixed car and PTWs flow.
- For the evaluation of different traffic policies.
- For the development of PTW-aware traffic management and control ITS applications.

In this dissertation, we analyze the impact of PTWs on road capacity and travel time. Understanding these behaviors is crucial to identify the opportunity PTWs provide to the traffic flow. As such, the traffic management or control strategies can be adapted to the prevailing traffic patterns. The mode shift towards PTWs has a contribution in relieving congestion. For proper utilization of this benefit, the use of PTWs has to be encouraged in different ways, e.g., by including PTWs in multi-modal transport planning systems. PTWs experience a shorter travel time than cars because of their ability to filter between traffic to escape congestion. The developed model can be applied to design a smart two-wheeler navigation system which is well aware of PTWs' capability to move through congested car traffic and provides a route plan accordingly.

We also study the operation of adaptive traffic light control systems and show how the efficiency of the system can be improved by integrating PTWs into the system. Furthermore, we developed a vehicle-classed based variable speed limit control system. We illustrate the advantage of optimizing the speed limit to the maneuvering behavior of PTWs to enhance the flow efficiency as well as traffic safety.

6.2 Future research direction

In this section, we recommend directions for future research. We discuss the two aspects of the model, the theoretical model development and the model validation and calibration.

The model is developed based on the requirements set out on the fundamental relations. However, the requirements has to be further refined to include other empirical observations. Explicit identification of the behavior rule for the two vehicle classes is also important. One can argue that the rule applied to describe PTWs is insufficient to represent the traffic characteristics of cars. Having a complete list of the individual vehicle class characteristics and interaction between them helps to include detailed traffic flow characteristics, thereby improving the model.

Another aspect is the simplification of the speed function. The complexity of the speed function hinders to analyze the mathematical properties of the model in detail. For this reason, using alternative formulation or simplifying the speed function is recommended. The porous flow method interestingly can describe the traffic patterns in mixed car and PTWs flow. Nevertheless, introducing a new approach to characterize the inter-vehicle spacing would add improvement. No distribution can describe the inter-vehicle spacing at all traffic states. Combining different distributions increases the complexity of the model, rather finding an alternative way to define the inter-vehicle spacing is preferable.

It is also important to investigate the model properties with a higher number of vehicle classes, that have different characteristics. Explicit consideration of the behavior of non-lane based and lane-following vehicles would also be useful for the model improvement.

For model calibration and validation, we employed data from a micro simulation tool. However, the procedures are limited to a simple case study. Moreover, although there is an advantage in using simulation tools in terms of flexibility and the possibility to study a wider range of scenarios, synthetic data are not sufficient to observe all real-world traffic behaviors. The challenge of getting real mobility traces remains an issue. Nonetheless, an exhaustive model validation/calibration should be done using real traffic data.

Appendix A

The parameters used For the fundamental diagrams

Common parameters	$v_1^{max}=70\text{km/hr}$, $v_2^{max}=65\text{km/hr}$, $q_{cap}=7500\text{ veh/hr}$ $l_1=3\text{m}$, $l_2=5\text{m}$
	Units* Speed(v)=km/hr, Flow(q)=veh/hr Density(ρ)=veh/m, T=s, l=m
Model	Parameters
G. Wong and S. Wong, 2002	$\rho_0=0.08$
Chanut and Buisson, 2003	$\rho_{jam}^r=1/3$, $\rho_{cr}^r=0.15$, $V_c = 50$, $\alpha_1=1$, $\alpha_2=5/3$, $\zeta=0.5$
Ngoduy and R. Liu, 2007	$\rho_{jam}^r=1/3$, $\rho_{cr}^r=0.15$, $V_c = 50$, $\alpha_1=1$, $\alpha_2=5/3$
J Van Lint, Serge Hoogendoorn, and Schreuder, 2008	$\rho_{jam}^r=1/3$, $\rho_{cr}^r=0.15$, $V_c = 50$, $T_1=1.2$, $T_2=1.8$
S Logghe and L. H. Immers, 2008; Qian et al., 2017	$r_{1,cr}^h=0.04$, $r_{2,cr}^h=0.1$, $\rho_{jam} = 0.2$
H. Zhang and Jin, 2002	$\tau_1 = 0.5$, $\tau_2=1$
Benzoni-Gavage and Colombo, 2003	
Fan and Work, 2015	$r_1^{max}=1.8$, $r_2^{max}=1$
Nair, Mahmassani, and Miller-Hooks, 2012	$\alpha_r = \alpha_f = 1$, $l_{max}=3$, $l_{min} = 0.01$, $r_1^{cr} = 0.75$, $r_1^{cr} = 2$, $a_1 = 1.125$, $a_2 = 8$

TABLE A.1: Parameters used to reproduce the fundamental diagrams in Chapter 2

Appendix B

Model development

B.1 Pore size distribution

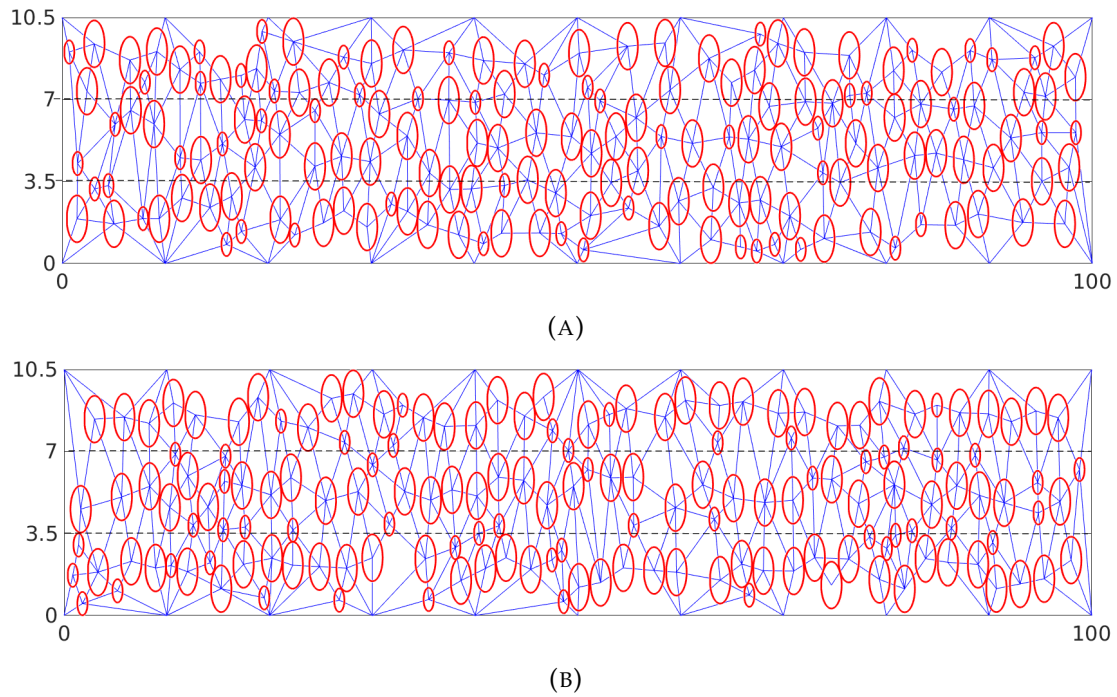


FIGURE B.1: Vehicle distribution in two different settings (A) Disordered flows (B) Semi-ordered flows, $\rho_1 = 0.05\text{veh}/\text{m}^2$, $\rho_2 = 0.1\text{veh}/\text{m}^2$

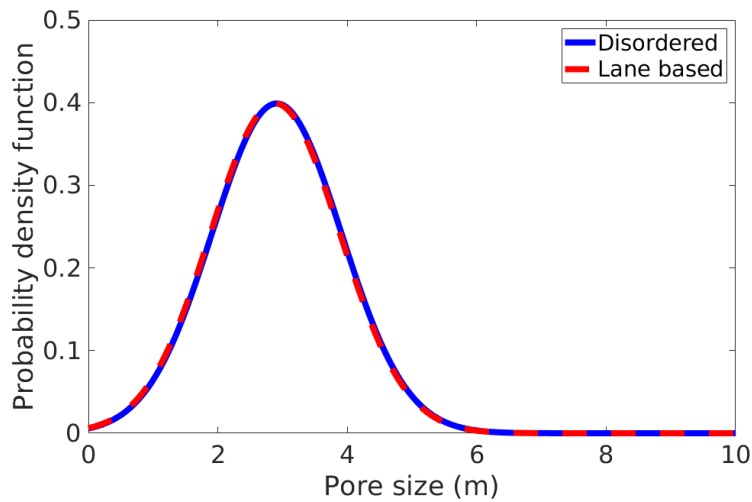


FIGURE B.2: Probability density functions extracted from the settings in FIGURE B.1

The variation of pore size distribution with traffic road width

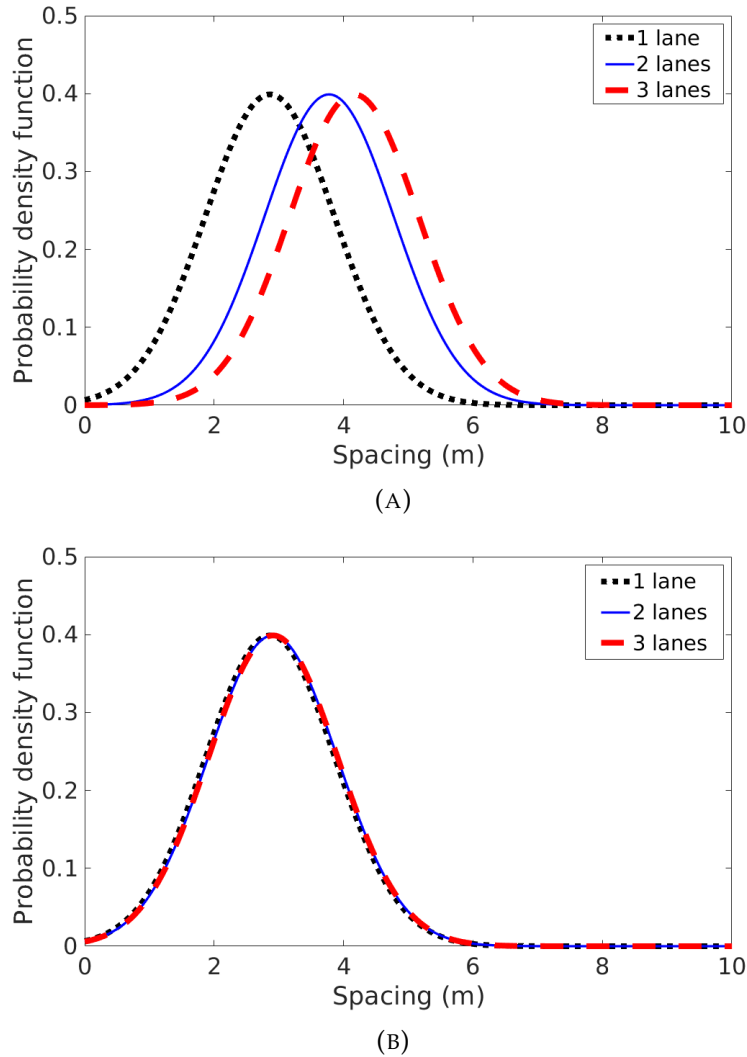


FIGURE B.3: Example of the variation in probability density function with road width (number of lanes)(A) Lower traffic densities ($\rho_1 = 0.01veh/m^2$, $\rho_2 = 0.04veh/m^2$) (B) Higher traffic densities ($\rho_1 = 0.05veh/m^2$, $\rho_2 = 0.1veh/m^2$)

Determination of the maximum area occupancy

We have distinguished the maximum total occupied area, which is the extreme total occupied areas corresponding to the null speed of a vehicle class, for the two classes in such a way that

We chose the value for the maximum total occupied area of cars on the basis of the following assumption: when we have car only traffic, jamming occurs at the point where $L_c * N_c = n * L$, here L_c, N_c, L, n denote length of car, number of cars, length of the road segment and number of lanes, respectively. Accordingly, the number of cars at the jammed condition equals $N_c = \frac{n*L}{L_c}$. Dividing the total area of cars to total area of the road segment, we can get the fraction of area occupied by cars.

$$A_{max}^c = \frac{N_c * A_c}{n * W * L'}$$

where W is the width of a single lane road and A_c is area of a car. Substituting N_c with $\frac{n*L}{L_c}$, $A_{max}^c = \frac{A_c}{L_c * W}$. In our case, $A_c = \pi * r_c^2$ and $L_c = 2 * r_c$, where r_c is the radius for cars. Taking $r_c = 1.5$ and $W = 3.2$, at the jammed condition the total area occupied

equals ≈ 0.79 . However, for mixed cars and PTWs traffic, in a single lane three PTWs can move side by side, and even if the total area occupied equals ≈ 0.79 there might be a space for cars. Thus, to take into account this situation we allowed the value to be a bit higher than the computed value, i.e. 0.85.

B.2 Lagrangian discretization method

The discretization scheme introduced in section 3.4.2.2 leads to the conservation law. We show here the derivation of the conservation law from the discretization method.

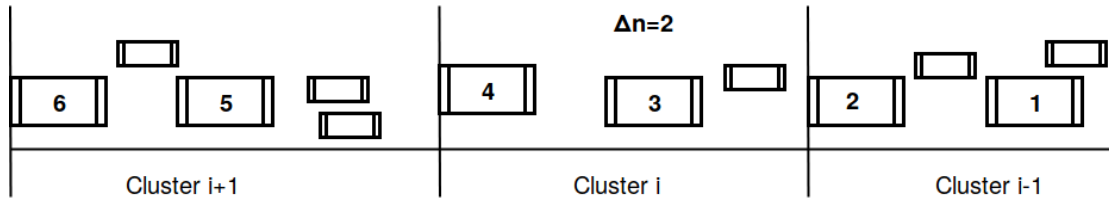


FIGURE B.4: Vehicle grouping according vehicle class 2 (cars), for the case $\Delta n = 1$

For the reference class,

$$(s_{r,i})^{t+\Delta t} \Delta n = (s_{r,i})^t \Delta n - v_{r,i}^t \Delta t + v_{r,i-1}^t \Delta t \quad (\text{B.1})$$

$$\frac{(s_{r,i})^{t+\Delta t} - (s_{r,i})^t}{\Delta t} = - \frac{v_{r,i}^t - v_{r,i-1}^t}{\Delta n} \quad (\text{B.2})$$

when $\Delta t \rightarrow 0, \Delta n \rightarrow 0$, equation (B.2) becomes

$$\frac{\partial s_r}{\partial t} + \frac{\partial v_r}{\partial n} = 0 \quad (\text{B.3})$$

If the relation $v_r > v_o$ holds always, then, for the non-reference class the conservation law is derived from the discretization scheme as follows:

$$N_{o,i}^{t+\Delta t} = N_{o,i}^t + \left(\frac{v_{r,i-1} - v_{o,i-1}}{s_{o,i-1}} \right)^t \Delta t - \left(\frac{v_{r,i} - v_{o,i}}{s_{o,i}} \right)^t \Delta t \quad (\text{B.4})$$

Equation (B.4) implies that the number of other class vehicle in the cluster i of the reference class changes by the number of vehicles entering from cluster $i-1$ and leaving cluster i to $i+1$.

$$N_{o,i} = \Delta n \frac{s_{r,i}}{s_{o,i}} \quad (\text{B.5})$$

Substituting N in equation (B.4) with equation (B.5),

$$\Delta n \left(\frac{s_{r,i}}{s_{o,i}} \right)^{t+\Delta t} = \Delta n \left(\frac{s_{r,i}}{s_{o,i}} \right)^t + \Delta t \left(\left(\frac{v_{r,i-1} - v_{o,i-1}}{s_{o,i-1}} \right)^t - \left(\frac{v_{r,i} - v_{o,i}}{s_{o,i}} \right)^t \right) \quad (\text{B.6})$$

$$\left(\frac{\left(\frac{s_{r,i}}{s_{o,i}} \right)^{t+\Delta t} - \left(\frac{s_{r,i}}{s_{o,i}} \right)^t}{\Delta t} \right) = - \left(\frac{\left(\frac{v_{r,i-1} - v_{o,i-1}}{s_{o,i-1}} \right)^t - \left(\frac{v_{r,i} - v_{o,i}}{s_{o,i}} \right)^t}{\Delta n} \right) \quad (\text{B.7})$$

Rearranging, and $\Delta t \rightarrow 0, \Delta n \rightarrow 0$ the conservation equation is obtained.

$$\frac{\partial (s_{r,i}/s_{o,i})}{\partial t} + \frac{\partial ((v_{r,i} - v_{o,i})/s_{o,i})}{\partial n} = 0 \quad (\text{B.8})$$

If the relation $v_r < v_o$ holds always, then, for the non-reference class the conservation law is derived from the discretization scheme as follows:

$$N_{o,i}^{t+\Delta t} = N_{o,i}^t + \left(\frac{v_{o,i+1} - v_{r,i}}{s_{o,i+1}} \right)^t \Delta t - \left(\frac{v_{o,i} - v_{r,i-1}}{s_{o,i}} \right)^t \Delta t \quad (\text{B.9})$$

Equation (B.9) implies that the number of other class vehicle in the cluster i of the reference class changes by the number of vehicles entering from cluster $i+1$ and leaving cluster i to $i-1$.

Substituting N in equation (B.9) with equation (B.5),

$$\Delta n \left(\frac{s_{r,i}}{s_{o,i}} \right)^{t+\Delta t} = \Delta n \left(\frac{s_{r,i}}{s_{o,i}} \right)^t + \left(\frac{v_{o,i+1} - v_{r,i}}{s_{o,i+1}} \right)^t \Delta t - \left(\frac{v_{o,i} - v_{r,i-1}}{s_{o,i}} \right)^t \Delta t \quad (\text{B.10})$$

$$\Delta n \left(\frac{s_{r,i}}{s_{o,i}} \right)^{t+\Delta t} = \Delta n \left(\frac{s_{r,i}}{s_{o,i}} \right)^t + \Delta t \left(\left(\frac{v_{o,i+1}}{s_{o,i+1}} - \frac{v_{o,i}}{s_{o,i}} \right) - \left(\frac{v_{r,i}}{s_{o,i+1}} - \frac{v_{r,i-1}}{s_{o,i}} \right) \right)^t \quad (\text{B.11})$$

From equation (B.2) we can get

$$v_{r,i-1} = \Delta n \frac{\Delta s_{r,i}}{\Delta t} + v_{r,i} \quad (\text{B.12})$$

Substituting equation (B.12) into equation (B.11)

$$\frac{\left(\frac{s_{r,i}}{s_{o,i}} \right)^{t+\Delta t} - \left(\frac{s_{r,i}}{s_{o,i}} \right)^t}{\Delta t} = \frac{\left(\frac{v_{o,i+1}}{s_{o,i+1}} - \frac{v_{o,i}}{s_{o,i}} \right)}{\Delta n} - v_{r,i} \frac{\frac{1}{s_{o,i+1}} - \frac{1}{s_{o,i}}}{\Delta n} + \frac{1}{s_{o,i}} \frac{\Delta s_{r,i}}{\Delta t} \quad (\text{B.13})$$

$$\frac{\Delta (s_r/s_o)}{\Delta t} = \frac{\Delta (v_o/s_o)}{\Delta n} - v_r \frac{\Delta (1/s_o)}{\Delta n} + 1/s_o \frac{\Delta s_r}{\Delta t} \quad (\text{B.14})$$

$\Delta t \rightarrow 0, \Delta n \rightarrow 0$

$$\frac{\partial (s_r/s_o)}{\partial t} - \frac{\partial (v_o/s_o)}{\partial n} + v_r \frac{\partial (1/s_o)}{\partial n} - 1/s_o \frac{\partial s_r}{\partial t} = 0 \quad (\text{B.15})$$

$$\frac{\partial s_o}{\partial t} + s_o/s_r \frac{\partial v_o}{\partial n} - \frac{v_o - v_r}{s_r} \frac{\partial s_o}{\partial n} = 0 \quad (\text{B.16})$$

equation (B.16) and equation (B.8) are equivalent.

Appendix C

VISSIM simulation

The following settings are used for Vissim simulation.

C.1 Vehicles parameter

TABLE C.1: Vehicles parameters

	Max. speed	length	Width
Cars	70km/hr	4.012m	1.852m
PTWs	60 km/hr	2m	0.848m

C.2 Parameter for Wiedemann model and Later distance

TABLE C.2: The parameters of the car following model (Wiedemann 99)

	CC0	CC1	min. lateral distance	
			Driving	Standing
Cars	0.8m	0.5s	0.6m	0.2m
PTWs	0.4m	0.25s	0.3m	0.1m

Appendix D

List of publications

1. Gashaw, S., Goatin, P. and Härrri, J., 2018. Modeling and analysis of mixed flow of cars and powered two wheelers. *Transportation research part C: emerging technologies*, 89, pp.148-167
2. Gashaw, S., Härrria, J. and Goatin, P., 2017. Adaptive Traffic Signal Control Under Mixed Traffic Condition. *International Scientific Conference on Mobility and Transport*, Munich, Germany
3. Gashaw, S., Härrri, J. and Goatin, P., 2018. Lagrangian formulation for mixed traffic flow including two-wheelers. *The 21st IEEE International Conference on Intelligent Transportation Systems*, Maui, Hawaii, USA
4. Gashaw, S., Goatin, P. and Härrri, J., 2017. Modeling and analysis of mixed flow of cars and powered two wheelers. *96th Annual Meeting of the Transportation Research Board*, Washington DC, USA. (presentation only)
5. Gashaw, S., Goatin, P. and Härrri, J., 2019. Variable Speed Limit Control for Mixed Powered Two-Wheelers and Cars Traffic. *98th Annual Meeting of the Transportation Research Board*, Washington DC, USA. (accepted for presentation)

Bibliography

- Abdel-Aty, Mohamed, Ryan Cunningham, et al. (2008). "Dynamic variable speed limit strategies for real-time crash risk reduction on freeways". In: *Transportation Research Record: Journal of the Transportation Research Board* 2078, pp. 108–116.
- Abdel-Aty, Mohamed, Jeremy Dilmore, and Albinder Dhindsa (2006). "Evaluation of variable speed limits for real-time freeway safety improvement". In: *Accident analysis & prevention* 38.2, pp. 335–345.
- Adler, Jeffrey L and Victor J Blue (1998). "Toward the design of intelligent traveler information systems". In: *Transportation Research Part C: Emerging Technologies* 6.3, pp. 157–172.
- Adnan, Muhammad (2014). "Passenger car equivalent factors in heterogenous traffic environment-are we using the right numbers?" In: *Procedia engineering* 77, pp. 106–113.
- Aghabayk, Kayvan et al. (2011). "Examining vehicle interactions during a vehicle-following manoeuvre". In: *Australasian Transport Research Forum (ATRF), 34th, 2011, vol. 34, Adelaide, South Australia, Australia*.
- Allen, D, S Bygrave, and H Harper (2005). "PUBLISHED PROJECT REPORT PPR240". In:
- Ambarwati, Lasmini et al. (2014). "Empirical analysis of heterogeneous traffic flow and calibration of porous flow model". In: *Transportation research part C: emerging technologies* 48, pp. 418–436.
- Arasan, V Thamizh and Reebu Zachariah Koshy (2005). "Methodology for modeling highly heterogeneous traffic flow". In: *Journal of Transportation Engineering* 131.7, pp. 544–551.
- Aupetit, Samuel, Stéphane Espié, and Samir Bouaziz (2015). "Naturalistic study of riders' behaviour in lane-splitting situations". In: *Cognition, Technology & Work* 17.2, pp. 301–313.
- Aw, AATM and Michel Rasclé (2000). "Resurrection of" second order" models of traffic flow". In: *SIAM journal on applied mathematics* 60.3, pp. 916–938.
- Barlovic, Robert et al. (1998). "Metastable states in cellular automata for traffic flow". In: *The European Physical Journal B-Condensed Matter and Complex Systems* 5.3, pp. 793–800.
- Barpounakis, Emmanouil N, Eleni I Vlahogianni, and John C Golias (2016). "Intelligent transportation systems and powered two wheelers traffic". In: *IEEE Transactions on Intelligent Transportation Systems* 17.4, pp. 908–916.
- Benekohal, Rahim Ray F (1991). *Procedure for validation of microscopic traffic flow simulation models*. 1320.
- Benzoni-Gavage, Sylvie and Rinaldo M Colombo (2003). "An n -populations model for traffic flow". In: *European Journal of Applied Mathematics* 14.05, pp. 587–612.
- Brackstone, Mark and Mike McDonald (1999). "Car-following: a historical review". In: *Transportation Research Part F: Traffic Psychology and Behaviour* 2.4, pp. 181–196.
- Caligaris, Carlo, Simona Sacone, and Silvia Siri (2007). "Optimal ramp metering and variable speed signs for multiclass freeway traffic". In: *Control Conference (ECC), 2007 European*. IEEE, pp. 1780–1785.
- Carlson, Rodrigo C et al. (2010). "Optimal mainstream traffic flow control of large-scale motorway networks". In: *Transportation Research Part C: Emerging Technologies* 18.2, pp. 193–212.

- Chanut, Stéphane and Christine Buisson (2003). "Macroscopic model and its numerical solution for two-flow mixed traffic with different speeds and lengths". In: *Transportation Research Record: Journal of the Transportation Research Board* 1852, pp. 209–219.
- Chen, Guangjiao et al. (2013). "A cell automation traffic flow model for mixed traffic". In: *Procedia-Social and Behavioral Sciences* 96, pp. 1412–1419.
- Cho, Hung-Jung and Yuh-Ting Wu (2004). "Modeling and simulation of motorcycle traffic flow". In: *Systems, Man and Cybernetics, 2004 IEEE International Conference on*. Vol. 7. IEEE, pp. 6262–6267.
- Chowdhury, Debashish, Ludger Santen, and Andreas Schadschneider (2000). "Statistical physics of vehicular traffic and some related systems". In: *Physics Reports* 329.4-6, pp. 199–329.
- Chu, Kang-Ching et al. (2011). "Validation of stochastic traffic flow model with microscopic traffic simulation". In: *Automation Science and Engineering (CASE), 2011 IEEE Conference on*. IEEE, pp. 672–677.
- Clark, Jim and Gene Daigle (1997). "The importance of simulation techniques in ITS research and analysis". In: *Proceedings of the 29th conference on Winter simulation*. IEEE Computer Society, pp. 1236–1243.
- Cohen, Adam and Susan Shaheen (2018). *Planning for Shared Mobility*.
- Cremer, M and Markos Papageorgiou (1981). "Parameter identification for a traffic flow model". In: *Automatica* 17.6, pp. 837–843.
- Dagan, Erez et al. (2004). "Forward collision warning with a single camera". In: *Intelligent Vehicles Symposium, 2004 IEEE*. IEEE, pp. 37–42.
- Daganzo, F. Carlos (1995). "Requiem for second-order fluid approximations of traffic flow". In: *Transportation Research Part B: Methodological* 29.4, pp. 277–286.
- (1997). "A continuum theory of traffic dynamics for freeways with special lanes". In: *Transportation Research Part B: Methodological* 31.2, pp. 83–102.
- (2002). "A behavioral theory of multi-lane traffic flow. Part I: Long homogeneous freeway sections". In: *Transportation Research Part B: Methodological* 36, pp. 131–158.
- Dang, Ruina et al. (2014). "A lane change warning system based on V2V communication". In: *Intelligent Transportation Systems (ITSC), 2014 IEEE 17th International Conference on*. IEEE, pp. 1923–1928.
- Dar, Kashif et al. (2010). "Wireless communication technologies for ITS applications". In: *IEEE Communications Magazine* 48.5, pp. 156–162.
- Del Castillo, JM and FG Benitez (1995). "On the functional form of the speed-density relationship—I: General theory". In: *Transportation Research Part B: Methodological* 29.5, pp. 373–389.
- Deo, Puspita, Bart De Schutter, and Andreas Hegyi (2009). "Model Predictive Control for Multi-Class Traffic Flows". In: *IFAC Proceedings Volumes* 42.15, pp. 25–30.
- Dervisoglu, Gunes et al. (2009). "Automatic calibration of the fundamental diagram and empirical observations on capacity". In: *Transportation Research Board 88th Annual Meeting*. Vol. 15.
- Dogan, Atakan et al. (2004). "Evaluation of intersection collision warning system using an inter-vehicle communication simulator". In: *Intelligent Transportation Systems, 2004. Proceedings. The 7th International IEEE Conference on*. IEEE, pp. 1103–1108.
- Doi, Ayumu et al. (1994). "Development of a rear-end collision avoidance system with automatic brake control". In: *Jsaе Review* 15.4, pp. 335–340.
- Edie, Leslie C (1961). "Car-following and steady-state theory for noncongested traffic". In: *Operations research* 9.1, pp. 66–76.
- El Faouzi, Nour-Eddin, Henry Leung, and Ajeesh Kurian (2011). "Data fusion in intelligent transportation systems: Progress and challenges—A survey". In: *Information Fusion* 12.1, pp. 4–10.
- Fan, Shimao and Daniel B Work (2015). "A heterogeneous multiclass traffic flow model with creeping". In: *SIAM Journal on Applied Mathematics* 75.2, pp. 813–835.

- Faye, Sébastien, Claude Chaudet, and Isabelle Demeure (2012). "A distributed algorithm for adaptive traffic lights control". In: *Intelligent Transportation Systems (ITSC), 2012 15th International IEEE Conference on*. IEEE, pp. 1572–1577.
- Fellendorf, Martin and Peter Vortisch (2010). "Microscopic traffic flow simulator VIS-SIM". In: *Fundamentals of traffic simulation*. Springer, pp. 63–93.
- FEMA (2009). *A European Agenda for Motorcycle Safety, The Motorcyclists' Point of View*. Tech. rep. The Federation of European Motorcyclists' Associations (FEMA).
- Gazis, Denos C, Robert Herman, and Richard W Rothery (1961). "Nonlinear follow-the-leader models of traffic flow". In: *Operations research* 9.4, pp. 545–567.
- Ghods, Amir Hosein, Ashkan Rahimi Kian, and Masoud Tabibi (2009). "Adaptive freeway ramp metering and variable speed limit control: a genetic-fuzzy approach". In: *IEEE Intelligent Transportation Systems Magazine* 1.1, pp. 27–36.
- Gipps, Peter G (1981). "A behavioural car-following model for computer simulation". In: *Transportation Research Part B: Methodological* 15.2, pp. 105–111.
- (1986). "A model for the structure of lane-changing decisions". In: *Transportation Research Part B: Methodological* 20.5, pp. 403–414.
- Greenberg, Harold (1959). "An analysis of traffic flow". In: *Operations research* 7.1, pp. 79–85.
- Greenshields, BD, Ws Channing, Hh Miller, et al. (1935). "A study of traffic capacity". In: *Highway research board proceedings*. Vol. 1935. National Research Council (USA), Highway Research Board.
- Guerrero-Ibáñez, Juan, Sherali Zeadally, and Juan Contreras-Castillo (2018). "Sensor technologies for intelligent transportation systems". In: *Sensors* 18.4, p. 1212.
- Gupta, Arvind Kumar and VK Katiyar (2007). "A new multi-class continuum model for traffic flow". In: *Transportmetrica* 3.1, pp. 73–85.
- Habenicht, Stefan et al. (2011). "A maneuver-based lane change assistance system". In: *Intelligent Vehicles Symposium (IV), 2011 IEEE*. IEEE, pp. 375–380.
- Hadiuzzaman, Md, Tony Z Qiu, and Xiao-Yun Lu (2012). "Variable speed limit control design for relieving congestion caused by active bottlenecks". In: *Journal of Transportation Engineering* 139.4, pp. 358–370.
- Hegyi, A and SP Hoogendoorn (2010). "Dynamic speed limit control to resolve shock waves on freeways-Field test results of the SPECIALIST algorithm". In: *Intelligent Transportation Systems (ITSC), 2010 13th International IEEE Conference on*. IEEE, pp. 519–524.
- Hegyi, Andreas, Bart De Schutter, and J Hellendoorn (2005). "Optimal coordination of variable speed limits to suppress shock waves". In: *IEEE Transactions on intelligent transportation systems* 6.1, pp. 102–112.
- Helbing, Dirk, Ansgar Hennecke, et al. (2001). "MASTER: macroscopic traffic simulation based on a gas-kinetic, non-local traffic model". In: *Transportation Research Part B: Methodological* 35.2, pp. 183–211.
- Helbing, Dirk and Benno Tilch (1998). "Generalized force model of traffic dynamics". In: *Physical review E* 58.1, p. 133.
- Hoogendoorn, Serge P and Piet HL Bovy (2000). "Continuum modeling of multiclass traffic flow". In: *Transportation Research Part B: Methodological* 34.2, pp. 123–146.
- (2001). "State-of-the-art of vehicular traffic flow modelling". In: *Proceedings of the Institution of Mechanical Engineers, Part I: Journal of Systems and Control Engineering* 215.4, pp. 283–303.
- Hoogendoorn, Serge and Raymond Hoogendoorn (2010). "Calibration of microscopic traffic-flow models using multiple data sources". In: *Philosophical Transactions of the Royal Society of London A: Mathematical, Physical and Engineering Sciences* 368.1928, pp. 4497–4517.
- Huber, Matthew J (1982). *Estimation of passenger-car equivalents of trucks in traffic stream (discussion and closure)*. 869.
- Jamson, A Hamish, Frank CH Lai, and Oliver MJ Carsten (2008). "Potential benefits of an adaptive forward collision warning system". In: *Transportation research part C: emerging technologies* 16.4, pp. 471–484.

- Jiang, Chunxiao et al. (2016). "Information-Sharing Outage-Probability Analysis of Vehicular Networks". In: *IEEE Transactions on Vehicular Technology* 65.12, pp. 9479–9492.
- Kesting, Arne and Martin Treiber (2013). "Traffic flow dynamics: data, models and simulation". In: *no. Book, Whole*(Springer Berlin Heidelberg, Berlin, Heidelberg, 2013).
- Kesting, Arne, Martin Treiber, and Dirk Helbing (2007). "General lane-changing model MOBIL for car-following models". In: *Transportation Research Record* 1999.1, pp. 86–94.
- Klar, Axel, Reinhart D Kühne, and Raimund Wegener (1995). "Mathematical models for vehicular traffic". In:
- Kockelman, Kara (1998). "Changes in flow-density relationship due to environmental, vehicle, and driver characteristics". In: *Transportation Research Record: Journal of the Transportation Research Board* 1644, pp. 47–56.
- Koyama, Yuichiro and Toshiyuki Tanaka (2011). "High-precision motorcycle trajectory measurements using GPS". In: *SICE Journal of Control, Measurement, and System Integration* 4.3, pp. 199–205.
- Krammes, Raymond A and Kenneth W Crowley (1986). "Passenger car equivalents for trucks on level freeway segments". In: *Transportation Research Record* 1091.
- Lämmer, Stefan and Dirk Helbing (2008). "Self-control of traffic lights and vehicle flows in urban road networks". In: *Journal of Statistical Mechanics: Theory and Experiment* 2008.04, P04019.
- Lan, Lawrence W and Chiung-Wen Chang (2005). "Inhomogeneous cellular automata modeling for mixed traffic with cars and motorcycles". In: *Journal of advanced transportation* 39.3, pp. 323–349.
- Lan, Lawrence W, Yu-Chiun Chiou, et al. (2010). "Cellular automaton simulations for mixed traffic with erratic motorcycles' behaviours". In: *Physica A: Statistical Mechanics and its Applications* 389.10, pp. 2077–2089.
- Leclercq, Ludovic (2005). "Calibration of flow-density relationships on urban streets". In: *Transportation Research Record: Journal of the Transportation Research Board* 1934, pp. 226–234.
- (2007). "Hybrid approaches to the solutions of the "Lighthill–Whitham–Richards" model". In: *Transportation Research Part B: Methodological* 41.7, pp. 701–709.
- Leclercq, Ludovic and Jorge A Laval (2009). "A multiclass car-following rule based on the LWR model". In: *Traffic and Granular Flow'07*. Springer, pp. 151–160.
- Leclercq, Ludovic, Jorge Andres Laval, and Estelle Chevallier (2007). "The Lagrangian coordinates and what it means for first order traffic flow models". In: *Transportation and Traffic Theory 2007. Papers Selected for Presentation at ISTTT17 Engineering and Physical Sciences Research Council (Great Britain) Rees Jeffreys Road Fund Transport Research Foundation TMS Consultancy Ove Arup and Partners, Hong Kong Transportation Planning (International) PTV AG*.
- Lee, Chris, Bruce Hellinga, and Frank Saccomanno (2004). "Assessing safety benefits of variable speed limits". In: *Transportation research record: journal of the transportation research board* 1897, pp. 183–190.
- Lee, Tzu-Chang, John W Polak, et al. (2012). "The kinematic features of motorcycles in congested urban networks". In: *Accident Analysis & Prevention* 49, pp. 203–211.
- Lee, Tzu-Chang, John Polak, and Michael Bell (2009). "New approach to modeling mixed traffic containing motorcycles in urban areas". In: *Transportation Research Record: Journal of the Transportation Research Board* 2140, pp. 195–205.
- Lenorzer, A et al. (2015). "Modelling and Simulation of Mixed Traffic". In: *Australasian Transport Research Forum (ATRF), 37th, 2015, Sydney, New South Wales, Australia*.
- LeVeque, Randall J (1992). *Numerical methods for conservation laws*. Vol. 132. Springer.
- Levinson, David (2003). "The value of advanced traveler information systems for route choice". In: *Transportation Research Part C: Emerging Technologies* 11.1, pp. 75–87.
- Li, Xin-Gang et al. (2006). "A realistic two-lane cellular automata traffic model considering aggressive lane-changing behavior of fast vehicle". In: *Physica A: Statistical Mechanics and its Applications* 367, pp. 479–486.

- Lighthill, MJ and GB Whitham (1955a). "On kinematic waves. I. Flood movement in long rivers". In: *Proceedings of the Royal Society of London A: Mathematical, Physical and Engineering Sciences*. Vol. 229. 1178. The Royal Society, pp. 281–316.
- (1955b). "On kinematic waves. II. A theory of traffic flow on long crowded roads". In: *Proceedings of the Royal Society of London A: Mathematical, Physical and Engineering Sciences*. Vol. 229. 1178. The Royal Society, pp. 317–345.
- Lin, Pei-Wei, Kyeong-Pyo Kang, and Gang-Len Chang (2004). "Exploring the effectiveness of variable speed limit controls on highway work-zone operations". In: *Intelligent transportation systems*. Vol. 8. 3. Taylor & Francis, pp. 155–168.
- Liu, Lan, Liling Zhu, and Da Yang (2016). "Modeling and simulation of the car-truck heterogeneous traffic flow based on a nonlinear car-following model". In: *Applied Mathematics and Computation* 273, pp. 706–717.
- Liu, Shuai, Hans Hellendoorn, and Bart De Schutter (2017). "Model predictive control for freeway networks based on multi-class traffic flow and emission models". In: *IEEE Transactions on Intelligent Transportation Systems* 18.2, pp. 306–320.
- Logghe, S and Lambertus H Immers (2008). "Multi-class kinematic wave theory of traffic flow". In: *Transportation Research Part B: Methodological* 42.6, pp. 523–541.
- Logghe, S. and LH. Immers (2003). "Heterogeneous traffic flow modelling with the LWR model using passenger-car equivalents". In: *Proceedings of the 10th World congress on ITS, Madrid (Spain)*.
- Maerivoet, Sven and Bart De Moor (2005). "Cellular automata models of road traffic". In: *Physics Reports* 419.1, pp. 1–64.
- Maimaris, Athanasios and George Papageorgiou (2016). "A review of intelligent transportation systems from a communications technology perspective". In: *Intelligent Transportation Systems (ITSC), 2016 IEEE 19th International Conference on*. IEEE, pp. 54–59.
- Mallikarjuna, C, Budde Tharun, and Dibyendu Pal (2013). "Analysis of the lateral gap maintaining behavior of vehicles in heterogeneous traffic stream". In: *Procedia-Social and Behavioral Sciences* 104, pp. 370–379.
- Mallikarjuna, Ch, A Phanindra, and K Ramachandra Rao (2009). "Traffic data collection under mixed traffic conditions using video image processing". In: *Journal of transportation engineering* 135.4, pp. 174–182.
- Mallikarjuna, Ch and K Ramachandra Rao (2006). "Area occupancy characteristics of heterogeneous traffic". In: *Transportmetrica* 2.3, pp. 223–236.
- (2009). "Cellular automata model for heterogeneous traffic". In: *Journal of Advanced Transportation* 43.3, pp. 321–345.
- Marsden, Greg, Mike McDonald, and Mark Brackstone (2001). "Towards an understanding of adaptive cruise control". In: *Transportation Research Part C: Emerging Technologies* 9.1, pp. 33–51.
- Mathew, Tom V, Caleb Ronald Munigety, and Ashutosh Bajpai (2013). "Strip-based approach for the simulation of mixed traffic conditions". In: *Journal of Computing in Civil Engineering* 29.5, p. 04014069.
- Meng, Jian-ping et al. (2007). "Cellular automaton model for mixed traffic flow with motorcycles". In: *Physica A: Statistical Mechanics and its Applications* 380, pp. 470–480.
- Miles, Roger E (1970). "On the homogeneous planar Poisson point process". In: *Mathematical Biosciences* 6, pp. 85–127.
- Miller, Ronald and Qingfeng Huang (2002). "An adaptive peer-to-peer collision warning system". In: *Vehicular technology conference, 2002. VTC Spring 2002. IEEE 55th*. Vol. 1. IEEE, pp. 317–321.
- Minh, Chu Cong, Kazushi Sano, and Shoji Matsumoto (2012). "Maneuvers of motorcycles in queues at signalized intersections". In: *Journal of advanced transportation* 46.1, pp. 39–53.
- MINH, Chu Cong, Kazushi SANO, et al. (2007). "Acceleration and deceleration models of motorcycle at signalized intersections". In: *Journal of the Eastern Asia Society for Transportation Studies* 7, pp. 2396–2411.

- Misener, James A, Raja Sengupta, and Hariharan Krishnan (2005). "Cooperative collision warning: Enabling crash avoidance with wireless technology". In: *12th World Congress on Intelligent Transport SystemsITS AmericaITS JapanERTICO*.
- Monamy, Thomas, Habib Haj-Salem, and Jean-Patrick Lebacque (2012). "A macroscopic node model related to capacity drop". In: *Procedia-Social and Behavioral Sciences* 54, pp. 1388–1396.
- Nagel, Kai and Michael Schreckenberg (1992). "A cellular automaton model for freeway traffic". In: *Journal de physique I* 2.12, pp. 2221–2229.
- Nair, Rahul, Hani S Mahmassani, and Elise Miller-Hooks (2011). "A porous flow approach to modeling heterogeneous traffic in disordered systems". In: *Transportation Research Part B: Methodological* 45.9, pp. 1331–1345.
- (2012). "A porous flow model for disordered heterogeneous traffic streams". In: *Transportation Research Board 91st Annual Meeting*. 12-3260.
- Newell, Gordon F (1993). "A simplified theory of kinematic waves in highway traffic, part I general theory, part II: Queueing at freeway bottlenecks, part III multi-destination flows". In: *Transportation Research Part B: Methodological* 27.4, pp. 281–313.
- Newell, Gordon Frank (2002). "A simplified car-following theory: a lower order model". In: *Transportation Research Part B: Methodological* 36.3, pp. 195–205.
- Ngoduy, D and SP Hoogendoorn (2003). "An automated calibration procedure for macroscopic traffic flow models". In: *IFAC Proceedings Volumes* 36.14, pp. 263–268.
- Ngoduy, D and R Liu (2007). "Multiclass first-order simulation model to explain non-linear traffic phenomena". In: *Physica A: Statistical Mechanics and its Applications* 385.2, pp. 667–682.
- Nguyen, Long Xuan and Shinya Hanaoka (2011). "An application of social force approach for motorcycle dynamics". In: *Proceedings of the Eastern Asia Society for Transportation Studies The 9th International Conference of Eastern Asia Society for Transportation Studies, 2011*. Eastern Asia Society for Transportation Studies, pp. 319–319.
- Nguyen, Long Xuan, Shinya Hanaoka, and Tomoya Kawasaki (2014). "Traffic conflict assessment for non-lane-based movements of motorcycles under congested conditions". In: *IATSS research* 37.2, pp. 137–147.
- Nguyen, Long, Shinya Hanaoka, and Tomoya Kawasaki (2012). "Describing non-lane-based motorcycle movements in motorcycle-only traffic flow". In: *Transportation Research Record: Journal of the Transportation Research Board* 2281, pp. 76–82.
- Ni, Daiheng (2007). "Determining traffic-flow characteristics by definition for application in ITS". In: *IEEE Transactions on Intelligent Transportation Systems* 8.2, pp. 181–187.
- OECD/ITF (2015). *Improving Safety for Motorcycle, Scooter and Moped Riders*. OECD Publishing, Paris. <http://dx.doi.org/10.1787/9789282107942-en>.
- Ossen, Saskia and Serge P Hoogendoorn (2011). "Heterogeneity in car-following behavior: Theory and empirics". In: *Transportation research part C: emerging technologies* 19.2, pp. 182–195.
- Ouellet, James V (2012). "Lane splitting on California freeways". In: *Proceedings of the Transportation Research Board 91st Annual Meeting*.
- Pandey, Gaurav, K Ramachandra Rao, and Dinesh Mohan (2017). "Modelling vehicular interactions for heterogeneous traffic flow using cellular automata with position preference". In: *Journal of Modern Transportation* 25.3, pp. 163–177.
- Papadimitratos, Panos et al. (2009). "Vehicular communication systems: Enabling technologies, applications, and future outlook on intelligent transportation". In: *IEEE communications magazine* 47.11.
- Papageorgiou, Markos (1983). *Applications of Automatic Control Concepts to Traffic Flow Modeling and Control*. Springer, Berlin, Heidelberg.
- Papageorgiou, Markos and Apostolos Kotsialos (2002). "Freeway ramp metering: An overview". In: *IEEE transactions on intelligent transportation systems* 3.4, pp. 271–281.

- Pasquale, C et al. (2016). "A multi-class ramp metering and routing control scheme to reduce congestion and traffic emissions in freeway networks". In: *IFAC-PapersOnLine* 49.3, pp. 329–334.
- Paveri-Fontana, SL (1975). "On Boltzmann-like treatments for traffic flow: a critical review of the basic model and an alternative proposal for dilute traffic analysis". In: *Transportation research* 9.4, pp. 225–235.
- Payne, Harold J (1971). "Model of freeway traffic and control". In: *Mathematical Model of Public System*, pp. 51–61.
- Pipes, Louis A (1953). "An operational analysis of traffic dynamics". In: *Journal of applied physics* 24.3, pp. 274–281.
- Pipes, Louis Albert (1966). "Car following models and the fundamental diagram of road traffic". In: *Transportation Research/UK/*.
- Ploeg, Jeroen et al. (2011). "Design and experimental evaluation of cooperative adaptive cruise control". In: *Intelligent Transportation Systems (ITSC), 2011 14th International IEEE Conference on*. IEEE, pp. 260–265.
- Pohlmann, Tobias and Bernhard Friedrich (2010). "Online control of signalized networks using the cell transmission model". In: *Intelligent Transportation Systems (ITSC), 2010 13th International IEEE Conference on*. IEEE, pp. 1–6.
- Praveen, Prema Somanathan and Venkatachalam Thamizh Arasan (2013). "Influence of traffic mix on PCU value of vehicles under heterogeneous traffic conditions". In: *International Journal of Traffic and Transport Engineering* 3.3, pp. 302–330.
- Priemer, Christian and Bernhard Friedrich (2009). "A decentralized adaptive traffic signal control using V2I communication data". In: *Intelligent Transportation Systems, 2009. ITSC'09. 12th International IEEE Conference on*. IEEE, pp. 1–6.
- Puppo, Gabriella et al. (2016). "Fundamental diagrams in traffic flow: The case of heterogeneous kinetic models". In: *Communications in Mathematical Sciences* 14.3, pp. 643–669.
- Qian, Zhen Sean et al. (2017). "Modeling heterogeneous traffic flow: A pragmatic approach". In: *Transportation Research Part B: Methodological* 99, pp. 183–204.
- Radin Umar, RS, GM Mackay, and Brian L Hills (1995). "Preliminary analysis of exclusive motorcycle lanes along the federal highway F02, Shah Alam, Malaysia". In: *Journal of IATSS Research* 19.2, pp. 93–98.
- Rakha, Hesham et al. (1996). "Systematic verification, validation and calibration of traffic simulation models". In: *75th Annual Meeting of the Transportation Research Board, Washington, DC*. Citeseer.
- Rice, Thomas, Lara Troszak, and Taryn Erhardt (2015). "Motorcycle lane-splitting and safety in California". In: *Berkeley: University of*.
- Richards, Paul I (1956). "Shock waves on the highway". In: *Operations research* 4.1, pp. 42–51.
- Robertson, Sandy (2002). "Motorcycling and congestion: Definition of behaviours". In: *Contemporary Ergonomics*, pp. 273–277.
- Robin, Th et al. (2009). "Specification, estimation and validation of a pedestrian walking behavior model". In: *Transportation Research Part B: Methodological* 43.1, pp. 36–56.
- Sarvi, Majid (2013). "Heavy commercial vehicles-following behavior and interactions with different vehicle classes". In: *Journal of advanced transportation* 47.6, pp. 572–580.
- Schakel, Wouter J, Bart Van Arem, and Bart D Netten (2010). "Effects of cooperative adaptive cruise control on traffic flow stability". In: *Intelligent Transportation Systems (ITSC), 2010 13th International IEEE Conference on*. IEEE, pp. 759–764.
- Schreiter, Thomas et al. (2012). "Vehicle class-specific route guidance of freeway traffic by model-predictive control". In: *Transportation Research Record: Journal of the Transportation Research Board* 2324, pp. 53–62.
- Seiler, Peter, Bongsob Song, and J Karl Hedrick (1998). *Development of a collision avoidance system*. Tech. rep. SAE Technical Paper.
- SHIOMI, Yasuhiro et al. (2012). "Modeling traffic flow dominated by motorcycles based on discrete choice approach". In: *Proceedings of 1st LATSIS Conference*.

- Smulders, Stef (1990). "Control of freeway traffic flow by variable speed signs". In: *Transportation Research Part B: Methodological* 24.2, pp. 111–132.
- Sperley, Myra, Amanda Joy Pietz, et al. (2010). *Motorcycle lane-sharing: literature review*. Tech. rep. Oregon. Dept. of Transportation.
- Spiliopoulou, A et al. (2014). "Macroscopic traffic flow model validation at congested freeway off-ramp areas". In: *Transportation Research Part C: Emerging Technologies* 41, pp. 18–29.
- Tang, TQ et al. (2009). "A new dynamic model for heterogeneous traffic flow". In: *Physics Letters A* 373.29, pp. 2461–2466.
- Tordeux, Antoine, Sylvain Lassarre, and Michel Roussignol (2010). "An adaptive time gap car-following model". In: *Transportation research part B: methodological* 44.8-9, pp. 1115–1131.
- Treiber, Martin and Dirk Helbing (1999). "Macroscopic simulation of widely scattered synchronized traffic states". In: *Journal of Physics A: Mathematical and General* 32.1, p. L17.
- Underwood, Robin T (1961). "Speed, volume, and density relationships". In: *Quality and Theory of Traffic Flow*, pp. 141–188.
- Van Arem, Bart, Cornelie JG Van Driel, and Ruben Visser (2006). "The impact of cooperative adaptive cruise control on traffic-flow characteristics". In: *IEEE Transactions on Intelligent Transportation Systems* 7.4, pp. 429–436.
- Van Lint, J, Serge Hoogendoorn, and Marco Schreuder (2008). "Fastlane: New multi-class first-order traffic flow model". In: *Transportation Research Record: Journal of the Transportation Research Board* 2088, pp. 177–187.
- Vlahogianni, Eleni I (2014). "Powered-Two-Wheelers kinematic characteristics and interactions during filtering and overtaking in urban arterials". In: *Transportation research part F: traffic psychology and behaviour* 24, pp. 133–145.
- Wageningen-Kessels, Femke van, Hans Van Lint, et al. (2010). "Lagrangian formulation of multiclass kinematic wave model". In: *Transportation Research Record: Journal of the Transportation Research Board* 2188, pp. 29–36.
- Wageningen-Kessels, Femke van, Yufei Yuan, et al. (2013). "Discontinuities in the Lagrangian formulation of the kinematic wave model". In: *Transportation Research Part C: Emerging Technologies* 34, pp. 148–161.
- Wageningen-Kessels, FLM van (2013). "Multi-class continuum traffic flow models: analysis and simulation methods". PhD thesis. TRAIL.
- Wagner, Peter, Kai Nagel, and Dietrich E Wolf (1997). "Realistic multi-lane traffic rules for cellular automata". In: *Physica A: Statistical Mechanics and its Applications* 234.3-4, pp. 687–698.
- Walton, D and J Buchanan (2012). "Motorcycle and scooter speeds approaching urban intersections". In: *Accident Analysis & Prevention* 48, pp. 335–340.
- Wang, Ruili et al. (2007). "Synchronized flow and phase separations in single-lane mixed traffic flow". In: *Physica A: Statistical Mechanics and its Applications* 378.2, pp. 475–484.
- Wegener, Raimund and Axel Klar (1996). "A kinetic model for vehicular traffic derived from a stochastic microscopic model". In: *Transport Theory and Statistical Physics* 25.7, pp. 785–798.
- Wigan, Marcus (2002). "Motorcycles as a full mode of transportation". In: *Transportation Research Record: Journal of the Transportation Research Board* 1818, pp. 39–46.
- Wong, GCK and SC Wong (2002). "A multi-class traffic flow model—an extension of LWR model with heterogeneous drivers". In: *Transportation Research Part A: Policy and Practice* 36.9, pp. 827–841.
- Wong, KI, Tzu-Chang LEE, and Yen-Yu CHEN (2016). "Traffic Characteristics of Mixed Traffic Flows in Urban Arterials". In: *Asian Transport Studies* 4.2, pp. 379–391.
- Yang, Da et al. (2015). "A cellular automata model for car–truck heterogeneous traffic flow considering the car–truck following combination effect". In: *Physica A: Statistical Mechanics and its Applications* 424, pp. 62–72.
- York, I et al. (2010). "Assessment of TfL's experimental scheme to allow motorcycles onto with-flow bus lanes on the TLRN". In: *Final Project Report PPR* 495, p. 126.

- Yperman, I (2011). "Commuting by motorcycle: impact analysis". In: *Transport and Mobility Leuven, Leuven, Belgium*.
- Yuan, Yufei, JWC Van Lint, et al. (2012). "Real-time Lagrangian traffic state estimator for freeways". In: *IEEE Transactions on Intelligent Transportation Systems* 13.1, pp. 59–70.
- Yuan, Yufei, FLM van Wageningen-Kessels, et al. (2011). "Two modeling and discretization choices for Lagrangian multi-class firstorder traffic flow model and their related (dis-) advantages". In: *The Ninth International Conference on Traffic and Granular Flow, 2011. Abstract Book., Moscow, proceedings to be published*. Vol. 125, pp. 200–237.
- Zegeye, Solomon K et al. (2009). "Model-based traffic control for balanced reduction of fuel consumption, emissions, and travel time". In: *Proceedings of the 12th IFAC Symposium on Transportation Systems*, pp. 149–154.
- Zhang, H Michael (1998). "A theory of nonequilibrium traffic flow". In: *Transportation Research Part B: Methodological* 32.7, pp. 485–498.
- (2002). "A non-equilibrium traffic model devoid of gas-like behavior". In: *Transportation Research Part B: Methodological* 36.3, pp. 275–290.
- Zhang, H. and W. Jin (2002). "Kinematic wave traffic flow model for mixed traffic". In: *Transportation Research Record: Journal of the Transportation Research Board* 1802, pp. 197–204.
- Zhang, Peng et al. (2006). "Hyperbolicity and kinematic waves of a class of multi-population partial differential equations". In: *European Journal of Applied Mathematics* 17.2, pp. 171–200.
- Zhou, Binbin et al. (2010). "Adaptive traffic light control in wireless sensor network-based intelligent transportation system". In: *Vehicular technology conference fall (VTC 2010-Fall), 2010 IEEE 72nd. IEEE*, pp. 1–5.